This is to certify that the

dissertation entitled

A Gallium-Arsenide Magnetostatic
Surface-Wave Amplifier

presented by

Jeffrey P. Tate

has been accepted towards fulfillment
of the requirements for

Masters degree in Elect. Engr.

Jan C. Freeman
Major professor
Jan C. Freeman

Date 6/18/85

# A GALLIUM-ARSENIDE MAGNETOSTATIC SURFACE-WAVE AMPLIFIER

by

Jeffrey P. Tate

A THESIS

Submitted to
Michigan State University
in partial fulfillment of the requirements
for the degree of

MASTER OF SCIENCE

Department of Electrical Engineering and Systems Science

1985

ABSTRACT

A GALLIUM-ARSENIDE MAGNETOSTATIC
SURFACE-WAVE AMPLIFIER

By

Jeffrey P. Tate

An analytical treatment of the interaction between slow magnetostatic waves and drifting carriers in a ferrite-semiconductor structure is presented in the absence of the magnetostatic approximation. The analysis of a GENERAL layered structure involving two metal plates is also included. Relevant dispersion relations are evaluated numerically. Dispersion results are optimized by variation of device parameters. The optimized solutions are analyzed under convective instability criteria. Gain is possible theoretically under specific device conditions.

## DEDICATION

The author wishes to lovingly dedicate this paper to his mother, P.J. Warren and to all his family without whose unfailing support this would not have been possible.

## ACKNOWLEDGEMENT

The author wishes to thank his major professor, Dr. J.C. Freeman, for his guidance, helpful discussions, inspiration and advice. The author also wishes to thank Mr. E.D. Robinson for the careful drafting of figures used in this report.

TABLE OF CONTENTS

LIST OF FIGURES

CHAPTER 4



APPENDICES

# 1. INTRODUCTION

The objective of this paper is to investigate the feasibility for amplification of magnetostatic waves in a ferrite-semiconductor composite structure. The mechanism for amplification is based on the interaction of the slow wave with drifting carriers. These phenomena have been studied by several investigators, both theoretically and experimentally. The results however, have been inconclusive.

The existence of magnetostatic waves has been verified by numerous investigators. A representative sample of the contributions made in this area includes:

(1) Damon and Esbach (1960) who investigated theoretically the existence of volume and surface modes of a thin ferrite slab. Dispersion relations were developed in the magnetostatic limit [1].

(2) (1968) Brundle and Freedman experimentally verify the existence of propagating magnetostatic waves using group time delay measurements [2].

(3) (1970) Seshadri performed an analysis for the verification of wavenumber and group velocity. The property of nonreciprocal propagation for magnetostatic waves in a metal backed ferrite slab was presented for the first time [3].

(4) Merry and Sethares [4] observed magnetostatic waves at frequencies of up to 15 gigahertz (1973).

(5) Kawasaki et. al. observed Ferrite-Air and Ferrite-Metal modes. High correlation with theoretical dispersion characteristics was

also observed (1974) [5].

It has been shown through experiments that many signal processing tasks in the microwave frequency range can be performed using these slow waves. In 1973, Vaslow observed group time delay as a function of the externally applied magnetic field. The application of magnetostatic surface waves for variable time delay was then explored [6]. Various devices were also studied by Adam and Collins, e.g. the nondispersive and tapped delay lines which employ magnetostatic surface waves [7]

Presently signal processing tasks can be performed using surface acoustic wave devices. The technology however, has a useful upper limit of two gigahertz due to transducer fabrication complexity and the magnitude of propagation losses. Owens states that Yttrium Garnet (YIG) devices show losses of approximately 12 db/$\mu$s versus 100 db/$\mu$s for devices using SAW technology [8]. Merry and Sethares also found that magnetostatic surface waves exhibit lower loss than SAWs above four gigahertz [9].

Of principle importance for potential signal processing applications is the effect on the slow wave dispersion relation of a metal plate placed a finite distance from the ferrite surface. Bongianni (1971) provides experimental dispersion relations which show the effects on magnetostatic wave propagation characteristics [10]. Theoretical and experimental results have shown that dispersion curves of almost arbitrary shape can be obtained with optimal plate spacing [11, 12].

Due to the effects on YIG magnetostatic wave dispersions, the presence of a metal plate in the ferrite-semiconductor geometry has also been studied extensively. Vashkovskiy et. al. theoretically investigated the effect of a metal-air-YIG spacing on gain and bandwidth of

an amplifier using drifting carriers in semiconductors [13]. The key point is the optimization of bandwidth and gain by maximizing the region of synchronous interaction for carriers and magnetostatic waves. Experimental analyses of magnetostatic wave/carrier interaction have also been performed by several groups, however no significant work has occurred involving the use of metal plates.

The excitation of ferrite magnetostatic waves can be broken into three basic groups:

(1) Magnetostatic Surface Waves (MSSW), where
$\vec{k} \times \vec{H}_0 = \hat{n}$

(2) Magnetostatic Forward Volume Waves (MSFVW), where
$(\vec{k} \times \vec{H}_0) \cdot \hat{n} = 0$

(3) Magnetostatic Backward Volume Waves (MSBVW), where
$\vec{k} \times \vec{H}_0 = 0$

The surface or volume characteristic of the waves is determined by the orientation of the external static magnetic field $\vec{H}_0$ in relation to the direction of propagation. This is illustrated in Figure 1. The waves studied in this report are of the surface type. This means that the wave energy is concentrated on one surface of the ferrite slab. This condition is satisfied if the slab thickness is greater than a wavelength in the transverse direction as shown in Figure 2. Forward and backward waves are also useful in signal processing and devices have been developed using these propagation modes [14-16], but we restrict this investigation to surface modes.

If the ferrite technology continues to mature in a manner similar to that experienced in acoustics, then a means for the amplification of surface magnetostatic waves would be most useful. Theoretical analysis of magnetostatic wave interaction with drifting carriers has been

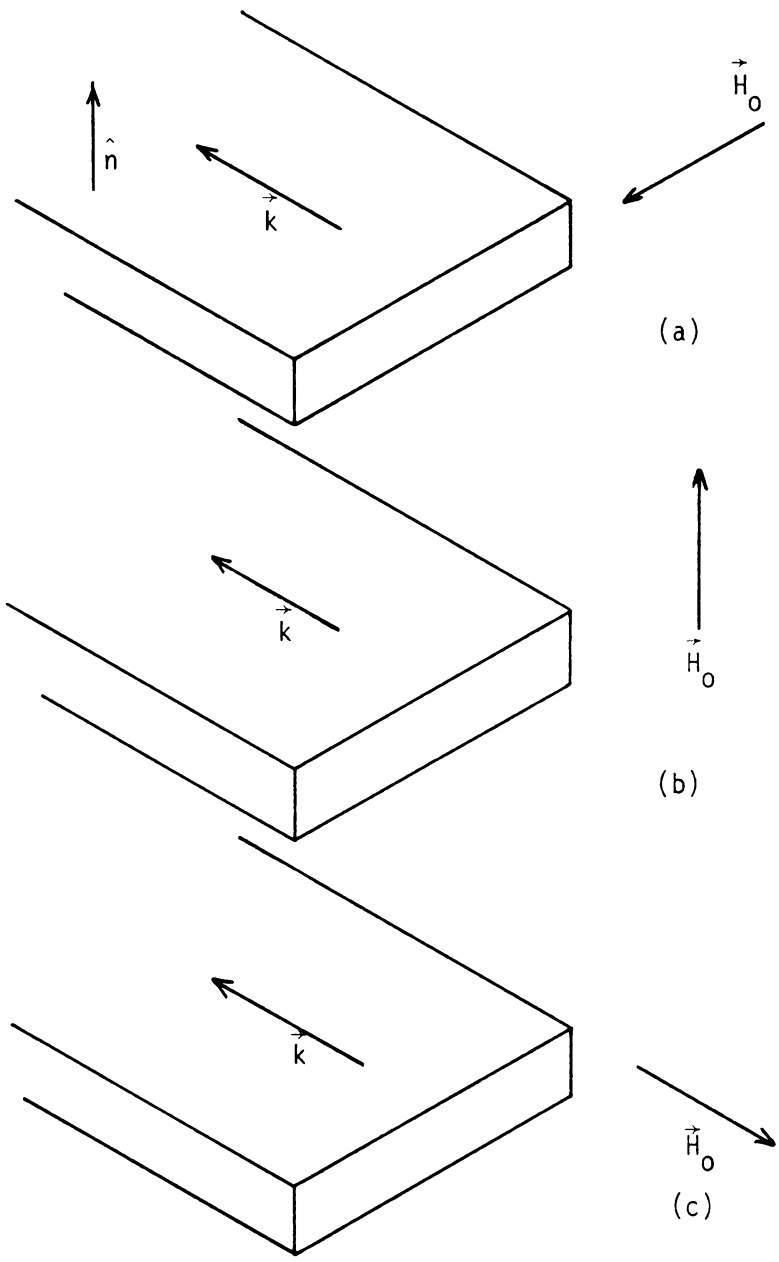


Figure 1. The three basic forms of magnetostatic wave propagation; (a) MSSW (b) MSFVW (c) MSBVW.

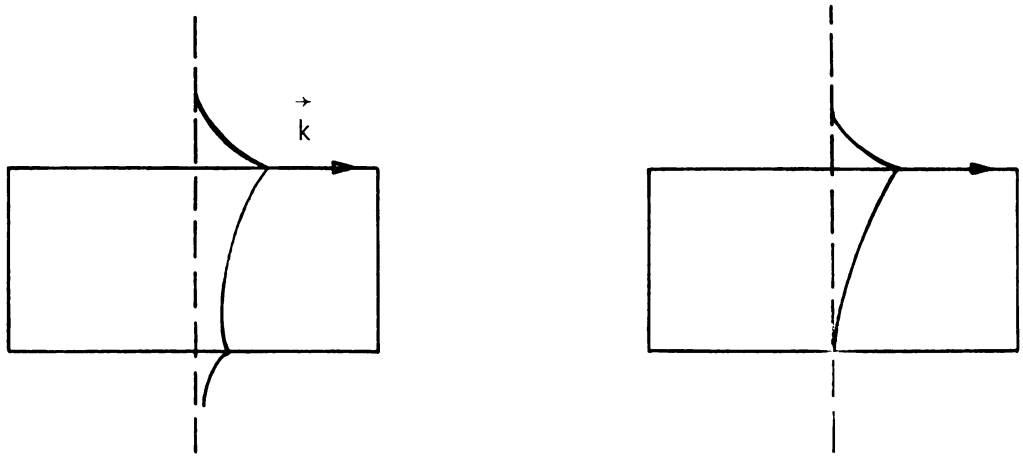


Figure 2. The effect of slab thickness on the mode character of the magnetostatic wave. The above sketch shows the transverse variation of wave field intensity.

performed by various researchers. Bini et al. have provided an "energetic approach" to describe the mechanism of energy transfer from drifting carriers to the slow waves. Analysis of a thin ferrite slab adjacent to a semiconductor half space was conducted. The development of a single surface model employing two semi-infinite half spaces was also presented. A bandwidth of 17 kilohertz for possible amplification was theoretically predicted; while for the thin slab, bandwidths should reach several hundred megahertz [17-20]. Awai and co-workers also performed numerical analyses of a finite YIG slab over InSb. Net amplification was predicted for the case of drifting carriers [21].

In bulk acoustic wave amplifiers a piezoelectric material adjacent to a semiconducting medium is used. The surface acoustic wave amplifier however, uses a thin film of semiconductor material in close proximity to the surface acoustic, or Rayleigh, wave. Because of the presence of an acoustic wave, close proximity without actual contact is required for the wave/carrier interaction to take place. This restriction can present difficulty in the manufacturing of these devices. This does not hold for the magnetostatic wave device. The YIG and semiconductor can be in direct physical contact. The device shall be referred to as a Magnetostatic Surface Wave Amplifier (MSSWA). It is anticipated that this device will operate up to about 10 gigahertz. Adam states however, that MSSW devices in general are narrowband at these frequencies, exhibiting approximately 300 megahertz of operating bandwidth [22].

This paper shall provide a thorough analysis of the MSSWA in the absence of the magnetostatic approximation. Of major importance is the velocity relationship between the carriers and magnetostatic waves. The conditions for which amplification is observed are inconclusive at present. Many reserachers have stated that the drifting carriers must

travel faster than the propagating magnetostatic wave. Kawasaki et al. state however, that even when the drift velocity is less than the phase velocity of the wave a reduction in losses is observed [23]. It is the author's belief that eventhough the carriers may possess a velocity greater than the slow wave phase velocity, some degree of synchronism must exist for energy transfer to occur.

This report shall also seek to determine the optimum geometry which will promote the desired synchronism for practical bandwidth and gain operation of the MSSWA. Some ideas regarding the implementation of this new geometry will also be discussed.

# 2. THE FERRITE SEMICONDUCTOR COMPOSITE STRUCTURE

In the analysis of the MSSW amplifier an understanding of the fundamental mechanisms on which potential amplification is based would be helpful. In this chapter the basic ideas behind ferrimagnetic resonance and the excitation of surface magnetostatic waves are discussed. The interaction of these waves with drifting carriers is also covered. The object is to present a qualitative description of this interaction as a foundation for detailed study of the MSSW amplifier dispersion relations in Chapter 3.

## 2.1. Ferrimagnetic Resonance

Ferro - and ferrimagnetic resonance effects are based on interaction of magnetic dipoles with magnetic fields. A spinning electron constitutes such a dipole. The magnetic moment associated with this spin motion is given by

$$\vec{\mu}_s = \gamma(s\bar{\hbar}) \qquad (2.1\text{-}1)$$

where $\gamma = -|e|/m$ is the gyromagnetic ratio. The value $s\bar{\hbar}$ is the electron spin angular momentum [24].

In the presence of a static magnetic field of magnitude $H_o$, a torque is experienced by the spinning electron. This torque is due to the time rate of change of the spin angular momentum. This can be written as

$$\frac{d(s\bar{\hbar})}{dt} = \mu_o \vec{\mu}_s \times \vec{H}_o \qquad (2.1\text{-}2)$$

which when (2.1-1) is used becomes

$$\frac{d\vec{\mu}_s}{dt} = \gamma_s(\vec{\mu}_s \times \vec{H}_o) \qquad (2.1\text{-}3)$$

where $\gamma_s = \mu_0\gamma$ and $\vec{H}_o$ is in the z-direction [25]. The motion described by (2.1-3) is of a precessional nature. The spinning electron precesses

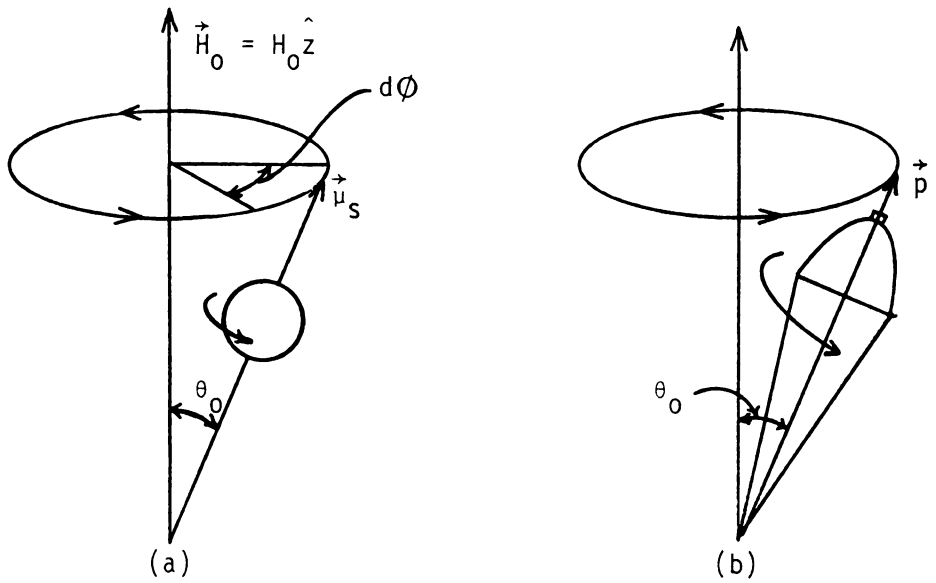


Figure 1. Illustration of the precessional motion for; (a) an electron in a static magnetic field and (b) a spinning top in a constant gravitational field. After B. Lax and K.J. Button.

about the static field in a manner similar to a top in the presence of a gravitational field. The torque relationship in the latter case is

$$\frac{d\vec{p}}{dt} = \vec{\omega}_o \times \vec{p} \qquad (2.1\text{-}4)$$

where $\omega_o$ is the precession frequency and $\vec{p}$ is the angular momentum [26]. A similar term can be developed for the electron and is given by

$$\omega_o = \gamma_s H_o \qquad (2.1\text{-}5)$$

This expression shows that electron precession frequency is determined by the strength of the applied field. The development of $\omega_o$ is given in [27]. In Figure 1 the two cases are shown, where the angle $\theta_o$ is the precession angle.

On the macroscopic level we are interested in the total magnetization of the ferrite system and the interaction it has with magnetic fields. The magnetization is defined as the magnetic moment per unit volume, so that $\vec{M}_o = N\vec{\mu}_s$ where N is the density of dipoles. Now we may write (2.1-3) as

$$\frac{d\vec{M}_o}{dt} = \gamma_s(\vec{M}_o \times \vec{H}_o) \qquad (2.1\text{-}6)$$

with $\vec{H}_o$ again in the z-direction. This equation describes the lossless case which is characterized by perpetual motion. The lossy case will be treated separately. It should be noted that $\vec{M}_o$ and $\vec{H}_o$ are nearly parallel in the first approximation [28]. This becomes significant in the analysis to follow.

If an alternating component of the magnetic field is introduced, the magnetization and field expressions become

$$\vec{M} = \vec{M}_o + \vec{m}e^{j\omega t} \qquad (2.1\text{-}7)$$

$$\vec{H} = \vec{H}_i + \vec{h}e^{j\omega t} \qquad (2.1\text{-}8)$$

where $\vec{H}_i$ and $\vec{M}_o$ represent the static magnetic field and magnetization.

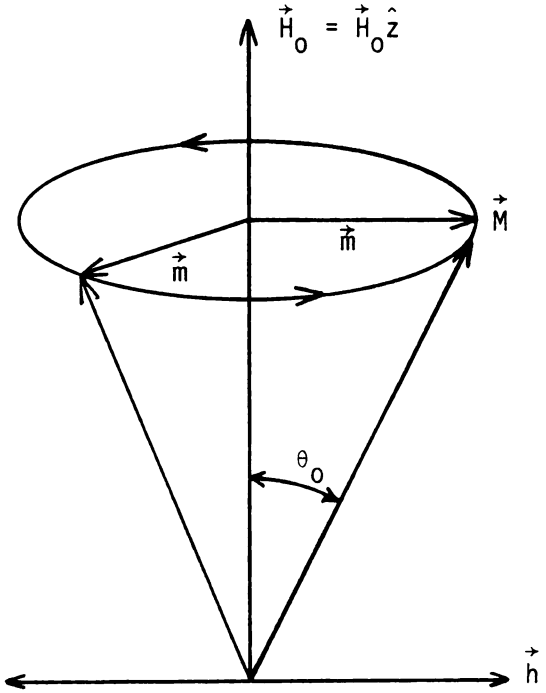


Figure 2. The rf and dc field and magnetization components. Note that $\vec{h}$ can be either circularly polarized or linearly polarized.

The rf components are $\vec{h}$ and $\vec{m}$ respectively. The field $\vec{H}_i$, called the static internal magnetic field is actually the vector sum of the external dc field and the components due to anisotropy and demagnetizing effects. For simplicity, we will assume a single crystalline ferrite slab that is infinite in extent. Under these conditions the above effects can be neglected and $\vec{H}_i = \vec{H}_0$.

The expressions for $\vec{H}$ and $\vec{M}$ are substituted into (2.1-6) to obtain

$$j\omega\vec{m} = \gamma_s(\vec{M}_0 \times \vec{h} + \vec{m} \times \vec{H}_0) \qquad (2.1\text{-}9)$$

where time-harmonic dependence ($e^{j\omega t}$) is implied. This is the linearized small signal approximation, where second order rf and dc terms are ignored [29]. The time variation of $\vec{m}$ as given by (2.1-9) is therefore a function of the first order interaction between dc and rf terms. The manner in which the rf magnetization changes with time determines the variation of the precession angle $\theta_0$. In Figure 2 these field and magnetization components are shown. It should be noted that since $\vec{m}$ is perpendicular to $\vec{H}_0$ that $\vec{h}$ must be also in order to obtain the most efficient energy transfer. If this spatial relationship between $\vec{H}_0$ and $\vec{h}$ is not satisfied, energy transfer does result, but at a reduced efficiency. This occurs for values of $\omega$ not equal to $\omega_0$ [30]. Figure 3 illustrates three cases; zero rf field, non-zero rf field at resonance and outside of resonance. Notice that an oscillatory motion occurs for $\vec{M}$ due to the nonresonant condition [31]. The oscillation shown is exaggerated for the purposes of illustration. In practice this "wobble" by the precessing magnetization would be noticeable only at very high values of the driving rf field and for frequencies not equal to $\omega_0$.

In order to illustrate this precession in more detail, consider a rotating coordinate system. This system rotates about the field $\vec{H}_0$ with angular velocity $\vec{\omega}_r$. The equation of motion becomes

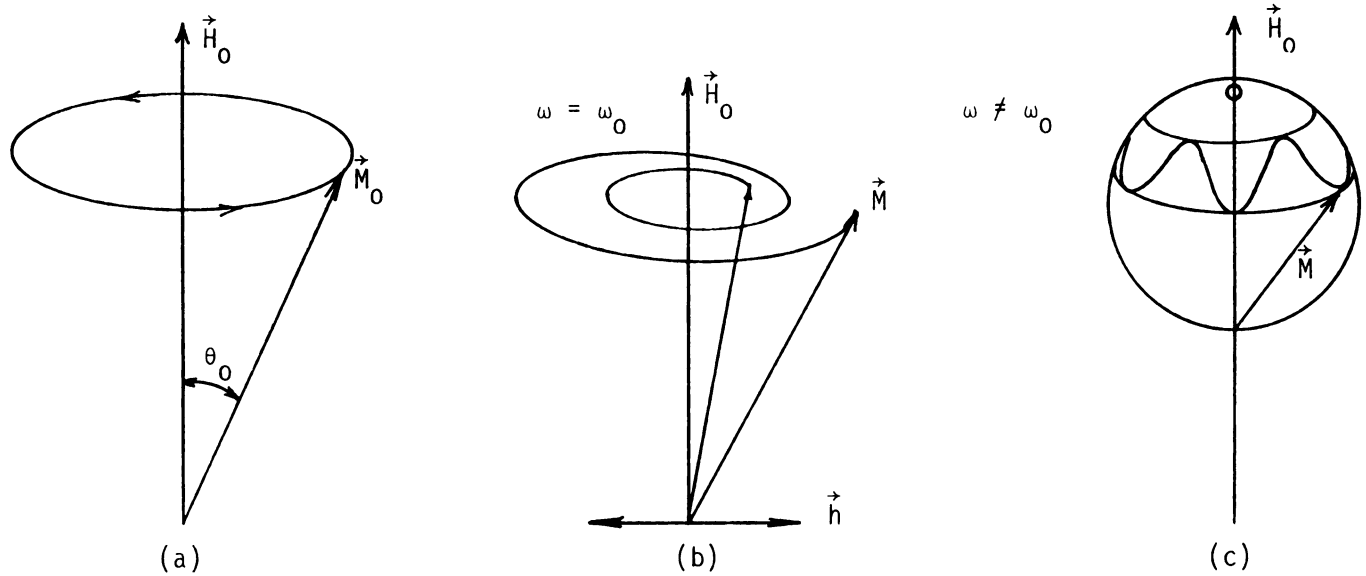


Figure 3. Three conditions for the variation in precessional motion; (a) $\vec{h} = 0$, (b) $\vec{h} \neq 0$, at resonance, (c) $\vec{h} \neq 0$, outside of resonance. After B. Lax and K.J. Button.

$$\frac{d\vec{M}_o}{dt} = \gamma_s \vec{M}_o \times (\gamma_s \vec{H}_o + \vec{\omega}_r) \qquad (2.1\text{-}10)$$

which is the same as (2.1-6) in the stationary reference frame if $H_o$ is replaced by

$$\vec{H}_{eff} = \vec{H}_o - \frac{\vec{\omega}_r}{\gamma_s} \qquad (2.1\text{-}11)$$

If an alternating field is introduced, e.g. one which is circularly polarized with frequency $\omega_r$ the equation of motion is

$$\frac{d\vec{M}}{dt} = \gamma_s (\vec{M} \times [\vec{H}_{eff} + \vec{h}(t)]) \qquad (2.1\text{-}12)$$

where $\vec{h}(t) = \vec{h}e^{j\omega t}$ and the new effective field is

$$\vec{H}_{eff} = \hat{z}\left(H_o - \frac{\omega_r}{\gamma_s}\right) + \hat{y}h(t) \qquad (2.1\text{-}13)$$

with $\hat{z}$ and $\hat{y}$ indicating the z and y directions respectively. The field component h(t) is stationary in the rotating frame [32].

When the magnetization experiences this effective field there is precession about both $\vec{H}_o$ and $\vec{h}(t)$ in the stationary reference frame. In most cases, $\vec{h}(t)$ is small compared to $\vec{H}_o$ so that the precession due to the rf component is ignored. Figure 4 gives an illustration of this total motion and also shows the variation of $\theta_o$ for precession about $\vec{H}_o$ due to the phase relationship between $\vec{h}(t)$ and $\vec{M}$.

The mechanism which governs the variation of $\vec{m}$ and $\theta_o$ is the torque created based on the spatial relationship between $\vec{h}(t)$ and $\vec{H}_o$ as mentioned above. The phase relationship between $\vec{h}(t)$ and $\vec{M}$ is also very important in determining this torque. In order to promote growth in the precession angle the component $\vec{h}(t)$ must precede $\vec{m}(t)$ by a quarter period [33]. If this condition is not met then there are regions where zero or negative torque can result. The negative torque gives rise to

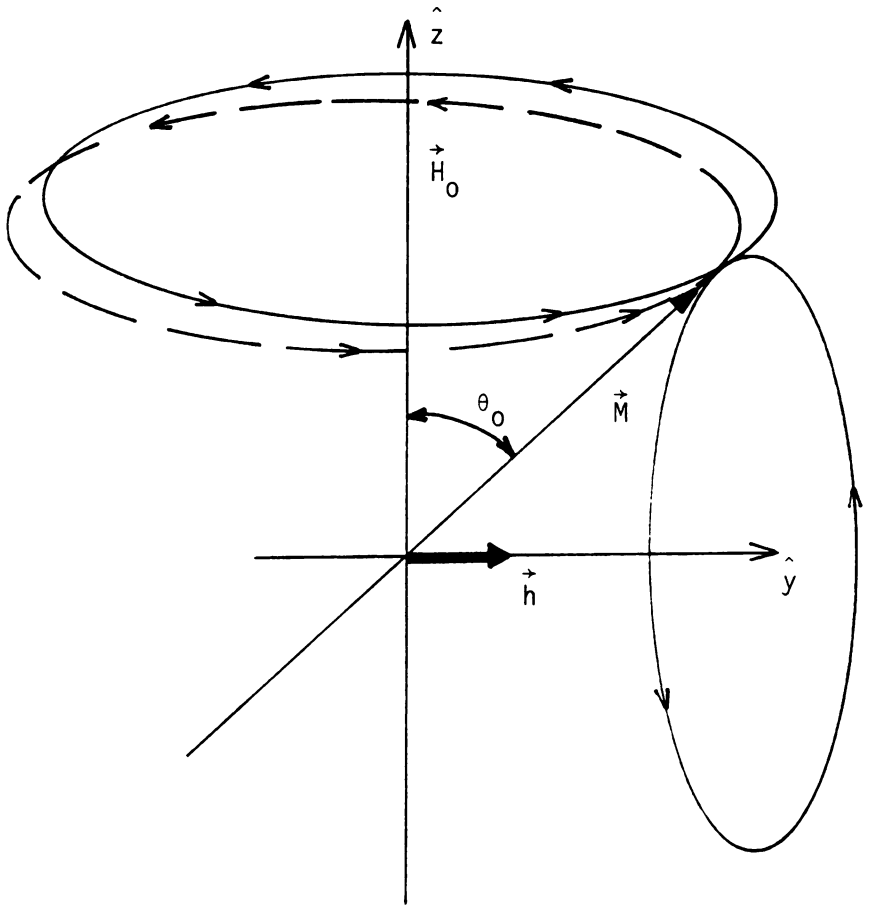


Figure 4. The resultant motion of $\vec{M}$ due to the precession about $\vec{H}$eff as shown by the dotted path. After R.F. Soohoo.

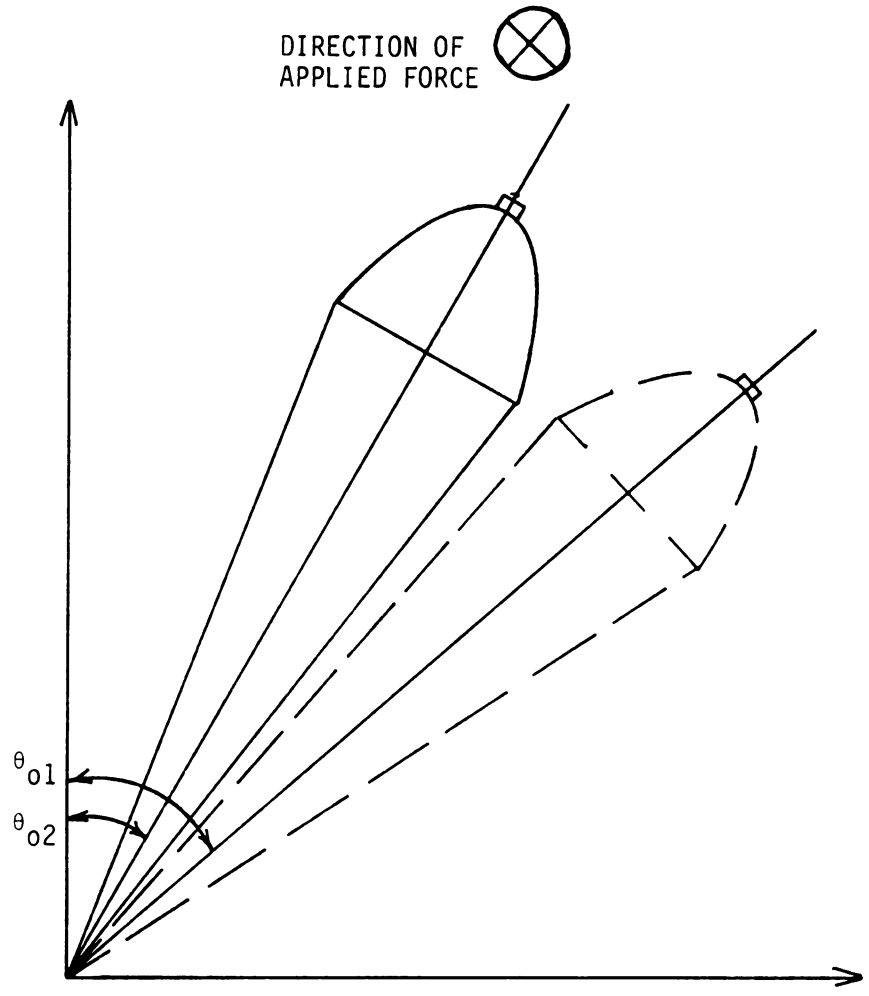


Figure 5. The effect of a positive torque on a spinning top. Note that $\theta_{o1} > \theta_{o2}$.

precessional damping. Note again Figure 4. When a positive torque is produced, it is directed in a downward fashion and tends to increase the precession angle $\theta_o$. This effect is similar to that experienced by the precessing top as shown in Figure 5.

The system described above does not account for losses which would relax the precessional motion. There are three forms for the phenomenological equation of motion in which the losses are included [34]. They are:

(1) The Landau - Lifshiftz form

$$\frac{d\vec{M}}{dt} = \gamma_s(\vec{M} \times \vec{H}) - \frac{\lambda}{M^2}[\vec{M} \times (\vec{M} \times \vec{H})] \qquad (2.1\text{-}14)$$

where $\lambda$ is the damping coefficient with units of frequency

(2) The Bloch - Bloembergen form

$$\frac{dM_T}{dt} = \gamma_s(\vec{M} \times \vec{H})_T - \frac{M_T}{\tau_2} \qquad (2.1\text{-}15)$$

$$\frac{dM_z}{dt} = \gamma_s(\vec{M} \times \vec{H})_z - \frac{M_z - M_o}{\tau_1} \qquad (2.1\text{-}16)$$

where $M_T$ and $M_z$ are the transverse and z-directed components of the magnetization. The constants $\tau_1$ and $\tau_2$ are related to the relaxation of the precessional motion. We cover this below in more detail.

(3) The Gilbert form

$$\frac{d\vec{M}}{dt} = \gamma_s(\vec{M} \times \vec{H}) + \frac{\alpha}{M}\vec{M} \times \frac{d\vec{M}}{dt} \qquad (2.1\text{-}17)$$

where $\alpha$ is the damping coefficient.

The Landau - Lifshiftz form is used most often in ferrimagnetic resonance and is incorporated in this paper. It should be noted that the various forms are equivalent for the case of small rf signals provided $\tau_2 = 1/\omega\alpha$ and $\alpha^2 << 1$ [35]. Therefore, for the purposes of illustration we will examine the Bloch - Bloembergen form in more detail.

If we look at the case of zero dc and rf fields we obtain

$$\frac{dM_z}{dt} = -\frac{(M_z - M_o)}{\tau_1} \tag{2.1-18}$$

$$\frac{dM_T}{dt} = -\frac{M_T}{\tau_2} \tag{2.1-19}$$

where $M_z$ and $M_T$ are as defined previously. The solutions to these equations are

$$M_z = M_o - \Delta M e^{-t/\tau_1} \tag{2.1-20}$$

$$M_T = M_{To} e^{-t/\tau_2} \tag{2.1-21}$$

where $\Delta M = M_o - M_z$ is assumed positive at time t=0. Based on these expressions we expect $\vec{M}_o$ to spiral inward to the z-axis in the absence of external excitation. This is shown in Figure 6. The losses which produce this motion must be overcome to obtain a net gain in the system.

The loss term is most commonly included in the development of the permeability tensor $\overleftrightarrow{\mu}$. This tensor relates magnetic induction $\vec{B}$ to the field intensity $\vec{H}$ in ferrimagnetic materials. In general, $\vec{B}$ and $\vec{H}$ possess both dc and rf components. One form for this tensor is

$$\overleftrightarrow{\mu} = \mu_o \begin{bmatrix} \mu & -jK & 0 \\ jK & \mu & 0 \\ 0 & 0 & 1 \end{bmatrix} \tag{2.1-22}$$

where

$$\mu = 1 + \frac{\omega_o \omega_m}{\omega_o^2 - \omega^2} \tag{2.1-23}$$

and

$$K = -\frac{\omega \omega_m}{\omega_o^2 - \omega^2} \tag{2.1-24}$$

where $\omega_m$ is the saturation magnetization frequency, a constant of the system. This form for the permeability tensor results if the external

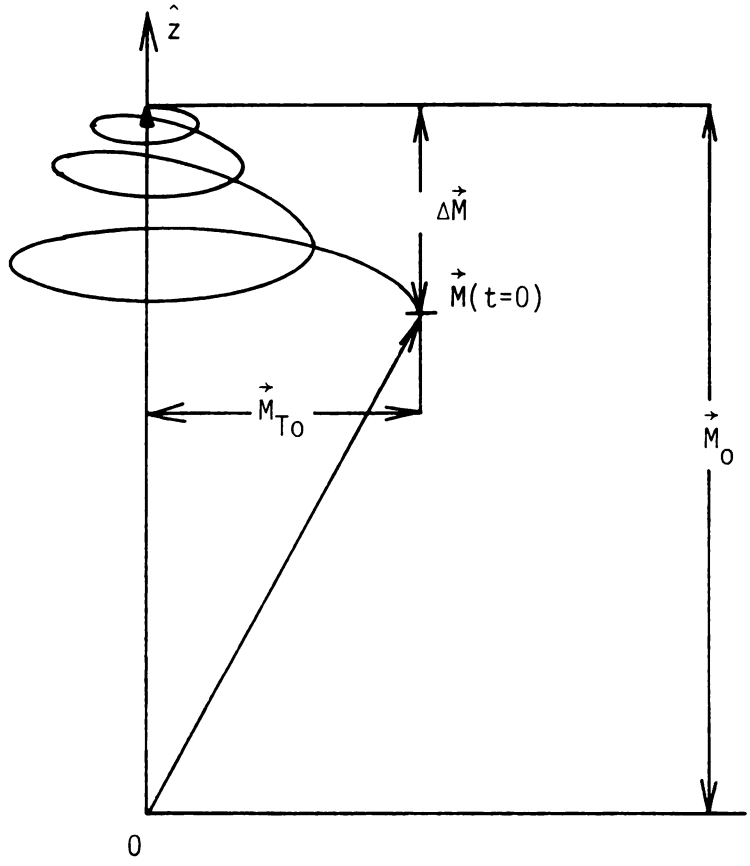


Figure 6. The Variation of the magnetization vector $\vec{M}$ in the absence of external excitation. After R.F. Soohoo.

dc field is in the z direction. Other forms for $\mu$ are given in Appendix A. The losses are included by replacing $\omega_o$ in the above expressions with

$$\omega_o' = \omega_o - j(1/T) \qquad (2.1\text{-}25)$$

which can also be written as

$$\omega_o' = \omega_o - j\frac{1}{2}\gamma_s \Delta H. \qquad (2.1\text{-}26)$$

The parameters T and $\Delta H$ are the precession relaxation time and the ferrimagnetic resonance linewidth respectively. Notice that $\Delta H$ is inversely proportional to the relaxation time. Ferrites with lower values of $\Delta H$ are therefore not as lossy as materials with broader resonance linewidths. Typical values for $\Delta H$ in materials such as Yttrium Iron Garnet (YIG) are on the order of one oersted. This gives a relaxation time of approximately $10^{-7}$ seconds. [36].

## 2.2. Spin and Magnetostatic Waves

Two forms of wave energy in ferrites will be discussed as they relate to propagation. These waves are distinguished by the relationship of their wavelengths to the magnetic dipole spacing. This will determine if exchange field effects between neighboring dipoles will be included. The exchange interaction gives rise to the effect which causes adjacent electron spins to precess in phase with each other. The formulation for incorporating this effect into the analysis is covered in Appendix A.

Magnetostatic waves are slow, dispersive waves which possess k values of less than $10^4$ $cm^{-1}$. This gives rise to large wavelengths with respect to the dipole spacing. Because of this, the exchange field interaction is small compared to the macroscopic magnetization field interaction [37].

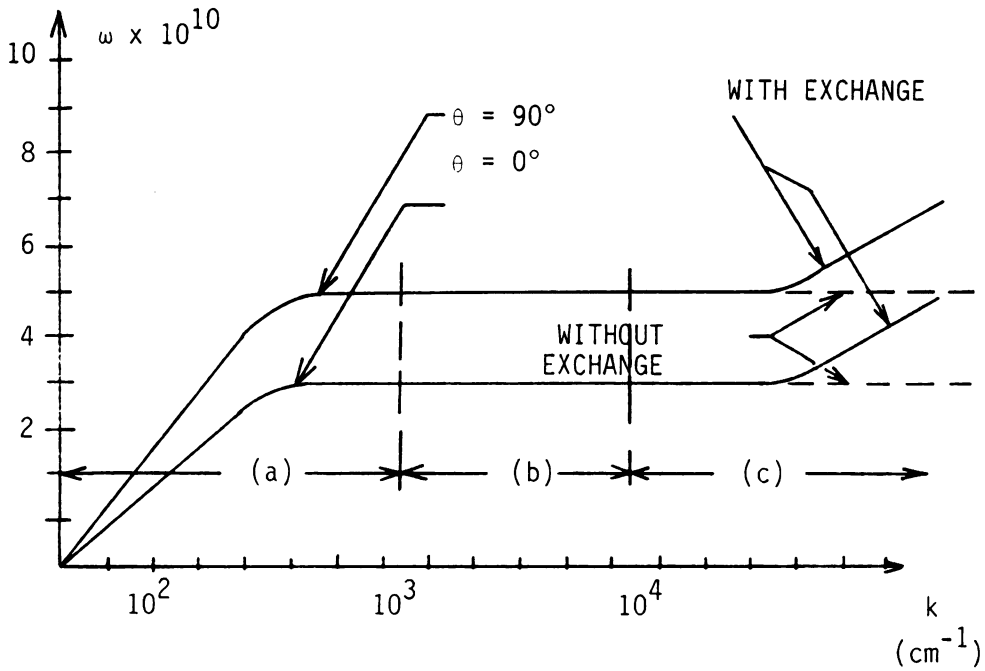


Figure 7. Dispersion curve schematic of three principal wave regions; (a) Electromagnetic, (b) Magnetostatic, and (c) Spin-exchange. The angle θ is for the direction of propagation in relation to the Z axis. After B.A. Auld.

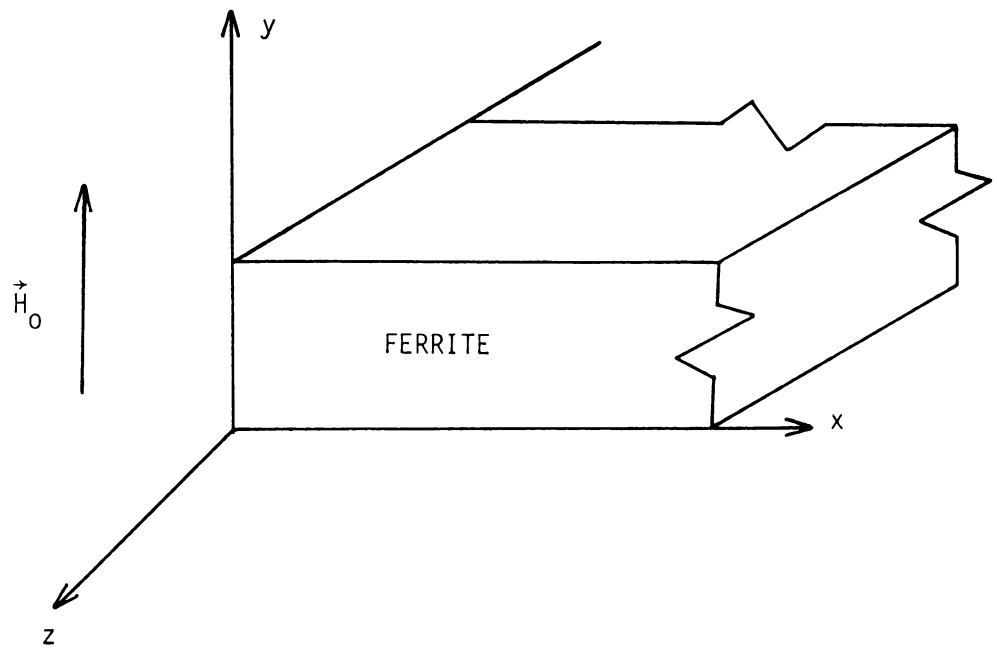


Figure 8. The basic coordinate system for description of wave propagation. The slab is assumed infinite in the xz plane.

The spin wave regime corresponds to wavenumber values larger than $10^4$ $cm^{-1}$. These are very high frequency waves so the exchange interaction is comparable to the macroscopic effects. For this reason, these waves are referred to as spin exchange waves [38]. A third major regime of wave propagation exists, the electromagnetic region. These waves are not examined here because their phase velocities are too great for interaction with drifting carriers [39]. Figure 7 shows a diagram of the dispersion relation which governs the electromagnetic, magnetostatic and spin wave regimes of propagation.

To provide a conceptual picture of wave propagation in ferrites let us consider several cases. Suppose we are given the following coordinate system for our sample as shown in Figure 8. Assume the ferrite is magnetized in the y-direction as shown. A uniform rf field is applied in a system where exchange interaction is assumed strong. This effect causes all dipoles to precess in phase as shown in Figure 9. If h(t) is varied uniformly then all dipoles will experience the same variation in $\theta_0$ but will continue to precess in phase. Now let us suppose the h(t) is nonuniform in the z direction. This causes a variation in $\theta_0$ along the sample as shown in Figure 10. Notice that as time increases, there is no movement of the wave in the direction of propagation and that neighboring dipoles are still in phase.

If exchange forces are ignored, i.e., we expand to the macroscopic level, two things occur; first, we must consider the precession of the magnetization vector instead of individual dipoles. Secondly, the phase of neighboring magnetization vectors is independent. This case is shown in Figure 11 where the rf field is assumed uniform in magnitude along the sample. The phase of adjacent $\vec{M}$ vectors differs depending on the position of the propagating wave. This is acceptable on the macroscopic

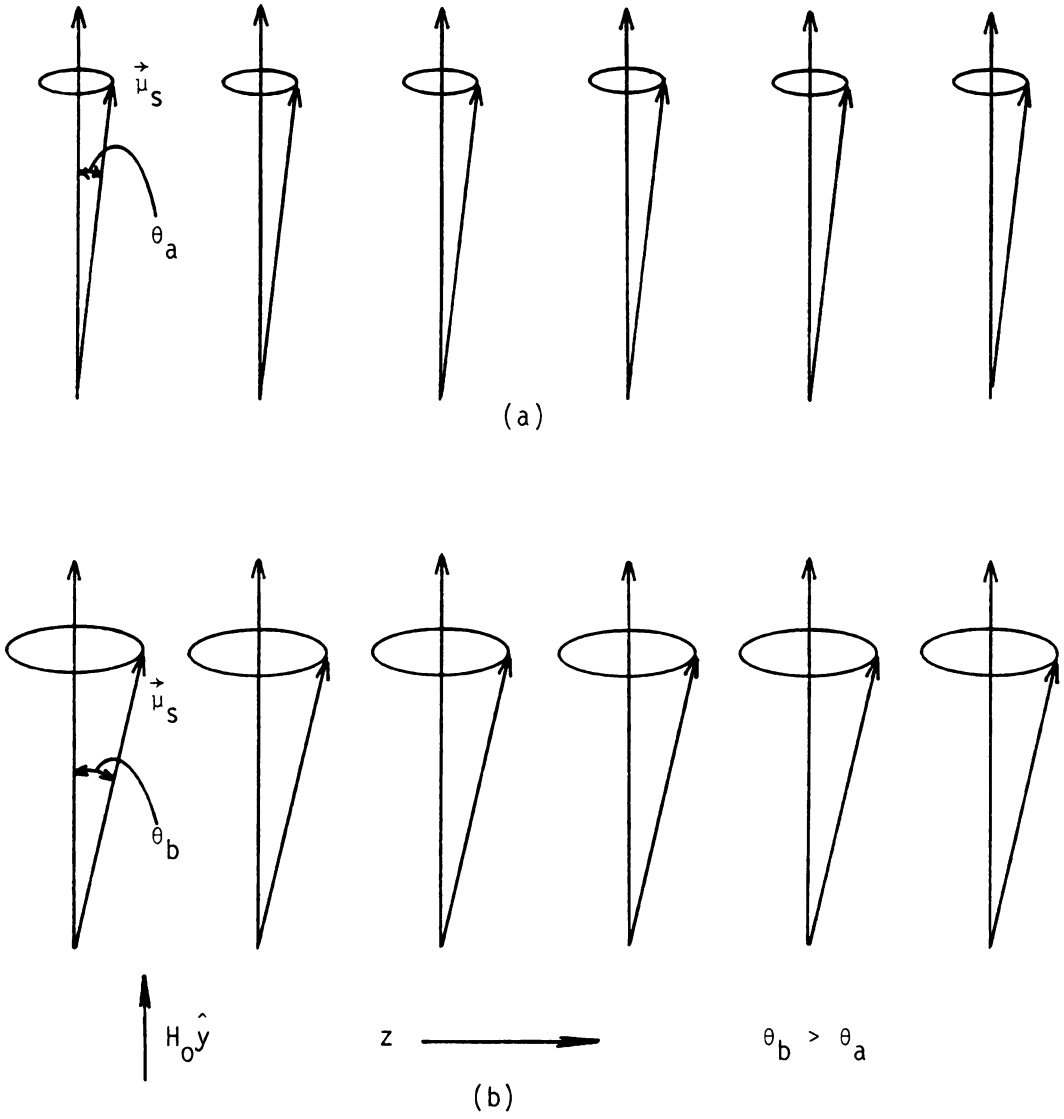


Figure 9. Magnetic dipoles in a ferrite slab under strong exchange interaction; (a) $h = 0$, (b) $h \neq 0$. All dipoles precess in phase.

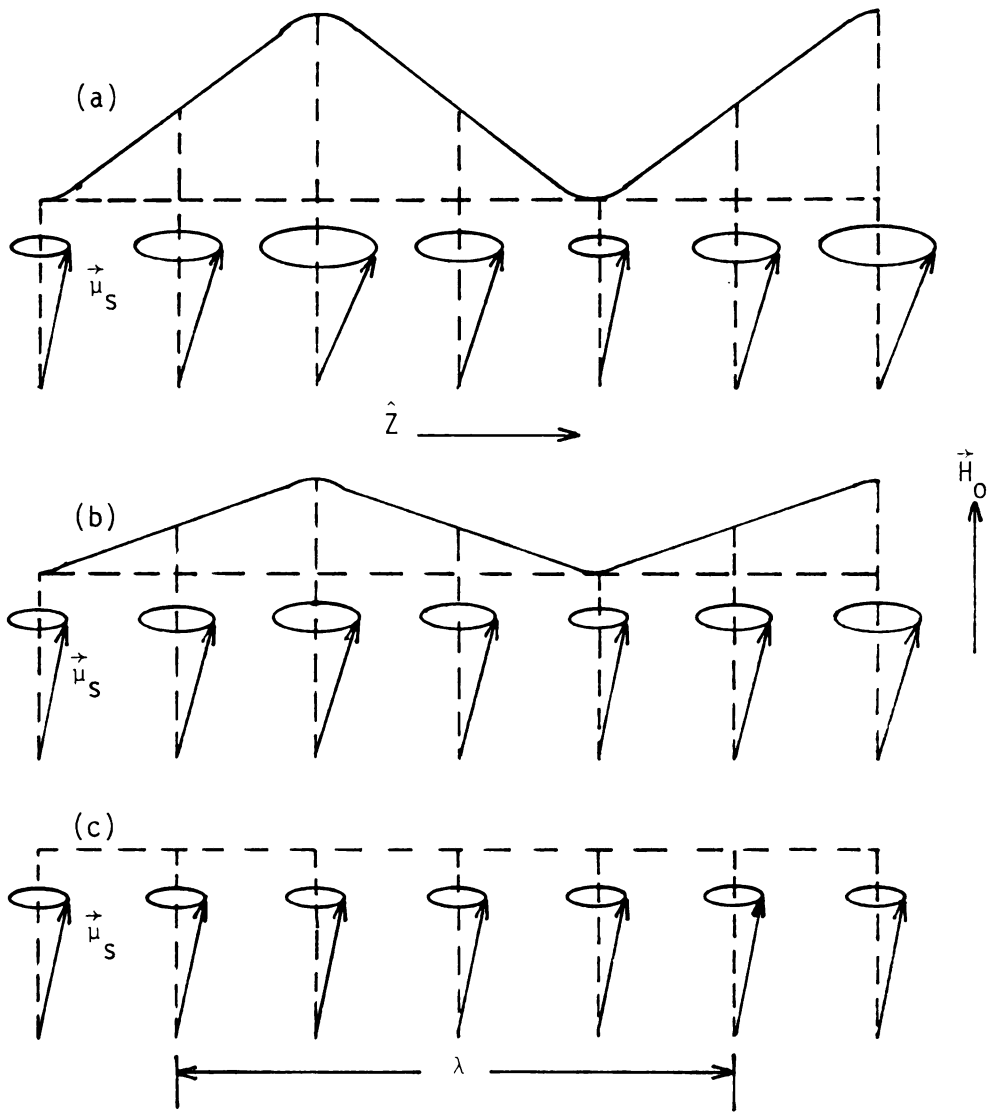


Figure 10. A standing spin-exchange wave of wavelength λ; (a) $t = t_o$, (b) $t = t_1 > t_o$ and (c) $t = t_2 > t_1$.

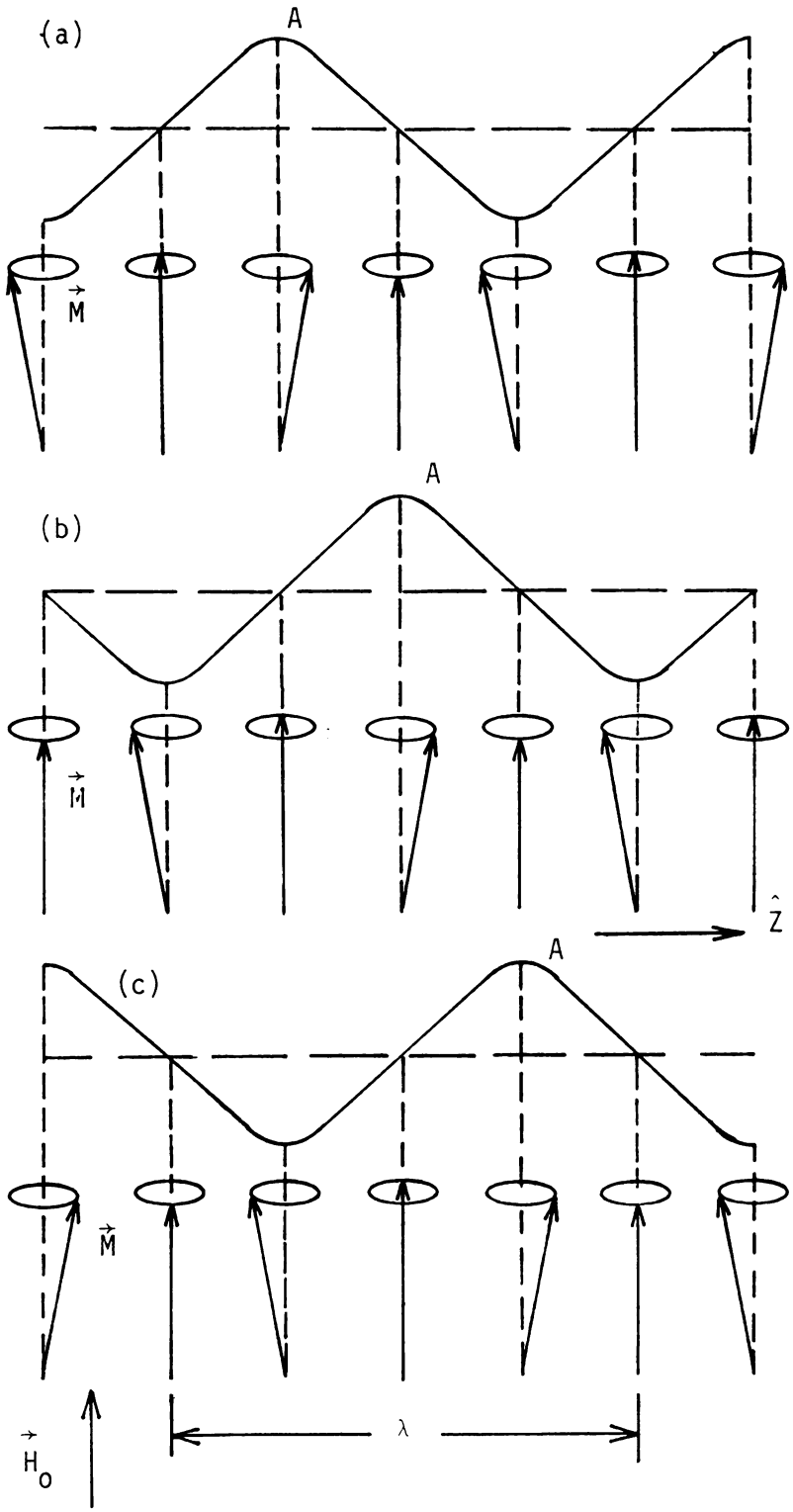


Figure 11. A travelling magnetostatic wave of wavelength $\lambda$; $t = t_o$, (b) $t = t_1 > t_o$ and (c) $t = t_2 > t_1$. Exchange is ignored here.

Figure 12. Generalized travelling magnetostatic wave of wavelength $\lambda$; (a) $t = t_0$, (b) $t = t_1 > t_0$ and (c) $t = t_2 > t_1$.

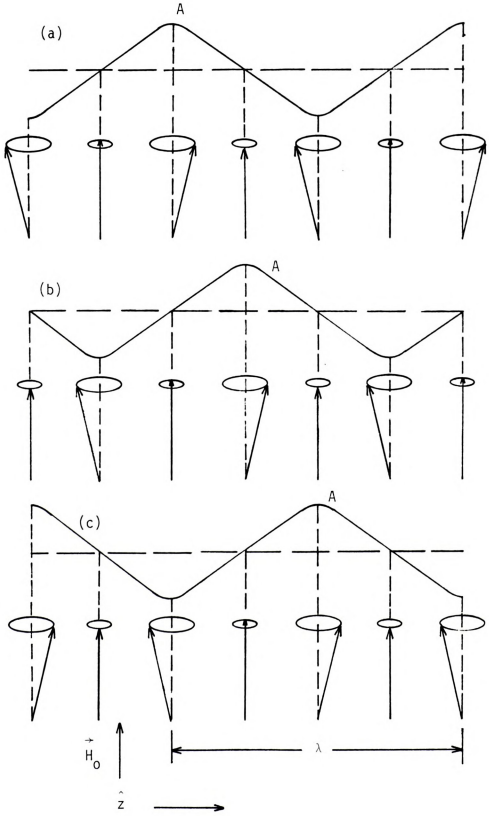


Figure 12

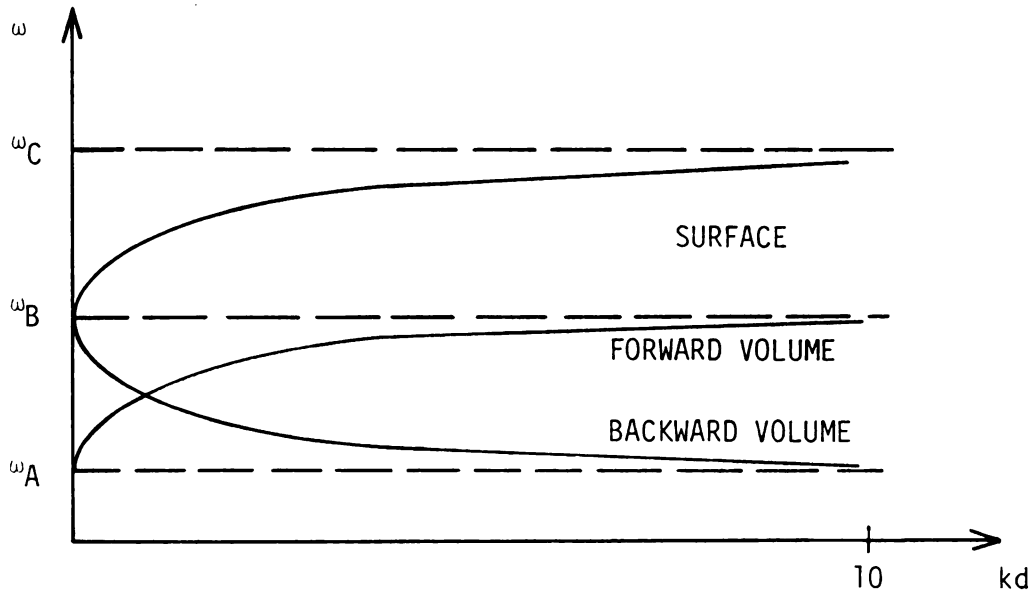


(a)

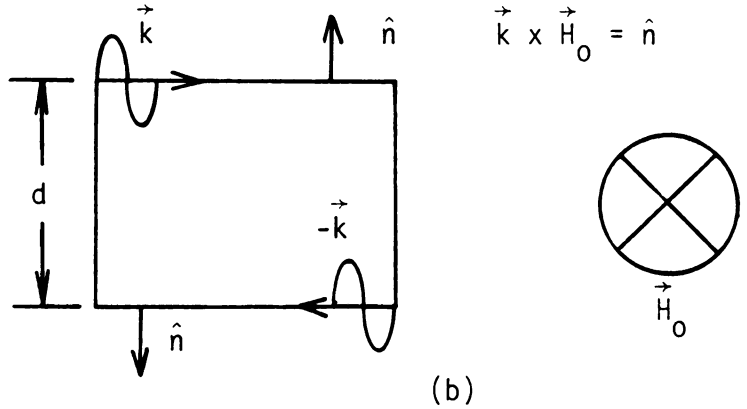


(b)

Figure 13. (a) Dispersion curves for the three forms of magnetostatic wave propagation in ferrites. (b) Orientation of the surface wave for a given $\vec{H}_o$.

level since the wavelength is so much larger than the dipole spacing.

In practice an rf disturbance will give rise to both amplitude and phase variations in the precessing magnetization vectors as the wave propagates. The complete description of this wave motion has not been clearly stated in the literature for the macroscopic case. We will interpret this motion in the following manner for an rf disturbance which is nonuniform. The propagation is determined by variation of both $\theta_0$ and the phase position of the vector $\vec{M}$. These two components of the motion are in phase with each other. This means a particular value of $\theta_0$ corresponds to a given phase position in the precession cycle [40]. A single wavelength will be defined using two corresponding points along the sample with the same value of $\theta_0$ and relative phase positions. This is illustrated in Figure 12.

The waves we are concerned with are surface magnetostatic waves. They are characterized by a concentration of wave energy on one face of the ferrite slab. Recall that the thickness of the sample is important in determining the degree of wave energy concentration on a single surface. The propagation of these waves is highly nonreciprocal. The direction of propagation, applied dc field and the outward pointing normal from the ferrite surface form a right hand coordinate system [41]. This means $\vec{k} \times \vec{H}_0$ will point away from the ferrite surface. The dispersion curves for these waves along with the forward and backward volume modes are given in Figure 13 [42].

## 2.3. The Semiconductor Carrier Wave System

The drifting of carriers in semiconductor material is basic to the amplification mechanism for magnetostatic waves. A geometry containing a slab adjacent to the ferrite is used. This is in contrast to magnetic semiconductors such as $CdCr_2Se_4$. It has been determined that the

resistivity must be reduced in these materials by several orders of magnitude before they can be useful in amplifier applications [43].

The carriers drift at a constant velocity, $u_o$, which is on the order of $2 \times 10^7$ cm/s. In order to keep the level of heating reasonable in these devices, high mobility semiconductors, such as GaAs, are used. Since the ferrite is adjacent to the semiconductor, the surface wave can penetrate as long as the carrier density is not too great. Typical values in the literature range from $10^{15}$ to $10^{20}$ $cm^{-3}$. The fields associated with this wave interact with the drifting carriers through the Lorentz force. This is given by

$$\vec{F} = \vec{u}_o \times \vec{h}_m(t), \qquad (2.1\text{-}27)$$

where $\vec{h}_m(t)$ is the rf component of the magnetostatic wave. The interaction is a Hall effect motion which is transverse to the dc drift motion of the carriers. This is shown in Figure 14.

The Hall field developed from this motion interacts with the magnetostatic wave, also shown in the figure. We will call this field component $\vec{h}_s(t)$. This component must have the correct phase relationship with $\vec{m}(t)$ in order to promote the desired amplification. The amplification results if the system losses can be overcome by the torque created from the interaction of $\vec{h}_s(t)$ and $\vec{m}(t)$. One must be careful to distinguish between $\vec{h}_m(t)$, the rf component of the magnetostatic wave and $\vec{h}_s(t)$ due to the rf Hall motion of the drifting carriers. The introduction of $\vec{h}_m(t)$ causes the variation of $\theta_o$ in phase with the wave propagation. The field $\vec{h}_s(t)$ is introduced to provide for the wave amplification.

Because it is the drifting carriers which drive the amplification in the MSSWA, a distinction between this device and the Traveling Wave Tube amplifier should be made. In the latter case the modulation of

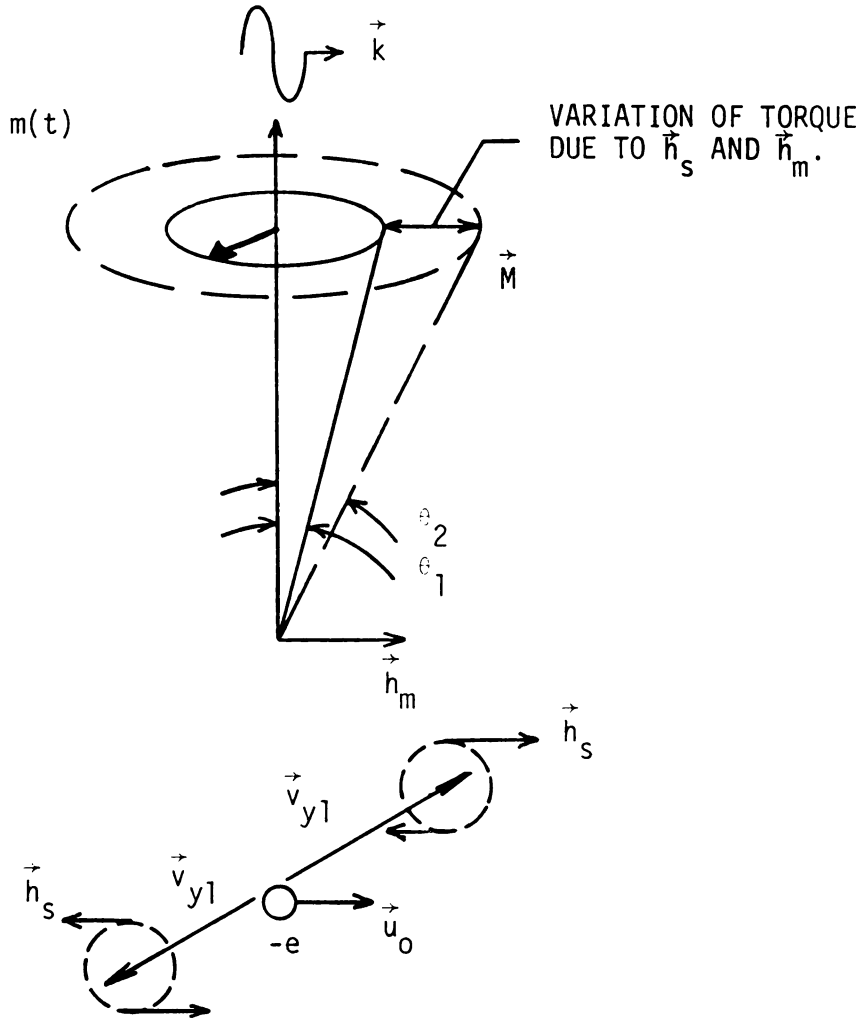


Figure 14. Interaction of a drifting electron in GaAs with the precessing $\vec{M}$ vector in the ferrite. Note that $u_o >> v_{y1}$ (i.e., $\vec{u}_o$ not to scale).

carrier motion is collinear with the overall dc drift motion. This gives rise to the carrier bunching or space charge wave from which signal amplification is obtained [44]. In the MSSWA the modulation is transverse to the dc carrier motion. Also of key importance is the fact that the space charge wave is weakly damped and inertia dominated in the TWT. The MSSWA, in contrast exhibits collision dominated waves whose normal modes are highly damped [45].

In this chapter the basic ferrimagnetic resonance interaction has been described. An illustration of carrier interaction with magnetostatic waves has also been discussed in order to provide an overview of the mechanisms of wave amplification. This gives the reader a foundation for the study of different dispersion relationships which describe the amplifier geometries of interest in this report.

# 3. ANALYSIS OF THE MSSWA

## 3.1. Relevant Properties of Magnetostatic Surface Waves

In this section the properties of magnetostatic surface waves are addressed in more detail. The literature on this topic is extensive and some controversy does exist [46, 47]. Here, we wish to present a detailed study of the effects of certain parameters such as slab thickness and metal plate spacing on the character of the dispersion relations.

The first case we examine is that of an unbounded ferrite slab of thickness d. The surface or (Damon-Esbach) mode has the property that wave energy is concentrated near one face of the ferrite as was stated in Chapter 2. The dispersion relation is affected by the thickness of the slab. It has been shown theoretically that the group velocity of the lowest order surface mode is dependent only on this parameter [48]. This effect tends to increase the velocity as d increases as shown in Figure 1(a). In order to maintain the velocity of the wave at reasonable values for amplification purposes, we conclude that a thinner slab is best. Recall that the drift velocity of carriers in GaAs reaches a practical maximum of $2 \times 10^7$ cm/s. A range of values for k in a ferrite of thickness d = 10$\mu$m is given in Figure 1(b).

The second case involves a metal plate adjacent to one face of the ferrite slab. This is shown in Figure 2. The wave on the top face is the Damon-Esbach wave treated above. This wave is also referred to as a Ferrite-Air (FA) mode. The wave on the lower face is called the Ferrite-Metal (FM) mode or Seshadri wave [49]. Notice that the FM mode has a larger passband. It has also been speculated that this mode is more lossy than the FA mode [50-52]. The resonance for the FM mode

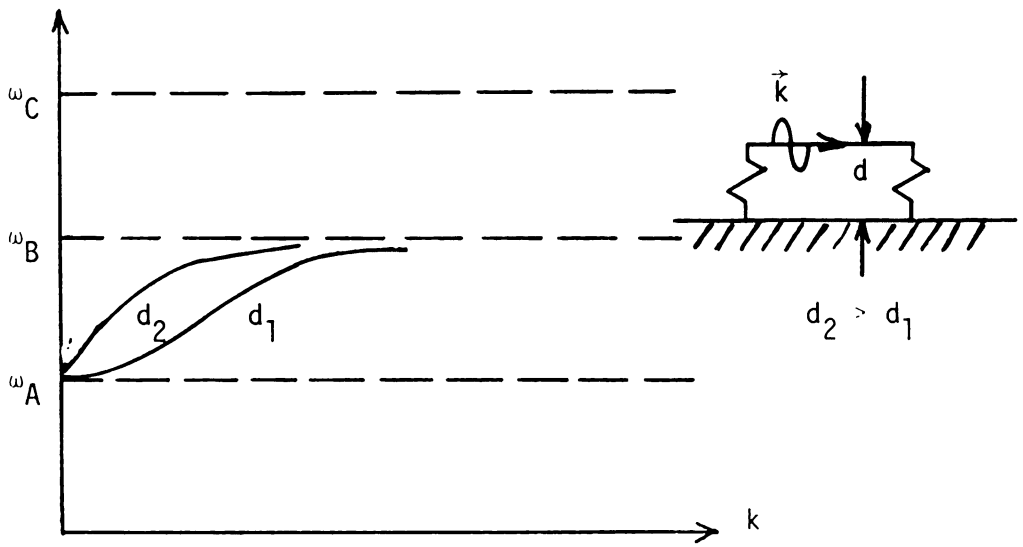


(a)

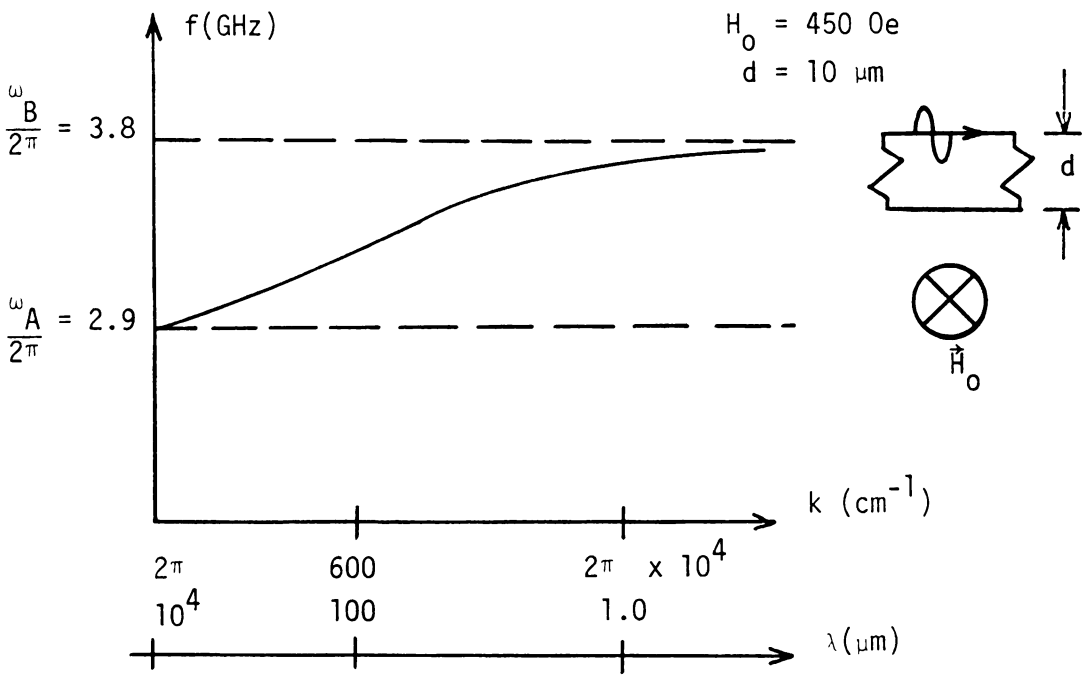


Figure 1. (a) Variation of dispersion curve for an unbound ferrite slab as a function of slab thickness. (b) a typical dispersion case.

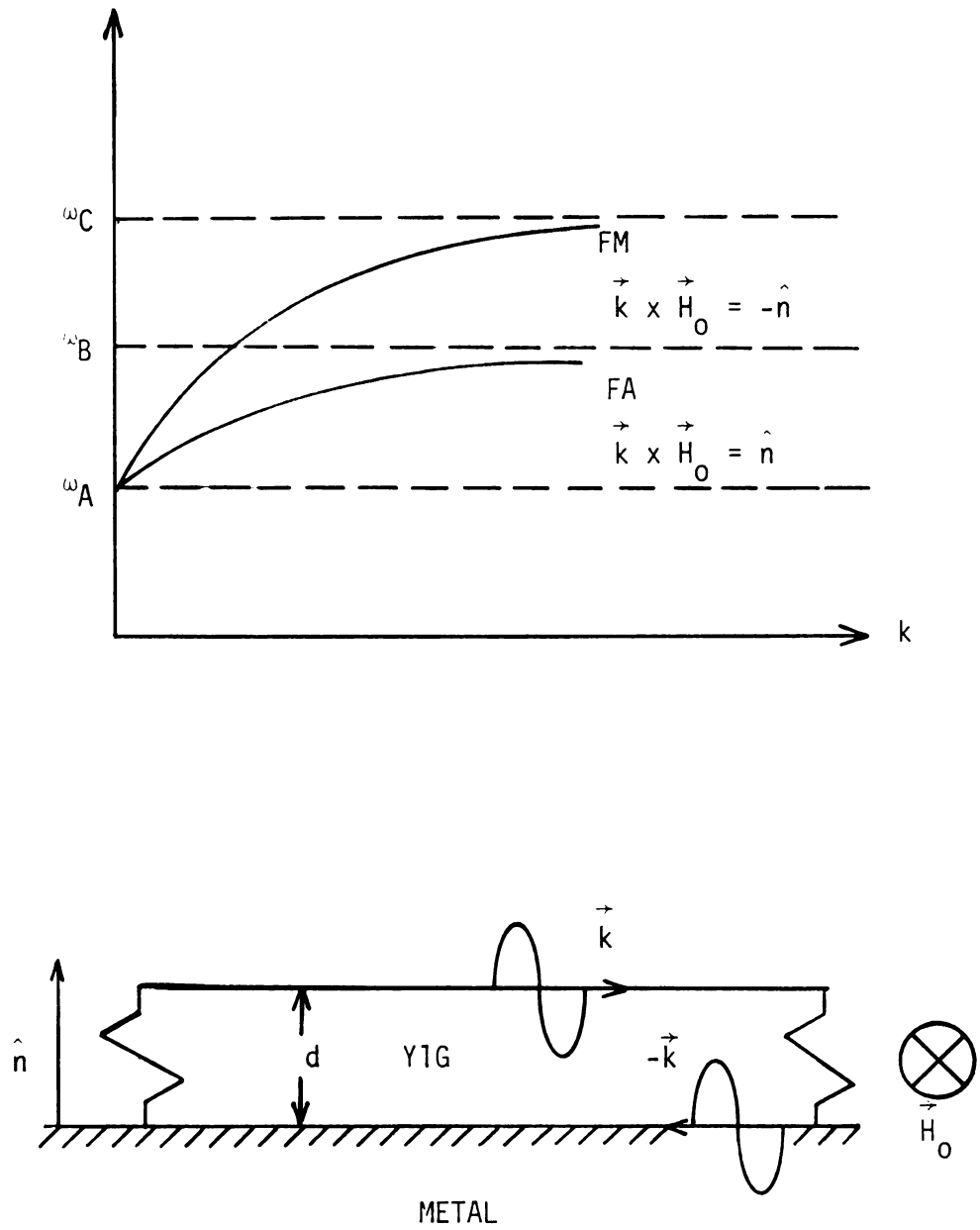


Figure 2. Dispersion curves for the FA and FM modes.

occurs at $\omega_o + \omega_M$ whereas the FA mode resonance is observed at $\omega_o + \frac{\omega_M}{2}$. These resonances are approached more quickly as $d \to \infty$. Therefore, in order to support a propagating mode with a finite passband a slab of finite thickness is required.

Now we consider the ferrite slab separated by a finite distance from the metal ground plane. The surface wave on the face opposite to the ground plane is just the FA mode of before. This wave is only slightly perturbed by the metal. We examine this more later. The wave on the bottom face is a hybrid mode referred to as a Ferrite-Air-Metal (FAM) mode. The spacing of the ground plane can create some interesting changes in the FAM dispersion curve. For spacings small compared to a wavelength the mode is basically the FM type. This wave is transformed into a FA mode as the ferrite to metal gap becomes very large. It is for intermediate values, such as $Ad = 1\mu m$, that the dispersion shows an interesting change. A region in the dispersion occurs where the group velocity goes to zero. The forward waves then become backward waves with negative group velocity as k is increased. This is shown in Figure 3.

If the gap between ferrite and metal is held constant as slab thickness is varied, the effects on both FA and FAM modes can be assessed. In the FA case, the variation in thickness gives rise to the same modifications in the dispersion as when the metal plate is absent. The FAM mode shows a more significant change over the same range of thickness values. The variation in d creates a dispersion curve which has a zero group velocity regime similar to the case treated above for variations in the ferrite-metal gap. Note Figure 4. In the limit as $d \to \infty$ a complete backward wave results as shown in Figure 5 for the frequency range ($\omega_A$, $\omega_B$) [53]. This result is not conclusive however; some authors have

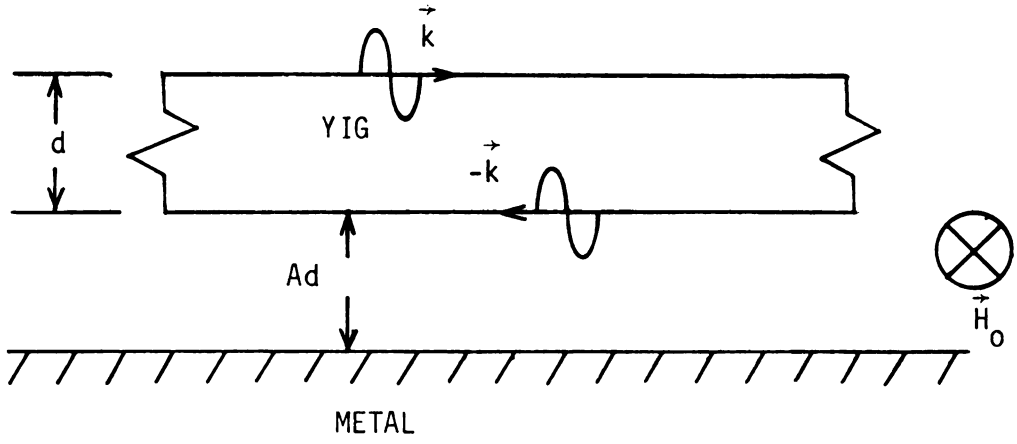


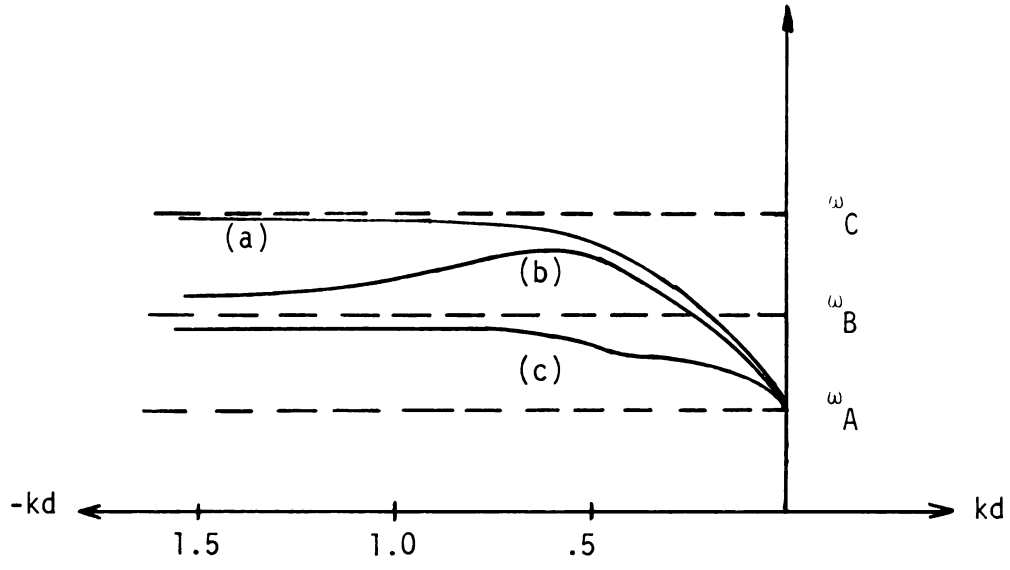


Figure 3. Variation of the ferrite dispersion curve due to metal-air-ferrite spacing; (a) A = 01μ, (b) A = 1.0μ and (c) A = 7.0μ. After Yukawa et al.

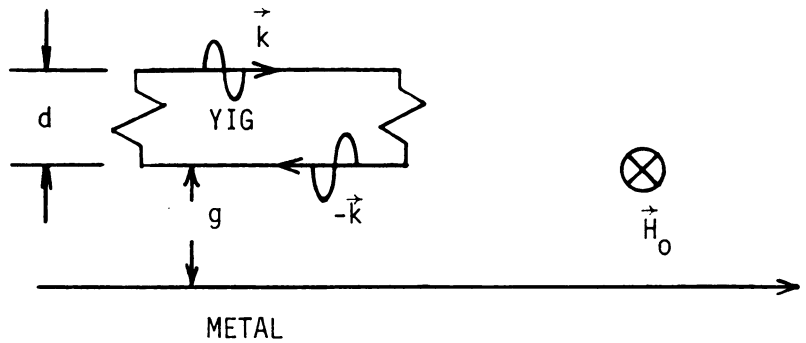


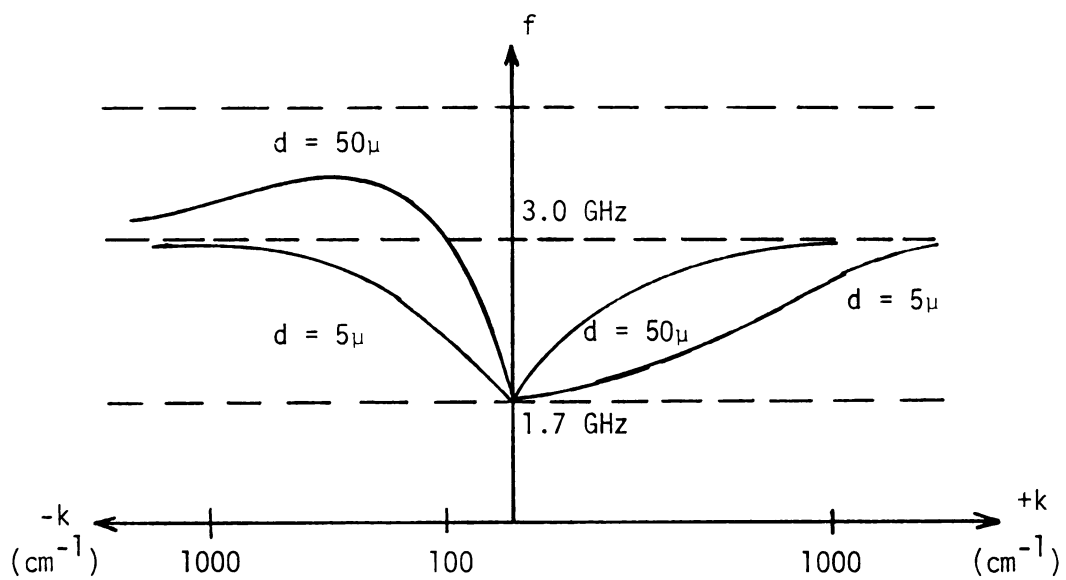


$H_o$ = 200 Oe

g = 25μ

Figure 4. Variation of the dispersion curve due to a change in slab thickness in the presence of a metal plate. After W.L. Bongianni.

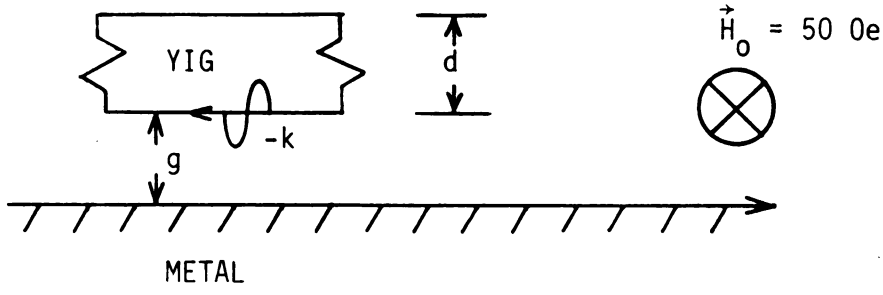


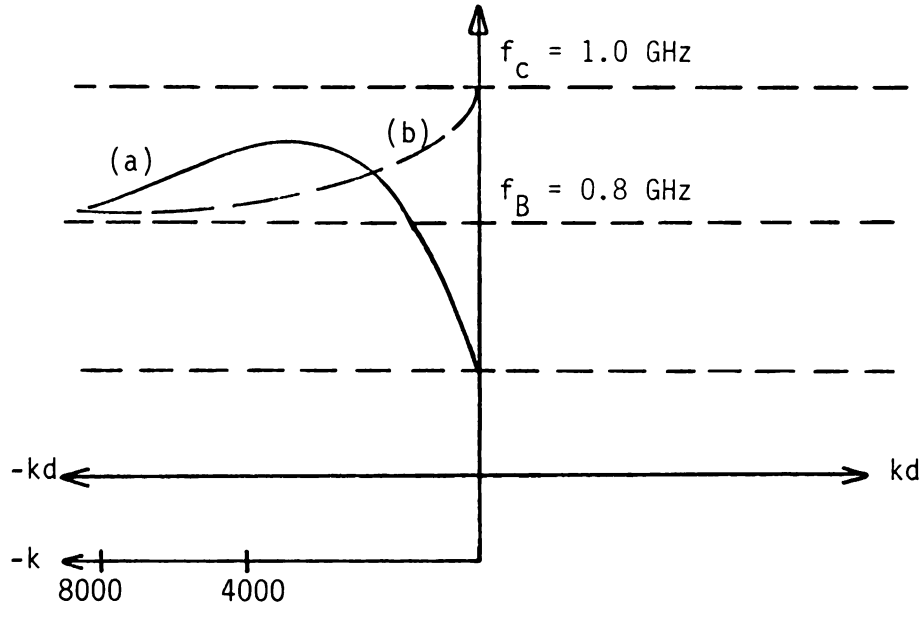


Figure 5. Variation in the dispersion curve for two limiting cases in the presence of metal; (a) d = 2μ g = .5μ and (b) d→∞ g = .5μ. After H. Van deVaart.

predicted that only a nonpropagating mode occurs at $\omega_B$ as d is increased without limit [54]. The dispersion curve for the FAM mode is summarized in Figure 6, where only the mode closest to the metal surface is considered. Unlike the FM mode, this wave is thought to have lower loss than the Ferrite-Air mode. This result was found by experiment [55] but the reliability is questionable.

In Figure 7 we show the effects of two metal plates on the dispersion relations. Notice in case (a) when A=B that the dispersion curve shows a backward wave being transformed into a D-E mode as the spacing is increased. This is significantly different from the dispersion curve behavior of the FAM mode in the case of one metal plate alone. In the case of A≠B shown in Figure 7(b) the maximum cutoff frequency can occur for +k or -k depending on the relationship between A and B. If A>B e.g. the upper cutoff occurs for -k because the metal is closer to the lower face of the ferrite slab [56]. This is especially evident in the case of Figure 8 where B=0 and A is finite.

A word should be said about the nonreciprocal nature of wave propagation in ferrite slabs. In the case of an ungrounded slab this shows up as one face being preferred for propagation from input to output based on the $\vec{k} \times \vec{H}_0$ relationship. Notice however, that the waves which propagate in the +k and -k directions have the same properties i.e. both are FA modes. In this sense the propagation might be thought of as reciprocal. If a metal plate is introduced, then one face will support an FA mode while the other side supports the FM mode. Recall that these modes are fundamentally different, e.g. the passband of the FM mode being larger. For a given transducer configuration and orientation of the static field $\vec{H}_0$, the propagation of the FA and FM modes is determined using the $\vec{k} \times \vec{H}_0$ relationship. If the input ports are switched the

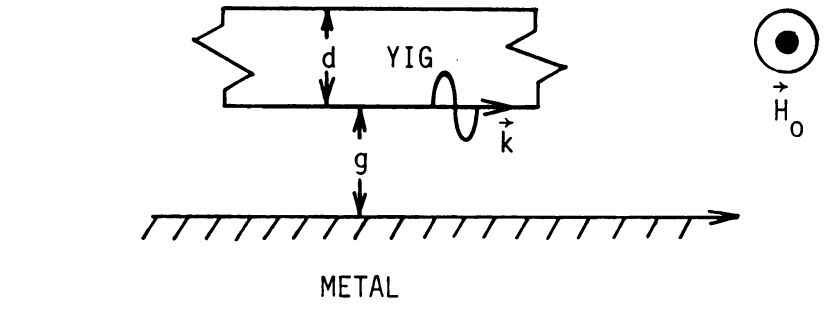


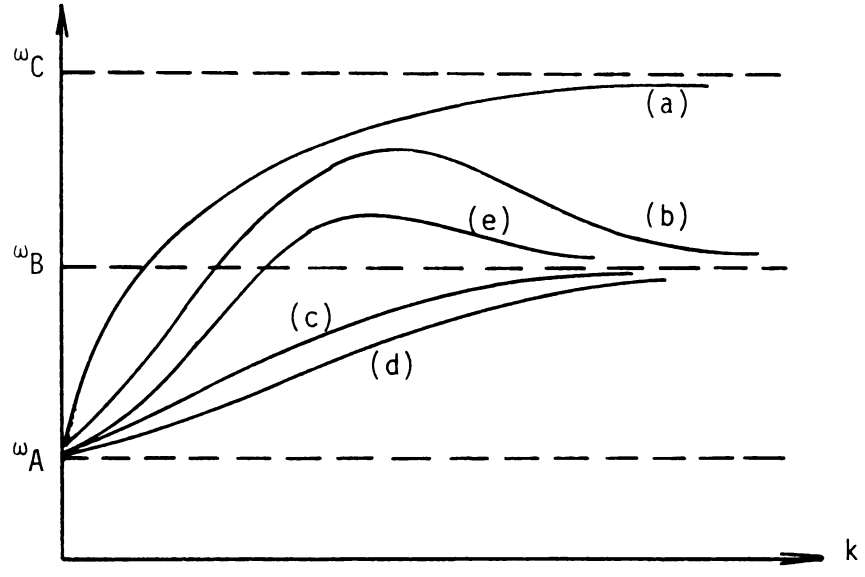


Figure 6. Summary of the dispersion curve variation for one metal plate; (a) g→0 (FM), (b) finite g (FAM), (c) g→∞(FA), (d) small d and (e) large d.

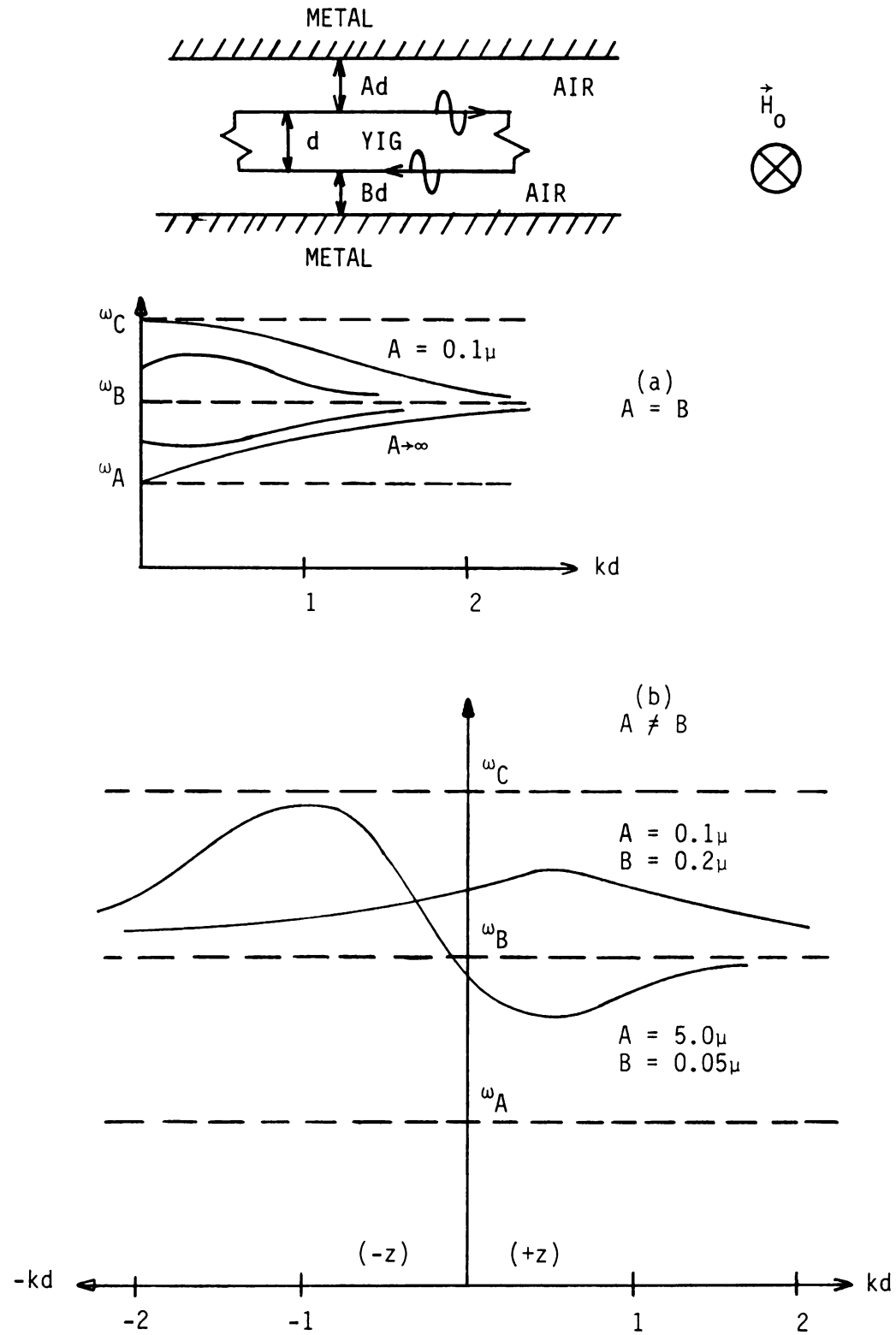


Figure 7. Variation of the dispersion curve in the presence of two metal plates; (a) A=B and (b) A≠B. After Yukawa et al.

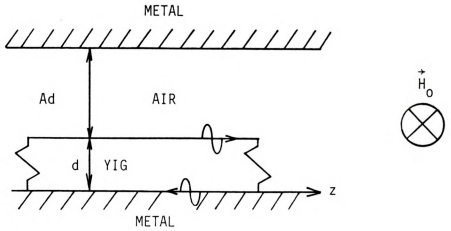


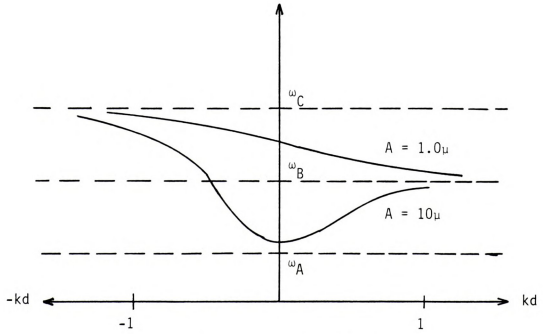


Figure 8. Variation of the dispersion curve for two metal plates where the lower plate is adjacent to the ferrite surface. After Yukawa et al.

signals detected would be different i.e. the propagation is non-reciprocal [57]. This is most important if you are operating below the cutoff for the FA mode and the conditions are such that this mode is required for detection at the output port. Figure 9 summarizes these remarks.

In the case of a FAM mode the nonreciprocity disappears when the ferrite to metal gap is above a certain value. This has been observed experimentally [58].

To summarize this section, we see that the dispersion relations for ferrite wave propagation are very sensitive to the variation of slab thickness, and the proximity of metal plates. The dispersion curves tend to stay within the passbands defined by $\omega_A$, $\omega_B$ and $\omega_C$ as shown in the diagrams. The variation in these curves provides the basis for achieving optimal gain and bandwidth operation when the amplification mechanism is introduced. The extreme degree of variability can also help to explain some of the controversy that exists in the literature.

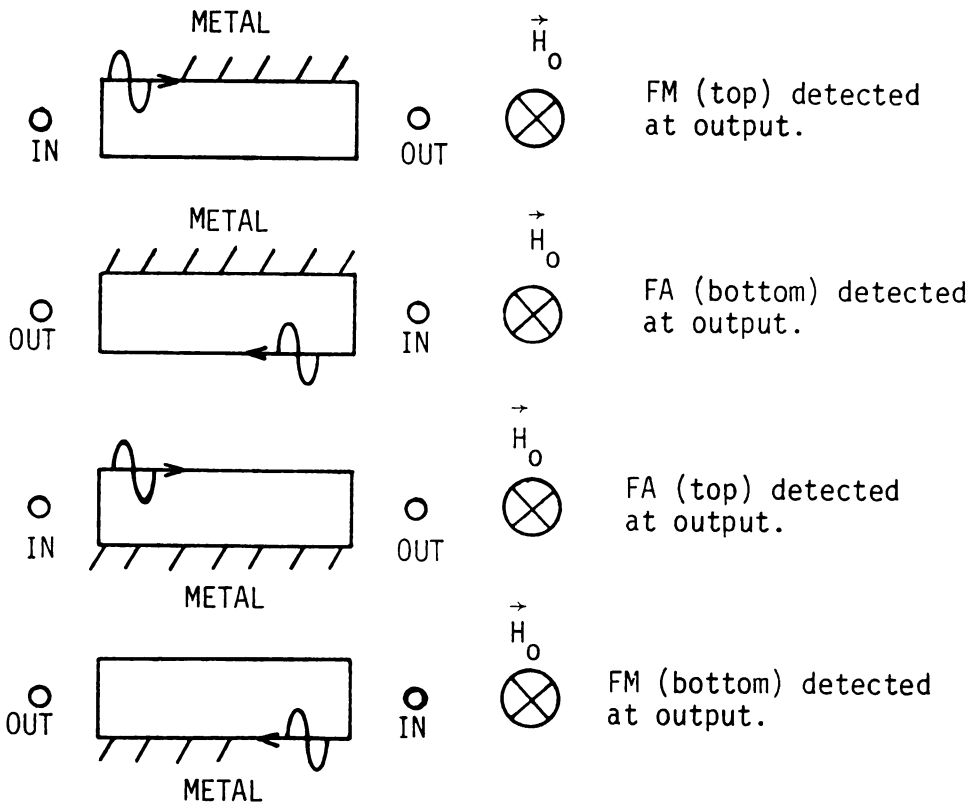


Figure 9. Illustration of the nonreciprocity of wave propagation for FA and FM modes in ferrites.

## 3.2. Description of Amplifier Geometries

In the last section a foundation was developed for the understanding of basic MSSW properties. It is the goal of this section to describe the geometries which will be encountered in our analysis of possible amplification of the magnetostatic waves. This will lead to the actual derivation of the relevant dispersion relations.

The actual MSSWA device might be fabricated as in Figure 10. The dielectric spacer between the YIG and GaAs serves as a tuning mechanism or as a region for exciting the MSSW's and subsequently detecting them. Because the interaction between the drifting carriers and the magnetostatic wave is based on the penetration of the wave in the semiconductor, the dielectric helps determine the strength of this interaction. We will check this later. It should be noted however that the YIG conductivity is sufficienty low so that it can be in direct contact with the GaAs and cause no problems. The top metal plate (called the gate) is used to counterbalance the dc Hall force due to the drift of carriers in the presence of the static $\vec{H}_0$ field. This force would cause a large variation in the semiconductor carrier density in the x-direction. If $\vec{H}_0=H_0\hat{y}$ the drifting electrons would accumulate on the GaAs-mylar interface. The presence of the metal tends to provide for a uniform background carrier density when a balancing E-field is applied. Recall that the metal plates also significantly effect the dispersion relation for the system. This is of course accounted for in the analysis. The overall effect of the gate and heat sink will depend on their separations from the region of interaction i.e. the GaAs-Dielectric-YIG region.

Before analysing the case depicted in Figure 10, we will study simpler models to develop a complete understanding of the interaction. We will begin with the first four cases illustrated in Figure 11. This

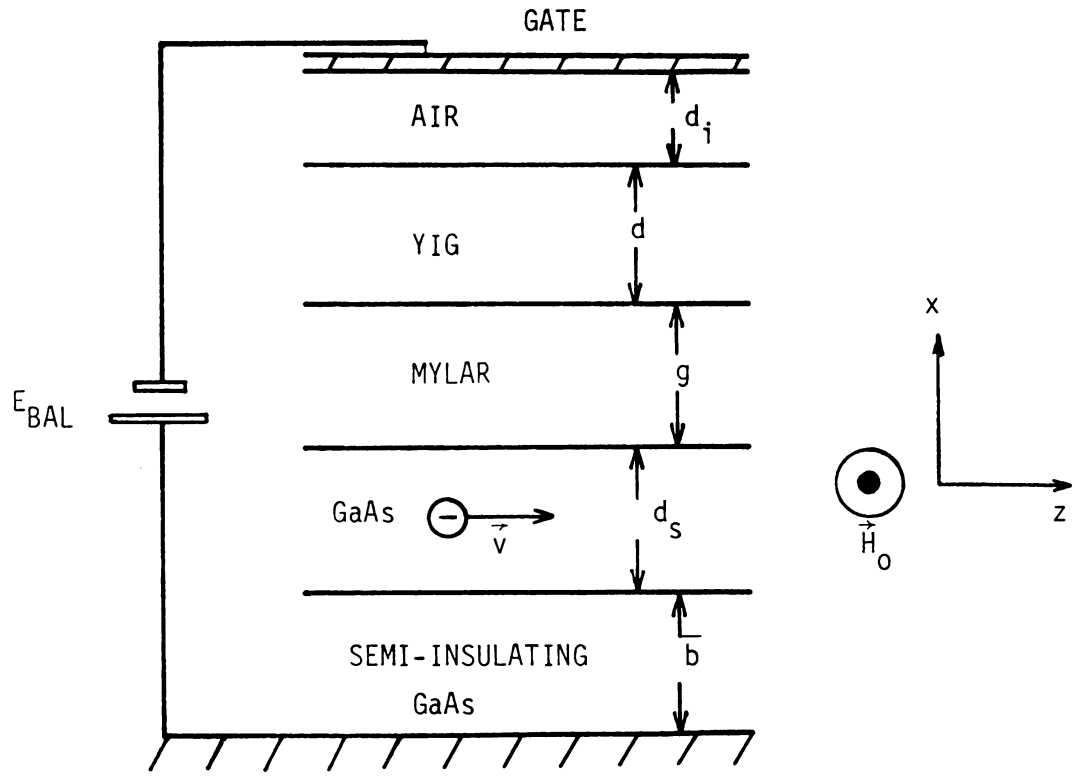


Figure 10. Illustration of the GENERAL case geometry.

first model is shown in Figures 11(a) and (b). Part (a) is referred to as the YIG-Dielectric-Semi (YDS) case. Note that the interaction is assumed to be confined to the interface between the ferrite and semiconductor. The YIG and semiconductor are treated as half spaces here. If the gap thickness is reduced to zero, the YDS case becomes SINGLE-SURFACE as shown.

The next model as shown in Figures 11(c) and (d) refers to a finite YIG slab separated from a semiconductor (GaAs) half-space. This case will be called YIGSLAB-GAP. Again, if the gap is allowed to vanish a limiting case is obtained. This model is referred to as YIGSLAB. If a metal plate is included a finite distance from the YIG we obtain the case in 11(e) called GATE. Finally the general case, which we denote as GENERAL will consider the complete device shown previously in Figure 10.

To gradually build up to the general case, each model will be analyzed in turn. This will be done to develop the appropriate dispersion relations. These relationships will lead to dispersion polynomials which are developed in Appendix B. It is these polynomials that are analyzed numerically to determine the feasibility of amplification for a particular model. Appendix C will develop the relevant approximations that are made in order to obtain these polynomials. The differences in approach of some key investigators in this area are discussed in detail in Appendix E.

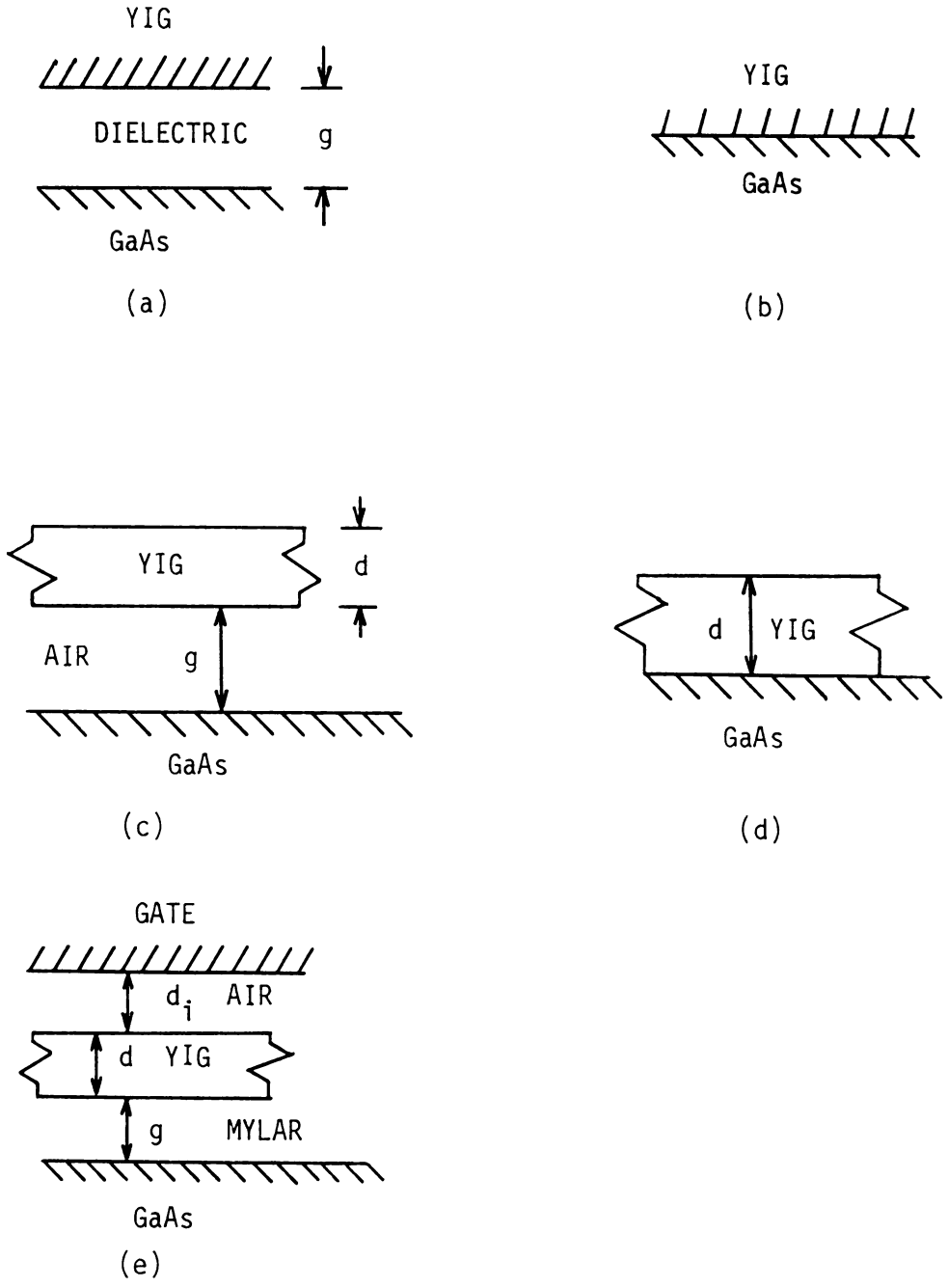


Figure 11. Illustration of all device model geometries. (a) YDS, (b) SINGLE-SURFACE, (c) YIGSLAB-GAP, (d) YIGSLAB, and (e) GATE.

## 3.3. Derivation of Ferrite Transverse Wavenumber

Basic to the operation of the MSSWA is the rate of decay for the magnetostatic wave energy in the plane transverse to the direction of propagation. In the analysis developed here we are concerned with the variation of the field strength in the x-direction. This is assumed to have a general form of $e^{\gamma x}$ where $\gamma$ is the transverse wavenumber. The plane wave propagation variation is also used so that in general the field components have the form

$$E, H \alpha e^{-j(kz-\omega t)}e^{\gamma x} \tag{3.3-1}$$

Note that $Re(\gamma)$ can be positive or negative depending on boundary conditions. The wavenumbers $\gamma$ and k are assumed to be complex in general.

In this section the transverse wavenumber for the TE mode of magnetostatic waves in the YIG is derived. This is denoted as $\gamma_f$. We begin with Maxwell's curl equations

$$\nabla \times \vec{E} = -j\omega\mu_0 \overleftrightarrow{\mu} \cdot \vec{H} \tag{3.3-2}$$

$$\nabla \times \vec{H} = j\omega\epsilon_0\epsilon_{rf}\vec{E}. \tag{3.3-3}$$

The latter equation is used in the form shown because the YIG is assumed to have zero conduction current i.e. $\sigma=0$. By substituting in the tensor form for $\mu$ we obtain for a coordinate system in Figure 12

$$\nabla \times \vec{E} = -j\omega\mu_0 \begin{bmatrix} \mu & 0 & -jSK \\ 0 & 1 & 0 \\ jSK & 0 & \mu \end{bmatrix} \begin{bmatrix} H_x \\ H_y \\ H_z \end{bmatrix} \tag{3.3-4}$$

where $S = \pm 1$ determines the orientation of $H_0$ along +y or -y. The above expression upon expansion becomes with $\frac{\partial}{\partial y} = 0$.

$$jkE_y = -j\omega\mu_0(\mu H_x - jSKH_z) \tag{3.3-5}$$

$$-jkE_x - \gamma E_z = -j\omega\mu_0 H_y \tag{3.3-6}$$

$$\gamma E_y = -j\omega\mu_0(jSKH_x + \mu H_z) \tag{3.3-7}$$

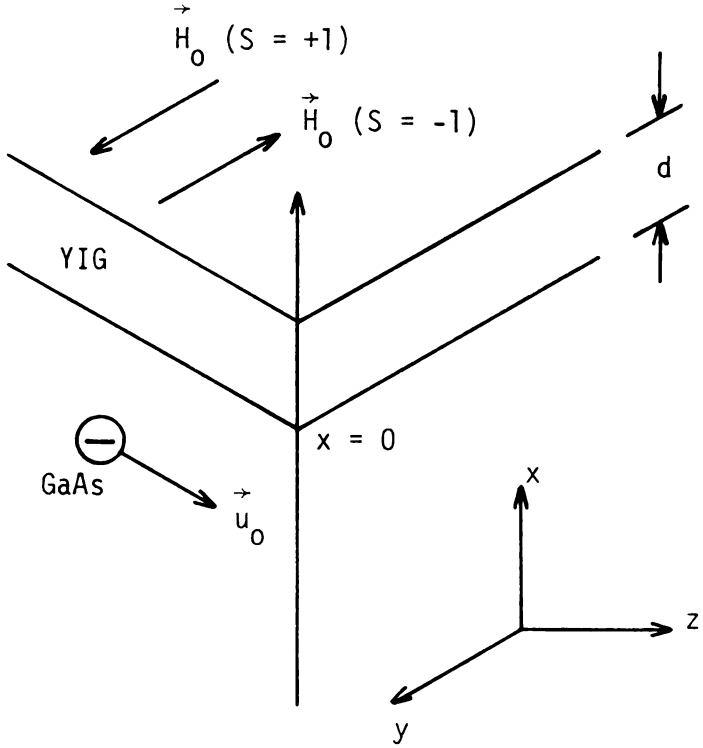


Figure 12. The coordinate system for derivation of transverse wavenumbers $\gamma_f$ and $\gamma_s$. Note that $\partial/\partial y \to 0$.

The expansion of the second curl equation yields with $-\frac{\partial}{\partial y} = 0$.

$$jkH_y = j\omega\varepsilon_f E_x \tag{3.3-8}$$

$$-jkH_x - \gamma H_z = j\omega\varepsilon_f E_y \tag{3.3-9}$$

$$\gamma H_y = j\omega\varepsilon_f E_z \tag{3.3-10}$$

Notice that the TE and TM modes are uncoupled for this case. This is observed because three of the equations relate to $H_z$, $H_x$ and $E_y$ only, while the other equations relate to $E_z$, $E_x$ and $H_y$. Of further importance is the fact that the TM mode is not directly coupled to the spin parameters $\mu$ and K of the ferrite. This indicates that the TM mode of the magnetostatic wave does not interact directly with the spin system. Note also that due to the small signal assumption the component $H_y$ is much smaller than the dc field $\vec{H}_o$ and therefore has negligible effect. For these reasons we neglect the TM field components. Manipulation of the equations involving the TE components yields.

$$j(k^2 - k_o^2\mu)H_x + (k\gamma - k_o^2 SK)H_z = 0 \tag{3.3-11}$$

$$j(-\gamma k - k_o^2 SK)H_x + (-\gamma^2 - k_o^2\mu)H_z = 0 \tag{3.3-12}$$

which in determinantal form is

$$\begin{vmatrix} j(k^2 - k_o^2\mu) & k\gamma - k_o^2 SK \\ -j(\gamma k + k_o^2 SK) & -(\gamma^2 + k_o^2\mu) \end{vmatrix} = 0. \tag{3.3-13}$$

The solution of this determinant yields the transverse wavenumber which is:

$$\gamma^2 \equiv \gamma_f^2 = k^2 + \frac{k_o^2}{\mu}(K^2 - \mu^2) \tag{3.3-14}$$

where $k_o^2 = \omega^2\mu_o\varepsilon_f$. For YIG, $\varepsilon_f \doteq 11$. The expression obtained above for $\gamma_f$ agrees with that obtained by Bini et al. [59].

For reference purposes, if a similar analysis is carried through

using the TM component equations the following results:

$$\gamma_f^2(TM) = k^2 - k_o^2. \qquad (3.3\text{-}15)$$

This shows us explicity that the transverse variation does not involve the spin system (note the absence of K and $\mu$.) Therefore, we see that the YIG appears as a simple dielectric for fields of TM mode configuration.

## 3.4. Derivation of Semiconductor Transverse Wavenumber

In this section, $\gamma_s$, the transverse wavenumber for the TE mode in the semiconductor is derived. The electrons drift with a constant speed $u_o$ in the +z direction. Note again Figure 12. Starting with Maxwell's curl equations again, the manipulation proceeds as follows.

$$\nabla x \nabla x \vec{E} = -j\omega\mu_o \nabla x \vec{H} \tag{3.4-1}$$

which becomes

$$\nabla(\nabla \cdot \vec{E}) - \nabla^2 \vec{E} = -j\omega\mu_o \vec{J} + k_s^2 \vec{E} \tag{3.4-2}$$

where $k_s^2 = \omega^2 \mu_o \varepsilon_s$ in the semiconductor and for GaAs the relative permittivity is $\varepsilon_{rs} = 12$. Continuing we have

$$\nabla(\nabla \cdot \vec{E}) - \nabla^2 \vec{E} - k_s^2 \vec{E} = -j\omega\mu_o \vec{J} \tag{3.4-3}$$

and if we write the electric field components,

$$\vec{E} = E_{x1}\hat{x} + E_{y1}\hat{y} + E_{z1}\hat{z}. \tag{3.4-4}$$

Then we obtain

$$\nabla(\nabla \cdot \vec{E}) = \gamma(\gamma E_{x1} - jkE_{z1})\hat{x} - jk(\gamma E_{x1} - jkE_{z1})\hat{z} \tag{3.4-5}$$

and

$$\nabla^2 \vec{E} = \hat{x}\nabla^2 E_{x1} + \hat{y}\nabla^2 E_{y1} + \hat{z}\nabla^2 E_{z1} = (\gamma^2 - k^2)\vec{E} \tag{3.4-6}$$

so that the left hand side of (3.2-3) becomes

$$\gamma(\gamma E_{x1} - jkE_{z1})\hat{x} - jk(\gamma E_{x1} - jkE_{z1})\hat{z} + (k^2 - \gamma^2)\vec{E} - k_s \vec{E}. \tag{3.4-7}$$

If we note that charge density and velocity possess both dc and rf terms we obtain for the right side of (3.4-3)

$$-j\omega\mu_o \vec{J} = -j\omega\mu_o(\rho_o \vec{v}_1 + \rho_1 u_o \hat{z}) \tag{3.4-8}$$

where the second order rf, and dc terms are ignored. Now using Poissons' equation we note that

$$\rho_1 = \varepsilon_s(\nabla \cdot \vec{E}) = \varepsilon_s(\gamma E_{x1} - jkE_{z1}) \tag{3.4-9}$$

so that (3.4-8) becomes

$$-j\omega\mu_o \vec{J} = -j\omega\mu_o \rho_o \vec{v}_1 - j\omega\mu_o \varepsilon_s u_o(\gamma E_{x1} - jkE_{z1})\hat{z} \tag{3.4-10}$$

Note that we can write the first term in the above expression as

$$-j\omega\mu_o\rho_o\vec{v}_1 = -j\omega\mu_o(-|e|n_o)\vec{v}_1 \qquad (3.4\text{-}11)$$

or

$$-j\omega\mu_o\rho_o\vec{v}_1 = j\left(\frac{k_s^2}{\omega}\right)\frac{|e|n_o}{\varepsilon_s}\vec{v}_1. \qquad (3.4\text{-}12)$$

Therefore equation (3.4-3) becomes

$$\gamma(\gamma E_{x1}-jkE_{z1})\hat{x}-jk(\gamma E_{x1}-jkE_{z1})\hat{z}+(k^2-\gamma^2)\vec{E}$$
$$-k_s^2\vec{E}+j\frac{k_s^2}{\omega}u_o(\gamma E_{x1}-jkE_{z1})\hat{z} = j\left(\frac{k_s^2}{\omega}\right)\frac{|e|n_o}{\varepsilon_s}\vec{v}_1. \qquad (3.4\text{-}13)$$

This expression is written in final form by expressing $\vec{v}_1$ in terms of the electric field of the TE mode. This comes from the phenomelogical equation of motion as follows

$$j\omega\vec{v} + \vec{v}\cdot\nabla\vec{v} = -\eta E-\eta(\vec{v}\times\vec{B}) -\nu\vec{v} - v_T^2\frac{\nabla\rho}{\rho_o} \qquad (3.4\text{-}14)$$

where $\eta = |e|/m^*$ and $\nu$ is the collision frequency. The term $v_T$ is the thermal velocity. Then we have

$$\vec{v}\cdot\nabla\vec{v} = \left[v_{x1}\frac{\partial}{\partial x} + (u_o+v_{z1})\frac{\partial}{\partial z}\right] v_{x1}\hat{x} + v_{y1}\hat{y} + (u_o+v_{z1})\hat{z} \qquad (3.4\text{-}15)$$

$$= -jku_o\vec{v}_1 \qquad (3.4\text{-}16)$$

where $\vec{v}_1 = \vec{v} - u_o\hat{z}$. Thus we have for (3.4-14) by rearranging terms,

$$[\nu + j(\omega-ku_o)]\vec{v}_1 = -\eta E - \eta(\vec{v}\times\vec{B}) + \frac{v_T^2}{|e|n_o}A \qquad (3.4\text{-}17)$$

with

$$A = [\gamma\hat{x}-jk\hat{z}]\varepsilon_s(\gamma E_{x1}-jkE_{z1}). \qquad (3.4\text{-}18)$$

We now work on the $\vec{v}\times\vec{B}$ term in Equation (3.4-17). The velocity and field terms can be written as

$$\vec{v} = u_o\hat{z} + \vec{v}_1 \qquad (3.4\text{-}19)$$

$$\vec{B} = SB_o\hat{y} + \vec{B}_1 \qquad (3.4\text{-}20)$$

for the case we are studying. This gives for the cross-product term in matrix form

$$\vec{v} \times \vec{B} = \begin{bmatrix} \hat{x} & \hat{y} & \hat{z} \\ v_{x1} & v_{y1} & v_{z1} \\ B_{x1} & SB_o+B_{y1} & B_{z1} \end{bmatrix} . \qquad (3.4\text{-}21)$$

Because we are considering only the TE case, only the terms involving $E_{y1}$ in Equation (3.4-13) are retained. This gives us

$$(k^2-\gamma^2-k_s^2)E_{y1}\hat{y} = j\left(\frac{k_s^2}{\omega}\right)\left(\frac{|e|n_o}{\varepsilon_s}\right)v_{y1}\hat{y} \qquad (3.4\text{-}22)$$

and thus only the y component of $\vec{v}_1$ is required from Equation (3.4-14). Which gives

$$[\nu + j\bar{\omega}]v_{y1}\hat{y} = -\eta E_{y1}\hat{y} - \eta(\vec{v} \times \vec{B})\Big|_{\hat{y}} + \frac{v_T^2}{|e|n_o} A\Big|_{\hat{y}} \qquad (3.4\text{-}23)$$

The third term on the right-hand side does not possess a y component and therefore will not contribute. The $(\vec{v} \times \vec{B})$ term becomes

$$(\vec{v} \times \vec{B})\Big|_{\hat{y}} = \hat{y}u_o B_{x1} \qquad (3.4\text{-}24)$$

to give

$$[\nu + j\bar{\omega}]v_{y1} = -\eta E_{y1} - \eta u_o B_{x1} \qquad (3.4\text{-}25)$$

where $\bar{\omega} = \omega - ku_o$. Note that the term in brackets is sometimes referred to as $\bar{\nu}$. Therefore, in the semiconductor for the TE mode case we have

$$(k^2-\gamma^2-k_s^2)E_y = \frac{jk_s^2}{\omega}\left(\frac{|e|n_o}{\varepsilon_s}\right)\frac{-\eta E_y - \eta u_o B_x}{\bar{\nu}} \qquad (3.4\text{-}26)$$

where the subscripts on field components have been dropped. Recall that the $E_y$ and $B_x$ terms represent small signal rf components. These are again related using Maxwell's equation as

$$B_x = -\frac{k}{\omega}E_y \qquad (3.4\text{-}27)$$

so that (3.4-26) becomes

$$\bar{\nu}(k^2 - \gamma^2 - k_s^2)E_y = j\left(\frac{k_s}{\omega}\right)^2 \frac{|e|n_o}{\varepsilon_s}\left[-\eta E_y + \eta u_o \frac{k}{\omega} E_y\right] \tag{3.4-28}$$

where recall that $\eta = \frac{|e|}{m^*}$. This equation is simplified to give the following

$$-\gamma^2 - k_s^2 + k^2 = -j\left(\frac{k_s \omega_p}{\omega}\right)^2 \frac{\bar{\omega}}{\bar{\nu}} \tag{3.4-29}$$

where $\omega_p^2 = n_o|e|^2/\varepsilon_s m^*$ which is the square of the plasma frequency. Solving for $\gamma^2$ yields

$$\gamma_{SEMI}^2 \equiv \gamma_s^2 = k^2 - k_s^2 + j\left(\frac{k_s \omega_p}{\omega}\right)^2 \left[\frac{(\nu - j\bar{\omega})\bar{\omega}}{\nu^2 + \bar{\omega}^2}\right] \tag{3.4-30}$$

This reduces to the final form of

$$\gamma_s^2 \doteq k^2 - k_s^2 + j\left(\frac{k_s}{\omega}\right)^2 \omega_c \bar{\omega} \tag{3.4-31}$$

for typical values of the variables involved. The term $\omega_c = \omega_p^2/\nu$ is the dielectric relaxation frequency.

The final Equation (3.4-31) is the same expression as stated by Bini et. al. [60] and used by Awai et. al. [61]. It is interesting to note that Awai obtained his expression from Vural [62], or the text by Vural and Steele [63]. This is important because the expressions given by Vural are for helicon waves which are TEM and propagate in the direction of the dc magnetic field (i.e. $\vec{k}$ is along $\vec{B}$ which is given by $B_o\hat{z}$.) Therefore it appears that $\gamma_s^2$ is the same for our TE case and the TEM case of Vural and Steele. This punctuates a general problem in this area of research i.e. the use of previously derived expressions without a thorough check of their validity and applicability to the investigator's special case. With the errors as mentioned in Appendix E, sign problems for instance, the situation can become confusing at best. The fact that our $\gamma_s^2$ expression is the same as the TEM helicon case is somewhat coincidental. If the orientation of $H_o$ is changed

this no longer holds true. It should also be noted that the presence or absence of the dc static field has an effect on the TM modes [64].

## 3.5. Derivation of YIG-Dielectric-Semiconductor (YDS) Dispersion Relations

In the previous sections the transverse wavenumbers for both ferrite and semiconductor were derived. We must now proceed to the development of the dispersion relations which are used to model the device geometry and propagation characteristics. This section will deal with the YDS model and the limiting case referred to as SINGLE-SURFACE, This latter case occurs in the limit as the dielectric thickness is reduced to zero. The ferrite and semiconductor regions are represented by semi-infinite half spaces. The geometries are as shown in Figure 13.

In the analysis of TE waves it is possible to begin with either $H_z$ or $E_y$ as the assumed field generating component without a loss of generality. As long as Maxwell's equations are satisfied, the solutions obtained are acceptable. In the first two regions we have

Region (1)

$$E_y = A_1 e^{\gamma_s x} \tag{3.5-1}$$

$$H_z = \frac{j\gamma_s}{\omega\mu_o} A_1 e^{\gamma_s x} \tag{3.5-2}$$

Region (2)

$$E_y = B_1 e^{kx} + B_2 e^{-kx} \tag{3.5-3}$$

$$H_z = \frac{jk}{\omega\mu_o} B_1 e^{kx} - B_2 e^{-kx} \tag{3.5-4}$$

where Equations (3.5-2) and (3.5-4) are obtained from Maxwell's $\nabla \times \vec{E}$ expression. The fields in Region (3) require more detail. In the ferrite recall that

$$\nabla \times \vec{E} = -j\omega\mu_o \bar{\bar{\mu}} \cdot \vec{H} \tag{3.3-5}$$

which yields

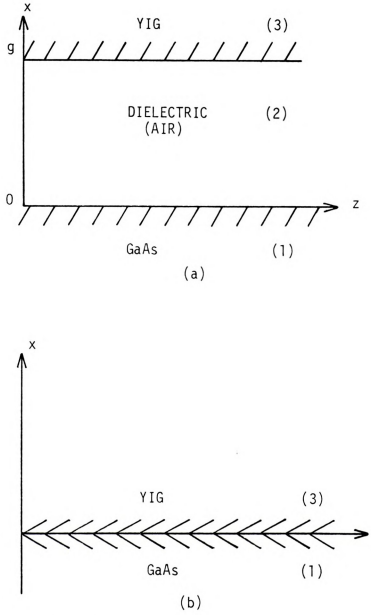


Figure 13. (a) YDS and (b) SINGLE-SURFACE geometries for development of dispersion relations.

$$\frac{-\partial E_y}{\partial z} = -j\omega\mu_o[\mu H_x - jSKH_z] \tag{3.5-6}$$

$$\frac{\partial E_y}{\partial z} = -j\omega\mu_o[jSKH_x + \mu H_z] \tag{3.5-7}$$

Whereas the equation $\nabla \times \vec{H} = j\omega\epsilon_o\epsilon_{rf}\vec{E}$ Yields

$$\frac{\partial H_x}{\partial z} - \frac{\partial H_z}{\partial x} = j\omega\epsilon_o\epsilon_{rf}E_y \tag{3.5-8}$$

If the Expressions (3.5-6) and (3.5-7) are used to relate $E_y$ and $H_z$ we obtain

$$-SKkE_y - \mu\frac{\partial E_y}{\partial x} = -j\omega\mu_o(K^2-\mu^2)H_z \tag{3.5-9}$$

which is derived by multiplying (3.5-6) by jSK and (3.5-7) by $\mu$. The above results when you subtract the two expressions. If we were to use (3.5-6), (3.5-7) and (3.5-8) the result which relates $E_y$ and $H_z$ appears different. We begin by differentiating (3.5-6) with respect to z.

$$\frac{-\partial^2 E_y}{\partial z^2} = -j\omega\mu_o\left[\mu\frac{\partial H_x}{\partial z} - jSK\frac{\partial H_z}{\partial z}\right] \tag{3.5-10}$$

If $\partial H_x/\partial z$ is substituted for in (3.5-10) using (3.5-8) the following is obtained

$$k^2E_y = \omega^2\mu_o\epsilon_o\epsilon_{rf}\mu E_y - j\omega\mu_o\mu\frac{\partial H_z}{\partial x} - \omega\mu_o SK\frac{\partial H_z}{\partial z} \tag{3.5-11}$$

The two expressions (3.5-9) and (3.5-11) seem to relate $E_y$ and $H_z$ in in different ways. It will be shown later that both lead to identical results for the dispersion equations. The interim equations however do not seem to be equivalent. If we begin with (3.5-9) we obtain for the fields

$$E_y = C_1e^{-\gamma_f x} \tag{3.5-12}$$

$$H_z = \frac{SKk - \mu\gamma_f}{j\omega\mu_o(K^2-\mu^2)}C_1e^{-\gamma_f x} \tag{3.5-13}$$

where $E_y$ is again the assumed generating component. In order to derive the dispersion relation the boundary conditions must be satisfied at all interfaces. We equate the tangential components because they must be continuous at the interface in our case. Therefore we match (3.5-1) and (3.5-2) with (3.5-3) and (3.5-4) at x = 0. Equations (3.5-3) and (3.5-4) are matched with (3.5-12) and (3.5-13) at x = d. For brevity we do not match $H_{x1}$, for this condition will be satisfied if the previous boundary conditions (i.e. on $E_y$ and $H_z$) are satisfied. Also we approximate $\gamma_f$ by k which simplifies the algebra but produces negligible error. The following equations result

$$A_1 - B_1 - B_2 = 0 \tag{3.5-14}$$

$$\gamma_s A_1 - kB_1 + kB_2 = 0 \tag{3.5-15}$$

$$B_1 e^{kg} + B_2 e^{-kg} - C_1 e^{-kg} = 0 \tag{3.5-16}$$

$$(K^2-\mu^2)B_1 e^{kg} - (K^2-\mu^2)B_2 e^{-kg} + (SK-\mu)C_1 e^{-kg} = 0 \tag{3.5-17}$$

If we let the term $(K^2 - \mu^2) = D$ and express the system of equations as a matrix, the following results

$$\begin{bmatrix} 1 & -1 & -1 & 0 \\ \gamma_s & -k & k & 0 \\ 0 & e^{kg} & e^{-kg} & -e^{-kg} \\ 0 & De^{kg} & -De^{-kg} & (SK-\mu)e^{-kg} \end{bmatrix} \begin{bmatrix} A_1 \\ B_1 \\ B_2 \\ C_1 \end{bmatrix} = 0 \tag{3.5-18}$$

By setting the determinant equal to zero we obtain the following upon expansion

$$e^{-2kg} = \frac{(\gamma_s+k)\,[SK-\mu+D]}{(\gamma_s-k)\,[SK-\mu-D]} \tag{3.5-19}$$

In the limit as $g \to 0$ we obtain

$$(K^2-\mu^2)\gamma_s + (SKk-k\mu) = 0 \tag{3.5-20}$$

which is the dispersion relation for the single surface limit.

At this point we demonstrate the apparent differences one obtains when choosing equations (3.5-11) versus (3.5-9). Let us consider the single surface case outright. Note again that the general field variation is $e^{-j(kz-\omega t)}e^{\gamma x}$ for the problem under consideration. In Region (1) we assume

$$E_y = Be^{\gamma_s x} \tag{3.5-21}$$

which gives

$$H_z = \frac{j\gamma_s}{\omega\mu_0} E_y \tag{3.5-22}$$

where the real part of $\gamma_s$ is greater than zero for $x < 0$ in order to satisfy boundary conditions.

In Region (2) we have

$$E_y = Ae^{-\gamma_f x} \tag{3.5-23}$$

which gives when equation (3.5-9) is used

$$H_z = \frac{(SKk-\mu\gamma_f)}{j\omega\mu_0(K^2-\mu^2)} Ae^{-\gamma_f x} \tag{3.5-24}$$

and for reference

$$H_x = \frac{(\mu k-SK\gamma_f)}{\omega\mu_0(K^2-\mu^2)} Ae^{-\gamma_f x} \tag{3.5-25}$$

If we match the tangential components at the boundary the following dispersion relation is obtained

$$\gamma_s(K^2-\mu^2) + (SKk-\mu\gamma_f) = 0 \tag{3.5-26}$$

which is just the result previously found in Equation (3.5-20) where $\gamma_f$ was approximated as k.

The dispersion relation can be determined in another manner as well. If we assume that $H_z$ is the generating component. This gives

$$H_z = a_1 e^{\gamma_s x} \tag{3.5-27}$$

and

$$E_y = \frac{-j\omega\mu_o}{\gamma_s} a_1 e^{\gamma_s x} \tag{3.5-28}$$

and in Region (2)

$$H_z = b_2 e^{-\gamma_f x} \tag{3.5-29}$$

which gives us $E_y$ and $H_x$ from Equation (3.5-11) as

$$E_y = \frac{-j\omega\mu_o(\mu\gamma_f + kSK)}{(k_o^2\mu - k^2)} b_2 e^{-\gamma_f x} \tag{3.5-30}$$

and

$$H_x = \frac{j(k_o^2 SK + \gamma_f k)}{(k_o^2\mu - k^2)} b_2 e^{-\gamma_f x} \tag{3.5-31}$$

where again $k_o^2 = \omega^2\mu_o\varepsilon_o\varepsilon_{rf}$. The tangential components are again matched at x = 0 to yield

$$(k_o^2\mu - k^2) - \gamma_s(\mu\gamma_f + SKk) = 0 \tag{3.5-32}$$

At first glance, Equations (3.5-26) and (3.5-32) do not look equivalent. If we equate them, however, an identity results. This is most easily shown by solving both equations for $\gamma_s$ and equating the resulting expressions. This gives

$$\frac{k_o^2\mu - k^2}{\mu\gamma_f + kSK} = \frac{\mu\gamma_f - kSK}{K^2 - \mu^2} \tag{3.5-33}$$

or

$$k_o^2\mu(K^2 - \mu^2) = \mu^2\gamma_f^2 - \mu^2 k^2 \tag{3.5-34}$$

$$k_o^2\mu(K^2 - \mu^2) = \mu^2\left[k^2 + \frac{k_o^2}{\mu}(K^2 - \mu^2)\right] - \mu^2 k^2 \tag{3.5-35}$$

which yields after simplification

$$k_o^2\mu(K^2 - \mu^2) = k_o^2\mu(K^2 - \mu^2) \quad \text{Q.E.D.} \tag{3.5-36}$$

Therefore we see that although the forms of the dispersion relation can appear to be different, they are actually identical results. This is especially important when comparing the various forms of the dispersion found in the literature.

## 3.6. Derivation of YIGSLAB and YIGSLAB-GAP Dispersion Relations

In the last section the development of YDS and the limiting case SINGLE-SURFACE were covered. In this section the dispersion relations for the YIGSLAB-GAP and its limiting case YIGSLAB are derived. The geometries are shown again in Figure 14. Listing the fields in all regions we obtain:

Region (1)

$$E_y = A_1 e^{\gamma_s x} \tag{3.6-1}$$

$$H_z = \frac{j\gamma_s}{\omega\mu_o} A_1 e^{\gamma_s x} \tag{3.6-2}$$

Region (2)

$$E_y = B_1 e^{kx} + B_2 e^{-kx} \tag{3.6-3}$$

$$H_z = \frac{jk}{\omega\mu_o} (B_1 e^{kx} - B_2 e^{-kx}) \tag{3.6-4}$$

Region (3)

$$E_y = C_1 e^{\gamma_f x} + C_2 e^{-\gamma_f x} \tag{3.6-5}$$

$$H_z = \frac{-jk}{\omega\mu_o D} \left[ C_1 e^{kx} (SK + \mu) + C_2 e^{-kx} (Sk - \mu) \right] \tag{3.6-6}$$

where equation (3.5-9) was used to obtain $H_z$, and $\gamma_f \doteq k$.

Region (4)

$$E_y = D_1 e^{-kx} \tag{3.6-7}$$

$$H_z = \frac{-jk}{\omega\mu_o} D_1 e^{-kx} \tag{3.6-8}$$

The field components are evaluated at x=0, x=g and x=g+d. Matching these components at the boundaries and solving as shown in previous sections yields the following dispersion equation

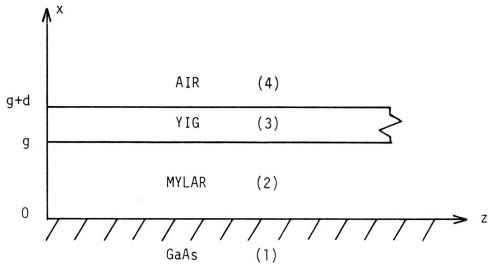


(a)

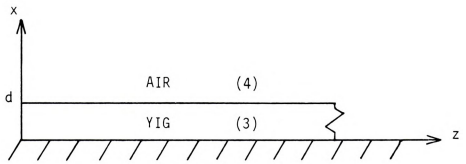


(b)

Figure 14. (a) YIGSLAB-GAP and (b) YIGSLAB geometries for development of dispersion relations.

$$\left[e^{-2kg} - \frac{\gamma_s+k}{\gamma_s-k}\right]\left[(SK+\mu)(SK-\mu-D)e^{-2kd} + (\mu-Sk)(SK+\mu-D)\right]$$

$$-D\left[e^{-2kg} + \frac{\gamma_s+k}{\gamma_s-k}\right]\left[(SK-\mu-D)e^{-2kd}-(SK+\mu-D)\right] = 0 \qquad (3.6\text{-}9)$$

Equation (3.6-9) is the dispersion relation for the YIGSLAB-GAP model. The limiting case for g→0 is best obtained by returning to the system determinant and setting $e^{-2kg} = 1$. A simplified version of this determinant is

$$\begin{vmatrix} e^{-2kg} - \frac{\gamma_s+k}{\gamma_s-k} & -1 & -e^{-2kg} \\ D\left[e^{-2kg} + \frac{\gamma_s+k}{\gamma_s-k}\right] & -(SK+\mu) & (\mu-SK)e^{-2kg} \\ 0 & (SK+\mu-D) & (Sk-\mu-D)e^{-2k(g+d)} \end{vmatrix} = 0 \qquad (3.6\text{-}10)$$

The solution of the determinant is

$$e^{-2kd} = \frac{(SK+\mu-D)\left[D\,\gamma_s-k(\mu-SK)\right]}{(SK-\mu-D)\left[D\,\gamma_s+k(\mu+SK)\right]} \qquad (3.6\text{-}11)$$

Recall that $D = (K^2 - \mu^2)$.

We now show an alternative method for developing eqn. (3.6-11). This involves using the standard decomposition of Maxwell's equations in free space,

$$H_x = \frac{1}{k^2-k_a^2}\left[jk\frac{\partial H_z}{\partial x} - j\omega\varepsilon_o\frac{\partial E_z}{\partial y}\right] \qquad (3.6\text{-}12)$$

$$H_y = \frac{1}{k^2-k_a^2}\left[jk\frac{\partial H_z}{\partial y} + j\omega\varepsilon_o\frac{\partial E_z}{\partial x}\right] \qquad (3.6\text{-}13)$$

$$E_x = \frac{1}{k^2-k_a^2}\left[jk\frac{\partial E_z}{\partial x} + j\omega\mu_o\frac{\partial H_z}{\partial y}\right] \qquad (3.6\text{-}14)$$

$$E_y = \frac{1}{k^2 - k_a^2}\left[ jk \frac{\partial E_z}{\partial y} - j\omega\mu_o \frac{\partial H_z}{\partial x} \right] \tag{3.6-15}$$

where $k_a^2 = \omega^2 \varepsilon_o \mu_o$ for air. For the YIGSLAB case i.e. $g \to 0$, we find the fields in all regions as before. Starting with region (4), the air region we have

$$H_z = b_4 e^{-\gamma_4 x} \tag{3.6-16}$$

and this gives

$$H_x = \frac{jk\gamma_4}{k_o^2 - k^2} b_4 e^{-\gamma_4 x} \tag{3.6-17}$$

where Re $(\gamma_4) > 0$ is assumed. The electric field component is then given by

$$E_y = \frac{j\omega\mu_o\gamma_4}{k^2 - k_a^2} b_4 e^{-\gamma_4 x} \tag{3.6-18}$$

In order to determine $\gamma_4$, Maxwell's curl equations are again used to yield

$$jkE_y = -j\omega\mu_o H_x \tag{3.6-19}$$

$$-\gamma_4 E_y = -j\omega\mu_o H_z \tag{3.6-20}$$

and

$$-jkH_x + \gamma_4 H_z = j\omega\varepsilon_o E_y \tag{3.6-21}$$

Setting the resulting determinant to zero yields

$$\gamma_4^2 = k^2 - k_a^2 \tag{3.6-22}$$

and since we are in the slow wave regime, $k_2 >> k_a^2$, so that

$$\gamma_4^2 \doteq k^2 \tag{3.6-23}$$

and thus for decay of the field intensity as $x \to \infty$ we choose the positive root i.e. $\gamma_4 = k$. This gives for the fields in Region (4)

$$H_z = b_4 e^{-kx} \tag{3.6-24}$$

$$H_x = -jb_4 e^{-kx} \tag{3.6-25}$$

$$E_y = \frac{j\omega\mu_o}{k} b_4 e^{-kx} \tag{3.6-26}$$

In Region (3) if $H_z$ is the assumed generating component again

$$H_z = a_3 e^{\gamma_f x} + b_3 e^{-\gamma_f x} \tag{3.6-27}$$

If the Equation (3.5-11) is used as in the YDS section we find that

$$E_y = \frac{j\omega\mu_o}{k_o^2\mu - k^2} \left[ (\mu\gamma_f - kSK) a_3 e^{\gamma_f x} - (\mu\gamma_f + kSK) b_3 e^{-\gamma_f x} \right] \tag{3.6-28}$$

and also

$$H_x = a_3 e^{\gamma_f x} \left[ \frac{j(k_o^2 SK - \gamma_f k)}{(k_o^2\mu - k^2)} \right] + b_3 e^{-\gamma_f x} \left[ \frac{j(k_o^2 SK + \gamma_f k)}{(k_o^2\mu - k^2)} \right] \tag{3.6-29}$$

In Region (1), the GaAs semiconductor, we have

$$H_z = b_1 e^{\gamma_s x} \tag{3.6-30}$$

$$H_x = \frac{jk}{\gamma_s} b_1 e^{\gamma_s x} \tag{3.6-31}$$

and

$$E_y = \frac{-j\omega\mu_o}{\gamma_s} b_1 e^{\gamma_s x} \tag{3.6-32}$$

Recall that in general the transverse wave numbers $\gamma_f$ and $\gamma_s$ are complex and are given by

$$\gamma_f^2 = k^2 + \frac{k_o^2}{\mu} (K^2 - \mu^2)$$

or

$$\gamma_f^2 = k^2 + k_o^2 \left[ \frac{\omega^2 - (\omega_m + \omega_o)^2}{\omega_o^2 + \omega_o\omega_m - \omega^2} \right] \tag{3.6-33}$$

and

$$\gamma_s^2 = k^2 - k_s^2 + j\left(\frac{k_s}{\omega}\right)^2 \omega_c \bar{\omega} \tag{3.6-34}$$

where $\bar{\omega} = (\omega - ku_o)$. Also recall that k, $k_s$ and $k_o$ are the general, semi-

conductor and ferrite propagation constants for the z directed magnetostatic wave respectively.

If we now match tangential components at all boundaries we obtain the final result of

$$e^{-2\gamma_f d} = \frac{[\gamma_s(\mu\gamma_f + SKk) + k^2]\,[k + (\mu\gamma_f - SKk)]}{[\gamma_s(\mu\gamma_f - SKk) - k^2]\,[-k + (\mu\gamma_f + SKk)]} \qquad (3.6\text{-}35)$$

for the dispersion equation of the YIGSLAB model. Notice that (3.6-35) and (3.6-11) appear to be different relations. A detailed analysis shows however, that the two expressions are indeed equivalent.

## 3.7. The GENERAL Case Dispersion Relation

The dispersion relations for four simpler models were developed in order to provide a foundation for this final case. In this section the GENERAL dispersion relation is presented. The algebraic manipulations required for this relation are very similar to those used in the previous sections. The fields in all regions are determined and boundary conditions at each interface are applied. For reference the geometry for this case is shown in Figure 10. Upon expansion of the matrix for this case the following relation results:

$$2e^{2k(d_i+d)}\, e^{3d_s k}\,[(\lambda_3+2) - \lambda_3 e^{-2k\bar{b}}][e^{-2kg}(\lambda_1-1) + (\lambda_1+1)]$$

$$[(\lambda_2-1) - e^{2kd_i}(\lambda_2+1)] - 2e^{2kd_i} e^{3kd_s}\,[(\lambda_3+2) - \lambda_3 e^{-2k\bar{b}}]$$

$$[e^{-2kg}(\lambda_2+1)+(\lambda_2-1)]\,[(\lambda_1+1) - e^{2kd_i}(\lambda_1-1)] + e^{2k(d_i+d)}\, e^{kd_s}$$

$$(1-e^{2kd_s})\,[e^{-2kg}(\lambda_1-1)+(\lambda_2+1)]\,[(\lambda_3+2)(\lambda_2-1) + e^{2kd_i}\lambda_3(1+\lambda_2)]$$

$$\left\{[(\lambda_3+2)-\lambda_3 e^{-2k\bar{b}}] - 2e^{kd_s} - 2(e^{kd_s} e^{-2k\bar{b}})\right\} - e^{2kd_i} e^{kd_s}$$

$$(1-e^{2kd_s})\,[e^{-2kg}(\lambda_2+1) + (\lambda_2-1)]\,[(\lambda_1+1)\,(\lambda_3+2) + e^{2kd_i}\lambda_3(\lambda_1-1)]$$

$$\left\{[(\lambda_3+2) - \lambda_3 e^{2k\bar{b}}] - 2e^{kd_s} - 2(e^{kd_s} e^{-2k\bar{b}})\right\} = 0 \qquad (3.7\text{-}1)$$

where the following definitions apply

$$\lambda_1 = \mu - SK \qquad (3.7\text{-}2)$$

$$\lambda_2 = \mu + SK \qquad (3.7\text{-}3)$$

$$\lambda_3 = \frac{j}{k^2}\,[SA + SBk] \qquad (3.7\text{-}4)$$

and from the geometry the thicknesses are as shown.

The GATE model is analyzed as a special case of the GENERAL model. The principle difference is that the GaAs region for the GATE model is semi-infinite and therefore no heat sink is included. The importance of this case is in investigating the effect of the single metal plate on the YIG-GaAs dispersion but with a model somewhat simpler than GENERAL. The heat sink of the GENERAL geometry is incorporated because any practical design of this device must account for the heating created in the GaAs region due to drifting carriers. The following conditions are used in the GENERAL model to simulate the GATE geometry:

(1) The semiconductor region is allowed to be as thick as possible for the thin slab approximation (i.e. $kd_s \leq 1.75.$); see Appendix C.

(2) The insulator between the GaAs and the heat sink is as large as possible.

These two conditions provide for a semiconductor region that appears semi-infinite in the transverse plane.

This chapter has been devoted to the analyses of device geometries and the development of the corresponding dispersion relations. The application of certain approximations (see Appendix C) will allow the development of dispersion polynomials for numerical analysis. The evaluation of numerical results is covered in the next chapter.

# 4. EVALUATION OF NUMERICAL DISPERSION RESULTS

In this chapter the numerical results of the various dispersion relations outlined in Chapter 3 are evaluated. This is done by developing approximate dispersion polynomials as set forth in Appendix B and using the computer for a numerical solution. We feel that this method will generate a more accurate set of results than perturbational methods.

## 4.1. Evaluation Procedure for Numerical Results

The procedure for the evaluation of the numerical solutions is as follows: (1) determine all roots for a given set of parameters, (2) optimize possible growing roots by examining the behavior of the roots under varying conditions, and (3) determine the behavior of optimized growing roots under the Bers-Briggs criteria.

The numerical analysis of dispersion polynomials is handled by a subroutine in the MSU computer library called ZPOLY. This subroutine will numerically solve complex polynomials up to 49th degree. The roots should follow the criteria below: (1) $k_r$ and $k_i$ must be positive, (2) $k_r$ must be between $10^3$ and $10^4 cm^{-1}$, (3) $k_i$ must be between 1% and 10% of $k_r$.

The second part of the procedure involves the evaluation of the results based on changes in relevant parameters. Notice that we have not as yet determined if the root(s) are physically realizable as growing root(s). At this stage we wish to obtain geometries which will optimize the root(s) in question. The following is a list of the parameters which we seek to optimize:

(1) d is the thickness of the YIG material in all cases studied.

(2) g is the thickness of the dielectric region separating the YIG and GaAs regions. It is instrumental in determining the strength of

interaction between the carriers and the magnetostatic wave.

(3) $n_o$ is the carrier density in the GaAs region.

(4) $\vec{u}_o$ is the carrier drift velocity. This is important based on synchronism arguments.

(5) $\vec{H}_o$ is the static magnetic field intensity applied to the device.

(6) $\Delta H$ is the ferromagnetic resonance linewidth of the YIG material.

(7) $d_i$ is the spacing from the top metal plate to the YIG material in the GENERAL case.

(8) $\bar{b}$ is the spacing from the bottom metal plate to the GaAs material in the GENERAL case.

The optimization of these parameters is done not only with the idea of maximizing gain and bandwith, but also to account for practical concerns such as semiconductor heating and the manufacturing of the actual device geometry.

The last part of the evaluation involves the determination of the physical applicability of possible growing roots. This is done using the Bers-Briggs criteria for convective instabilities. A convective instability is defined as one in which the energy flow of the magnetostatic wave and the carrier drift motion are in the same direction. This instability is spatial in nature. The transfer of energy between the two modes occurs when the carriers move faster than the wave. Under near-synchronous conditions the carriers lose energy to the wave and we have an instability. If the energy flows are in opposite directions, then a nonconvective or temporal instability occurs. This effect is demonstrated in the Backward Wave Oscillator [65].

In order to determine if a convective instability does in fact exist we use the Bers-Briggs criteria. This approach is based on the principal of causality and the initial value problem. It essentially studies the

asymtotic response of the system to a signal bounded both in space and time [66]. The practical usefulness of this criteria is in testing for the presence or absence of convective instabilities. A routine was developed to implement the Bers-Briggs criteria on the computer using the following steps [67]:

(1) Using existing programs which contain the complex dispersion polynomials we set a fixed frequency.

(2) A loop is used to step $\omega_i$ (the imaginary part of $\omega$) from -10 to $-10^{12}$.

(3) The roots of complex k are examined to determine if $k_i$ (the imaginary part of k) has a change of sign. This means we have a convective instability which convects energy in the +z direction. Recall that we are considering roots that correspond to growth in the +z direction. Therefore, any roots chosen for the Bers-Briggs test must have $k_i$ greater than zero prior to application of the criteria.

## 4.2. Evaluation of YDS and SINGLE-SURFACE

The dispersion polynomial for SINGLE SURFACE was analyzed using data sets from various researchers. This was done based on the fact that Bini et al. state that the single surface model can be used to simulate the interaction which occurs even in more complex geometries. The carrier density was varied over a range from $10^{15}cm^{-3}$ to $10^{20}cm^{-3}$. Drift velocities range from $7 \times 10^6$cm/s to $8 \times 10^7$cm/s. Semiconductor materials were InSb, GaAs and Ge. The principal researchers checked were Bini, Yamada, Chang and Matsuo, Awai, Vashkovskii and finally, Lukomskii. In all cases, there was no root observed which satisfies the stated criteria for roots to be selected. In the case of SINGLE SURFACE, the main problem was that $k_i$ was too large i.e., greater than $0.1k_r$. This would give rise to corresponding gain values that are not realizable

physically [68]. In the cases where $k_i$ was in range, $k_r$ was not, so that the root does not represent a slow magnetostatic wave.

In order to handle the above concerns, the YIG and Semiconductor regions are separated by a finite distance g. In this case again no slow wave with realizable positive gain was observed. This agrees with statements made by Awai et al., that a geometry in which the YIG and semiconductor appear infinite cannot support a slow magnetostatic wave [69]. We conclude from this that a more complex geometry is required in order to observe a growing root which is realizable by experiment.

## 4.3. Evaluation of YIGSLAB and YIGSLAB-GAP

The next order of complexity results if the YIG material has a finite thickness. Figure 1 shows the variation of $|\kappa_i|$ with frequency where $d_i$ is the parameter. Notice that as $d_i$ is increased the loss will decrease. The $|k_i|$ is plotted because for lower values of carrier density, net gain was not observed. The value of $k_r$ ranges from 1300 to 7500 for the root observed. Gain is observed for YIGSLAB if the carrier density is increased above $10^{17}cm^{-3}$. Values above this level are not practical however, for two reasons: (1) The semiconductor begins to function as a metal with the associated losses and (2) It is difficult to effectively dope GaAs so that it contains such a high level of carriers [70].

The case illustrated in Figure 1 is for the so-called thin slab approximation i.e., $kd \leq 1.75$. In the case of thick slabs where $kd > 1.75$ no slow wave was observed. This ties in with the previous discussion because the YIG again appears to be infinite.

Notice in Figure 1 that as d is changed, the bandwidth over which a slow, magnetostatic wave is present also varies. The peak value is

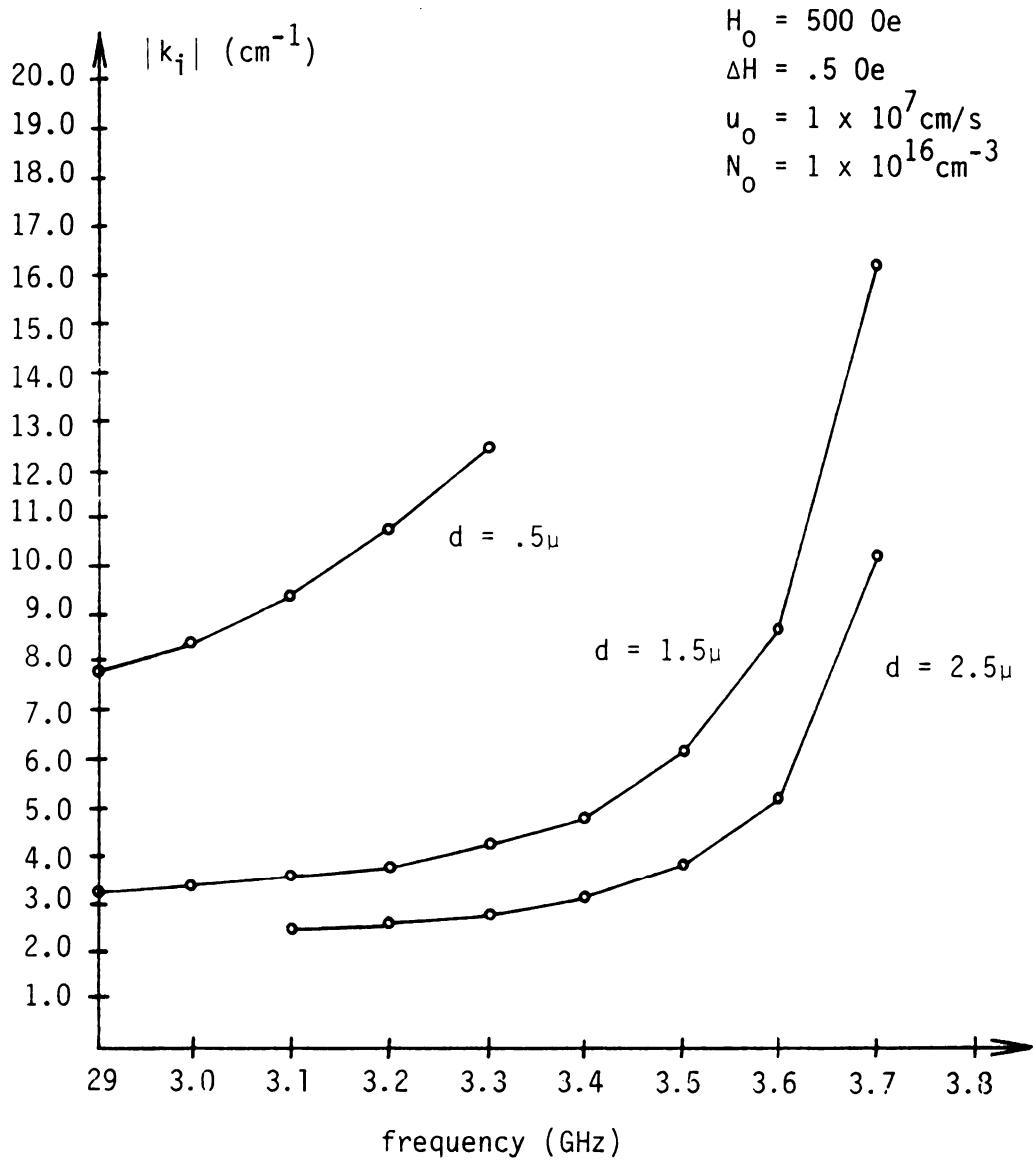


Figure 1. $|k_i|$ vs. frequency with YIG thickness as parameter for the YIGSLAB case.

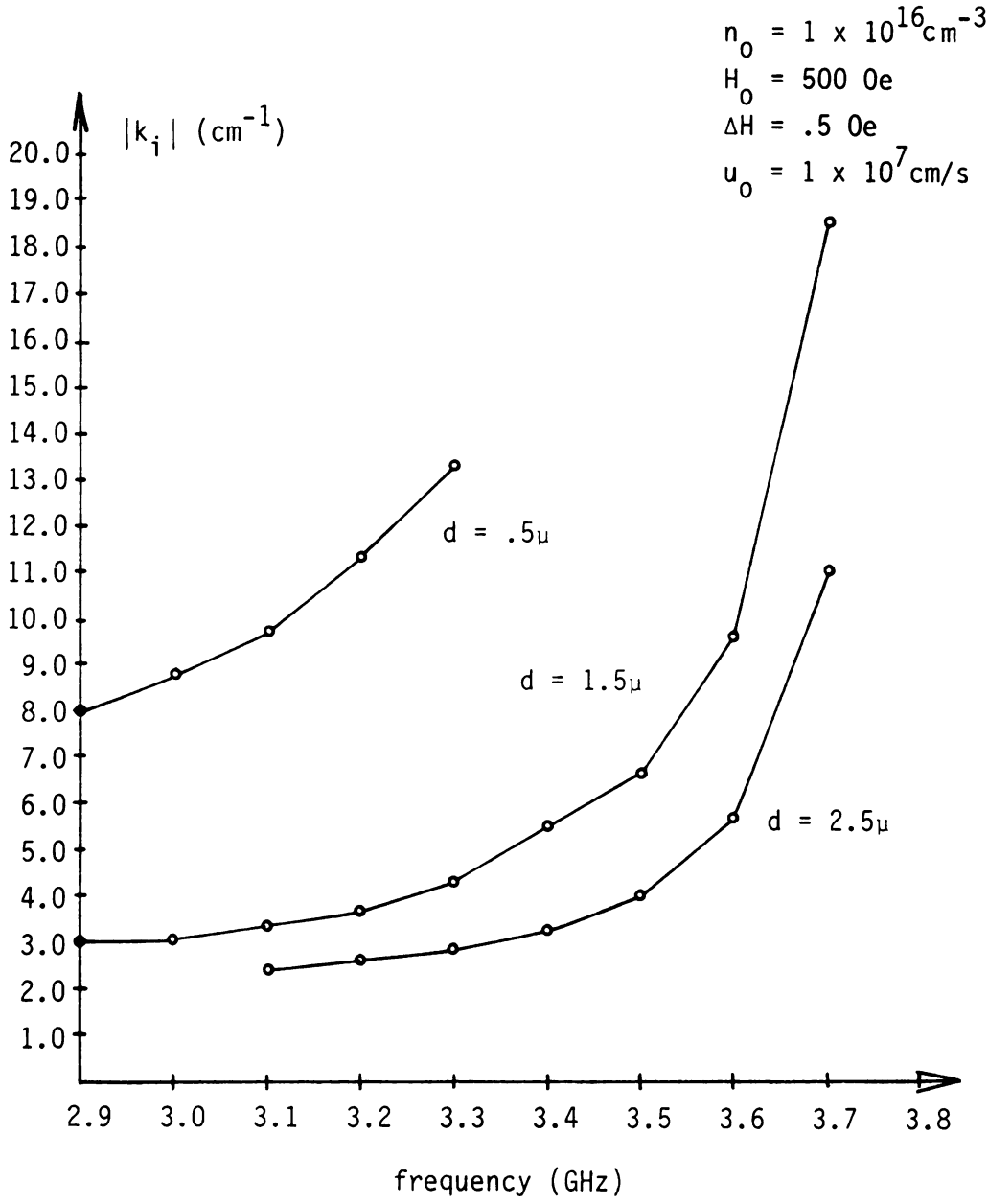


Figure 2. $k_i$ vs. frequency with YIG thickness as parameter for YIGSLAB-GAP case.

at d = 1.5μ as is shown. In all subsequent studies this value of YIG thickness is used.

If a gap is present (e.g., g = 1.0μ) we notice a small increase in loss as shown in Figure 2. It was also observed that for practical values of $n_0$ an increase in the gap thickness does not significantly affect the $k_i$ value. The increase observed is based on the strength of interaction between the drifting carriers and the magnetostatic wave. For this reason the gap is set to zero in remaining cases.

A word about the values of d and g that were selected. These values (d = 1.5μ and g = 0.0μ) were picked because they provide the best compromise for possible gain, bandwidth and accuracy of study. The concern for accuracy is based on the thin slab approximation where $kd \leq 1.75$. If d = 1.5μ e.g., then the maximum value of kd obtained is 1.126 when k = 7500 at 3.7 gigahertz. Therefore, it is possible that values of d greater than 1.5μ could be used. The problem is that as d is increased the bandwidth decreases because $k_r$ values are decreasing. This is evidenced by the fact that at 1.5μ the band of possible roots extends from 2.0 GHz to 3.7 GHz, whereas at 4.0μ the band is from 3.3 to 3.7 GHz. The effect on $k_i$ is the major concern when g is varied. Once g is greater than 1.0μ however, the values of $k_i$ are virtually unchanged. Therefore, a gap can be present for the purposes of signal excitation and detection but the gain will be improved if g = 0.0μ.

The variation of $k_i$ as a function of frequency with $u_0$ as parameter is shown in Figure 3 for the lossless case. Notice that as $u_0$ is increased $k_i$ increases as well. This also agrees with the work stated by Awai et al. The introduction of losses (i.e. $\Delta H \neq 0$) produces a significant reduction however, when the carriers are drifted at the maximum $\vec{u}_0$ for GaAs of $2 \times 10^7$ cm/s. This is shown in Figure 4. Since YIG films

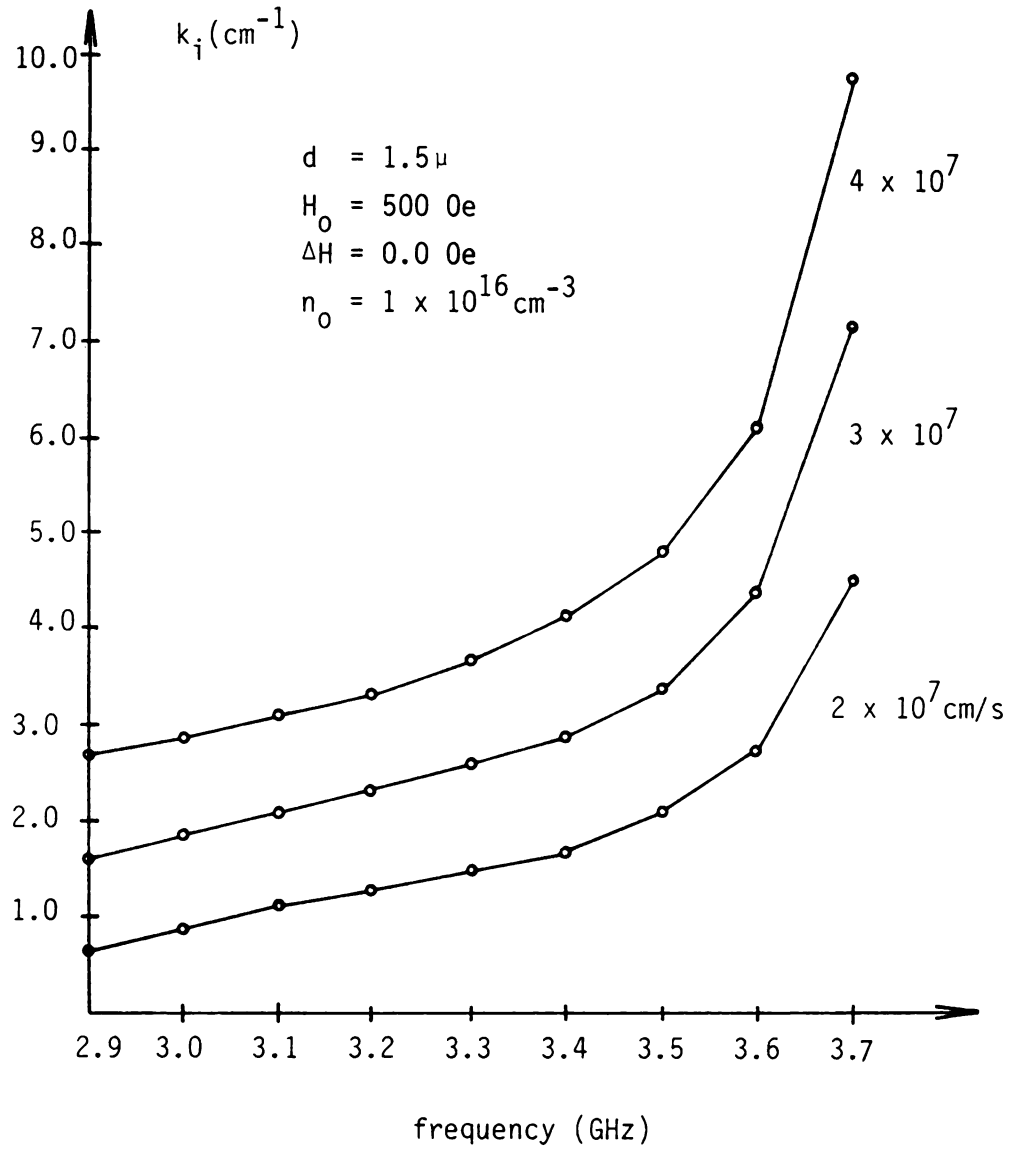


Figure 3. $k_i$ vs. frequency with $u_o$ as parameter for the lossless YIGSLAB case.

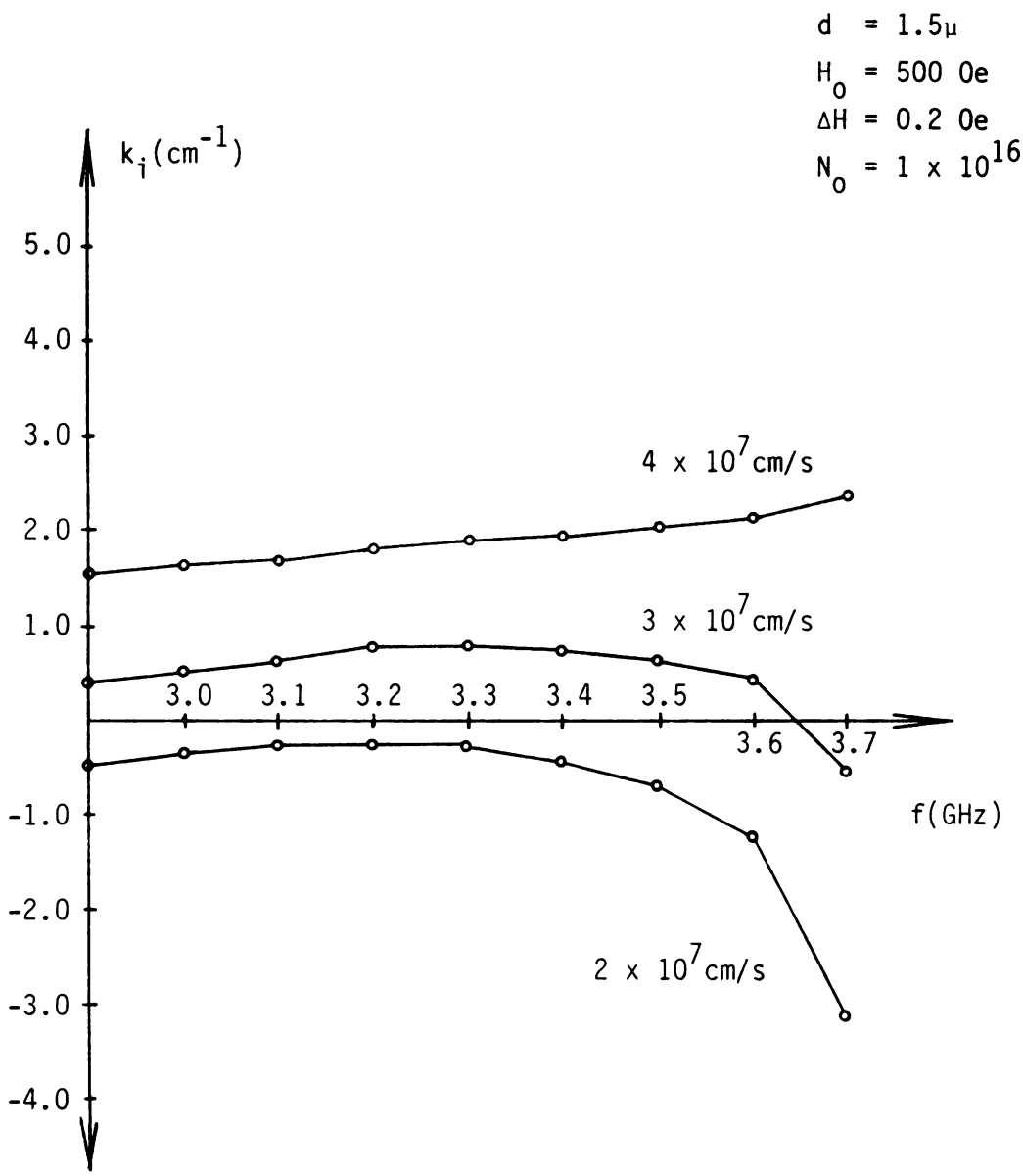


Figure 4. $k_i$ vs. frequency with $u_o$ as parameter for the lossy YIGSLAB case.

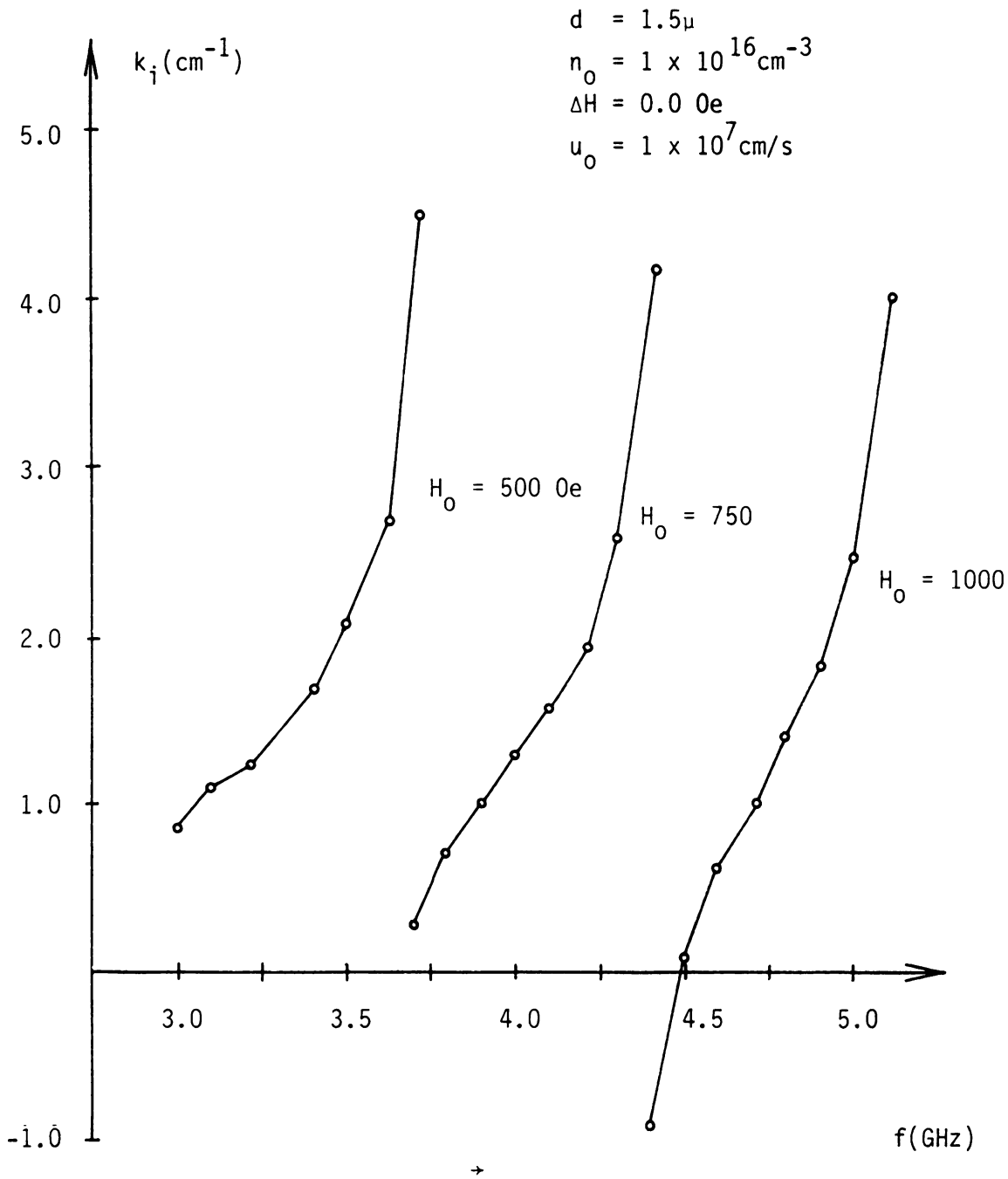


Figure 5. $k_i$ vs. frequency with $\vec{H}_o$ as parameter for the YIGSLAB case.

of highest quality may still possess $\Delta H$ values in the tenths of Oersteds, a geometry which provides for more gain at practical drift velocities is called for.

The variation of $k_i$ due to changes in $\vec{H}_o$, the static field is shown in Figure 5. Notice that as $\vec{H}_o$ is increased, the value of $k_i$ decreases slightly. The passband for wave propagation in the ferrite is shifted upward as $\vec{H}_o$ is increased. It is important to note that for possible operation above 5.0 GHz the static field must be greater than 1000 Oe, a fairly large field.

## 4.4. Evaluation of the GENERAL CASE

The introduction of metal plates serves three purposes: (1) to tailor the magnetostatic dispersion relation for the improvement of gain, (2) to provide a close to uniform carrier density in the GaAs region by counteracting the dc Hall-effect created by the static field $\vec{H}_o$, and (3) to provide a means for reducing the heat generated by the drifting carriers.

The geometry for the optimized YIGSLAB case is used with the exception that the GaAs region has a thickness $d_s = 1.0\mu$. This value is used because we want the heat generated to be reasonable. It is also a practical thickness from a fabrication standpoint.

The variation of $k_i$ versus frequency with $d_i$ as parameter is shown in Figure 6. This graph shows that gain is improved if the metal plate is closer to the YIG region. This agrees with work as stated by Vashkovskiy et al. [71]. The lower metal plate is also close to the GaAs region. Studies show that if $\bar{b}$ is greater than 0.2 the root disappears. This result is especially significant because none of the literature shows this case (thin semi region with metal plate) as having been examined in detail.

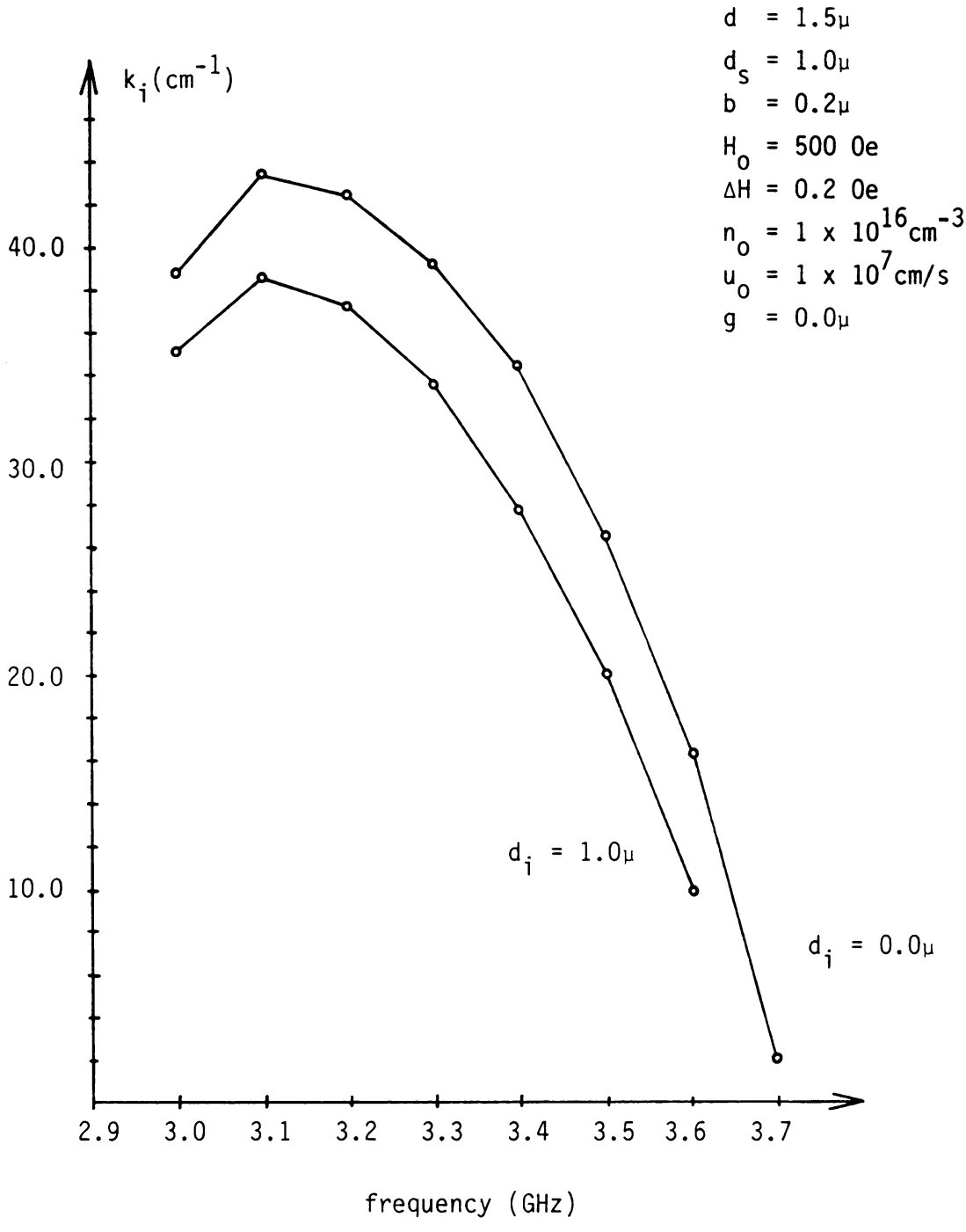


Figure 6. $k_i$ vs. frequency with $d_i$ as parameter for the GENERAL case.

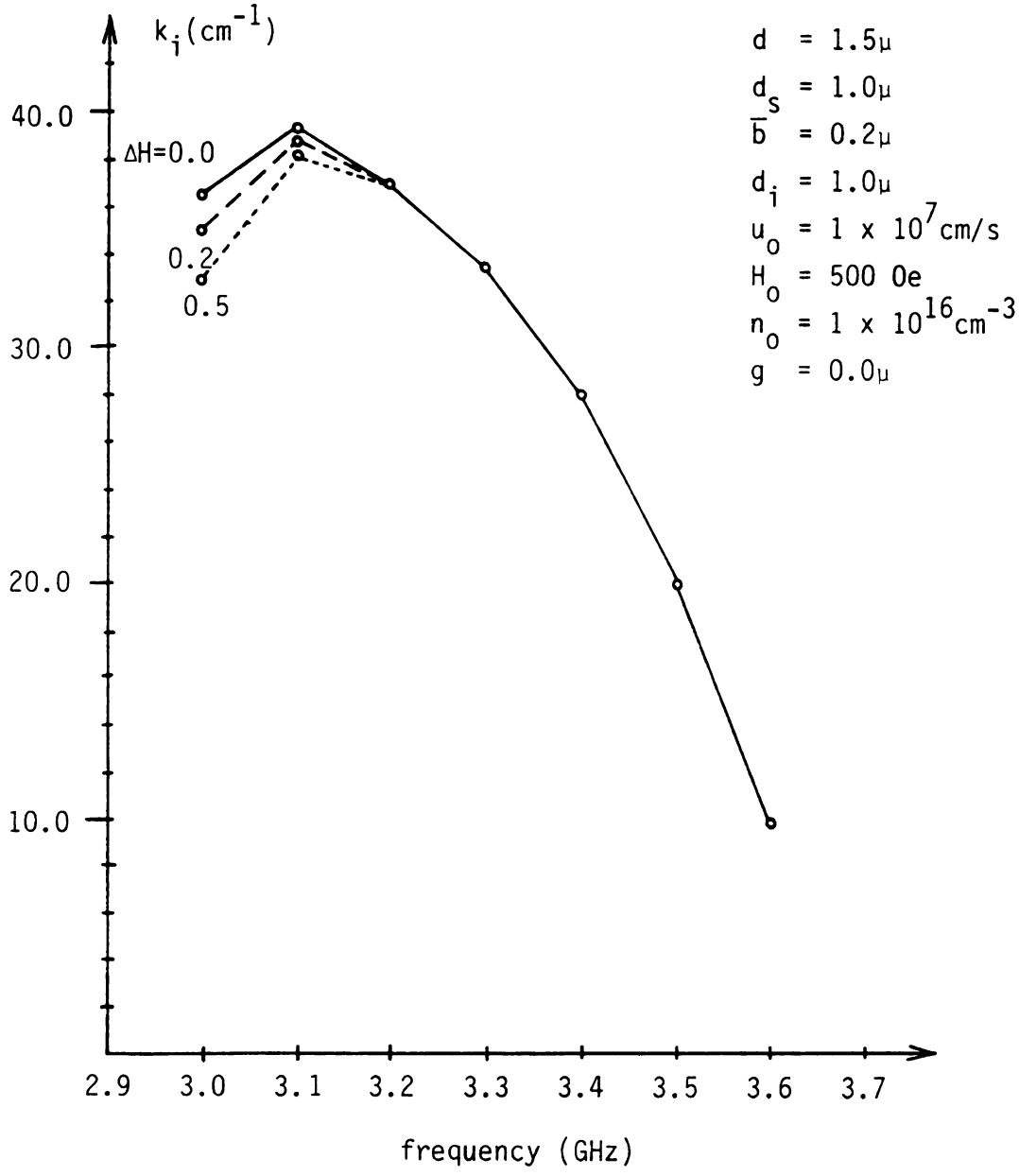


Figure 7. $k_i$ vs. frequency with ΔH as parameter for the GENERAL case.

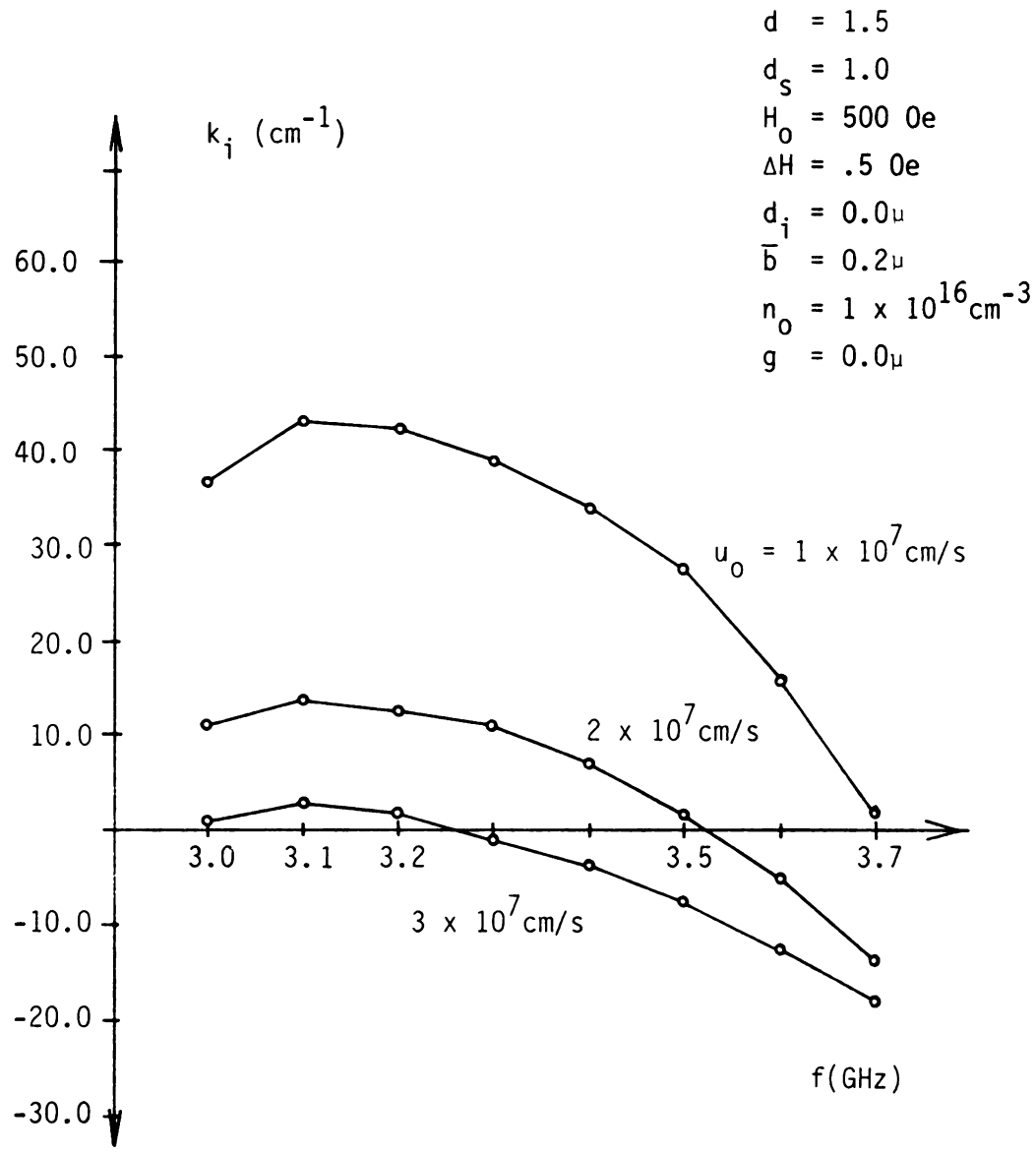


Figure 8. $k_i$ vs. frequency with $u_o$ as parameter for the GENERAL case.

If one examines the effect of losses we see a significant change from the YIGSLAB case. With values of $\Delta H$ as great as 0.5 Oe the $k_i$ is not significantly decreased over most of the frequency band from 3.2 to 3.7 GHz. This is shown in Figure 7. We believe the reason for this lies in the modification of the dispersion curve based on the presence of the two metal plates.

In Figure 8, $k_i$ as a function of frequency with $\vec{u}_0$ as parameter is shown. Notice that in the GENERAL case, positive $k_i$ values now occur if $\vec{u}_0$ is less than $2 \times 10^7$cm/s. This contrasts with the YIGSLAB case. If $\vec{u}_0$ is increased from $1 \times 10^7$cm/s to $2 \times 10^7$cm/s, there is now a significant decrease in the $k_i$ values (and hence the gain). This would tend to support the argument that the carriers and wave must be near synchronism. If the carriers are moving much faster than the wave, the gain is decreased and eventually lost. Further illustration of this is shown in Figure 9 where $k_i$ versus $u_0$ is shown.

In Figure 10, the effect of the static field variation on the GENERAL case is shown. Notice that in this case a peak in the $k_i$ values is obseved for $H_0$ = 750 Oe.

The GATE geometry was to be studied as a special case of the GENERAL configuration. This was to be achieved by allowing the GaAs region to be as large as possible for the thin slab approximation. It was discovered though that the lower plate plays a crucial part in obtaining net possible gain and therefore must be close. From a practical standpoint as well, the GaAs region should be as thin as possible to reduce heating loss. For these reasons the GATE geometry was not analyzed separately.

Finally, one must test the observed root to see if it gives rise to a convective instability using the Bers-Briggs criteria. This is

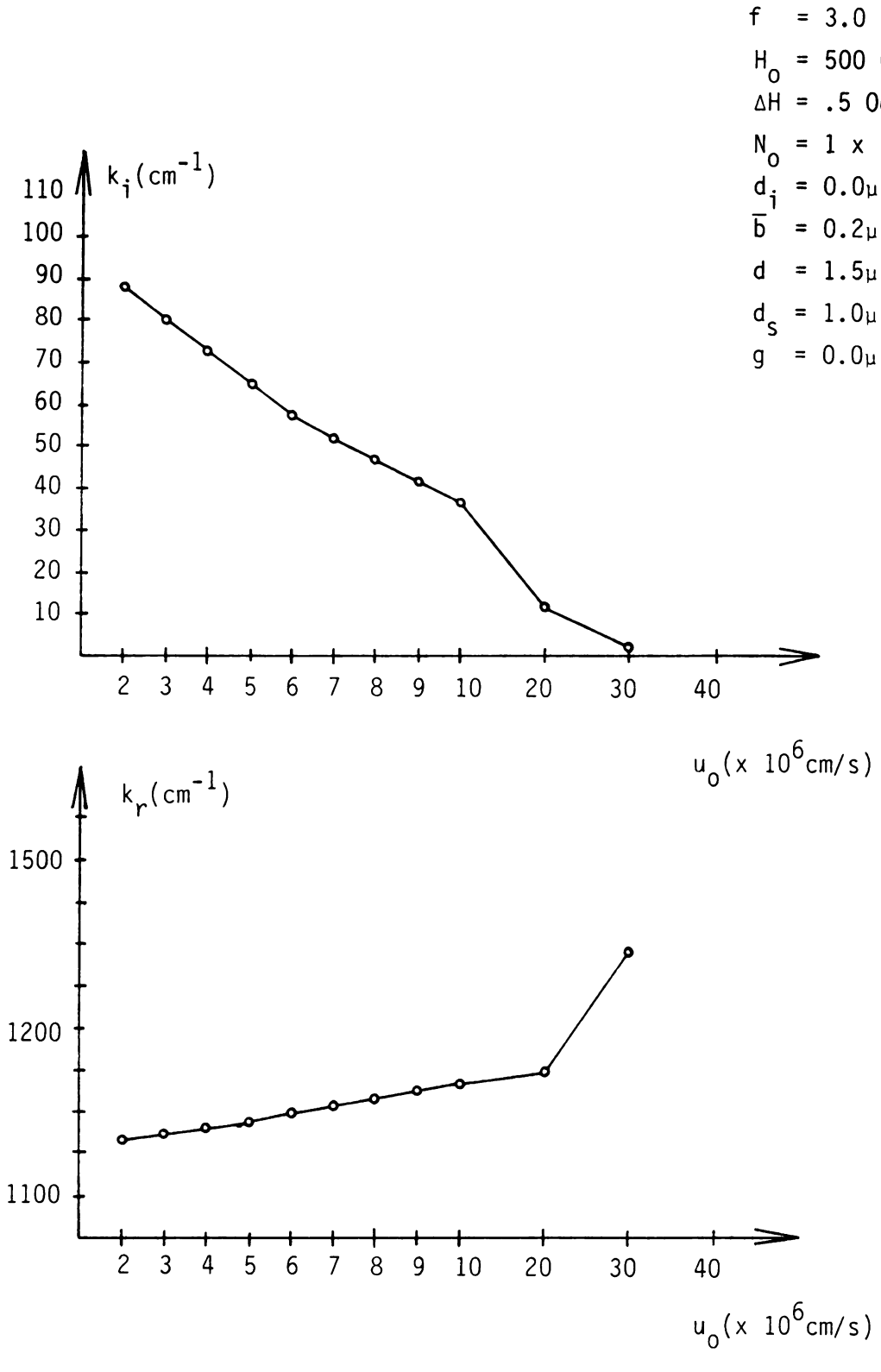


FIgure 9. $k_i$ and $k_r$ versus $u_o$ for GENERAL case.

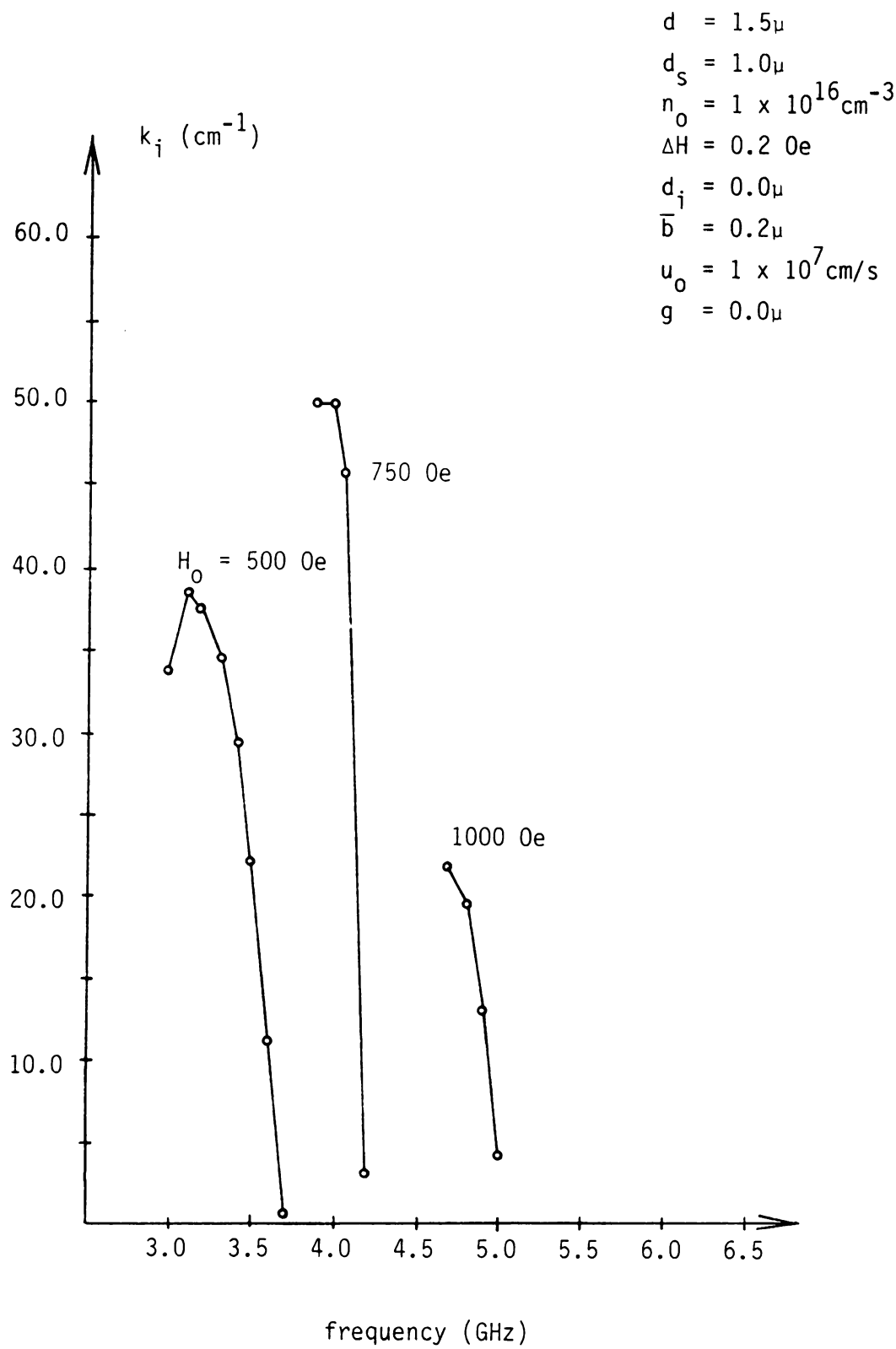


Figure 10. $k_i$ vs. frequency with $H_o$ as parameter for the GENERAL case.

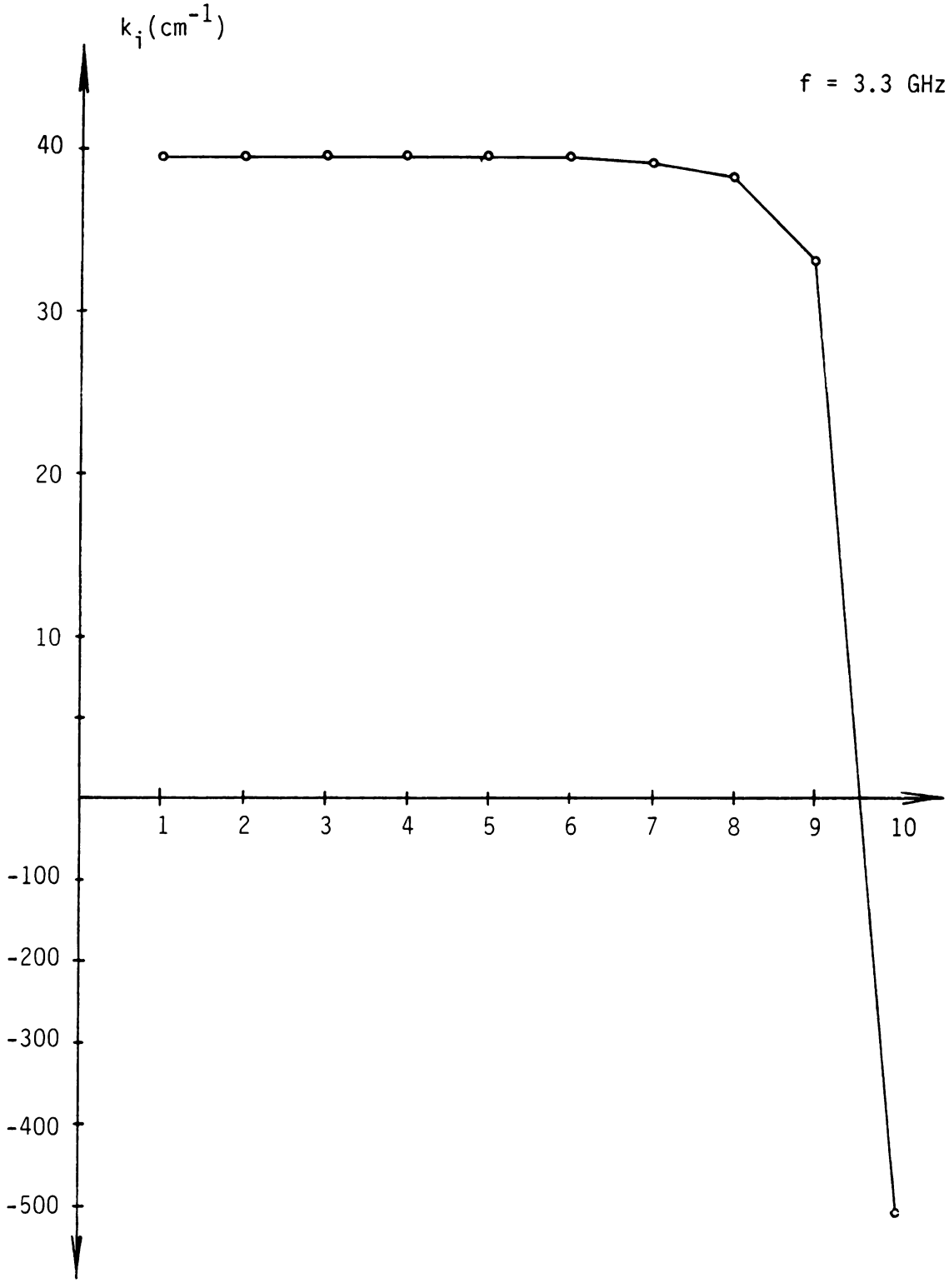


Figure 11. $k_i$ vs. log $|w_i|$ under the Bers and Briggs Criteria for GENERAL case.

shown in Figure 11. As indicated, the root is in fact "growing" since it experiences a change in sign. Therefore, energy is being convected in the +z direction.

This chapter has provided an evaluation of relevant dispersion results for the MSSWA. The criteria for the selection, evaluation and testing of possible growing roots is covered. This includes the Bers-Briggs criteria for convective instabilities. The geometry which will provide for optimal gain and bandwidth is presented. Trends which show the effect of certain parameters on gain and bandwidth behavior are also discussed.

# 5. SUMMARY AND CONCLUSION

## 5.1. Summary

The interaction of slow magnetostatic waves with drifting carriers in a layered ferrite-semiconductor structure has been studied in detail. The variation of the YIG-GaAs dispersion relation for different geometries has been modelled. The dispersion relations have been derived without the magnetostatic approximation. Using approximations for transverse wavenumber in the ferrite and semiconductor as well as an exponential approximation the dispersion polynomials were derived. Numerical evaluation of these polynomials was performed using a Fortran subroutine. The solutions of the dispersion polynomials were optimized with respect to certain device parameters. Possible growing roots were tested under the Bers and Briggs criteria for convective instabilities. Gain is predicted theoretically for the MSSWA.

## 5.2. Conclusion

The dispersion relations for geometries from a simple SINGLE-SURFACE to a more complex GENERAL layered structure have been theoretically analyzed. The results show that the YDS and SINGLE-SURFACE geometries will not support a slow magnetostatic wave. In the case of YIGSLAB and YIGSLAB-GAP, the following conclusions were drawn:

(1) The YIG region must be of finite thickness with respect to a wavelength in the transverse direction.

(2) Gain is improved if there is no gap between the YIG and GaAs regions, i.e., g = 0.

(3) Gain is obtained for velocities less than $2 \times 10^{7}$ cm/s only if carrier density is greater than $10^{18} cm^{-3}$.

(4) For practical values of carrier density, Gain increases as YIG thickness increases in general.

(5) Bandwidth decreases as YIG thickness increases.

The case of a GENERAL layered structure yields the following:

(1) The presence of the two metal plates is essential in order to achieve gain for practical carrier densities and drift velocities.

(2) The GaAs region must be of finite thickness with respect to a wavelength in the transverse direction if metal plates are present.

(4) $\Delta H$ can be 0.5 Oe and the gain is still significant over the frequency band of interest.

(5) The gain decreases significantly for $\vec{u}_0$ greater than $2 \times 10^7$ cm/s.

(6) Maximum gain occurs for $\vec{H}_0$ = 750 Oe.

The results of the Bers and Briggs criteria indicates that a convective instability is present. Due to the inconclusive nature of experimental results presented in the literature, we conclude that further investigations of the MSSWA using optimized parameters should be conducted.

# APPENDICES

# APPENDIX A

## BASIC ANALYSIS AND DEFINITIONS

The form for the permeability tensor $\overleftrightarrow{\mu}$ for a ferrite when the static magnetic field is along the +z axis is:

$$\overleftrightarrow{\mu} = \begin{bmatrix} \mu & jk & 0 \\ -jk & \mu & 0 \\ 0 & 0 & 1 \end{bmatrix} = \begin{bmatrix} \mu_{xx} & \mu_{xy} & \mu_{xz} \\ \mu_{yx} & \mu_{yy} & \mu_{yz} \\ \mu_{zx} & \mu_{zy} & \mu_{zz} \end{bmatrix} . \qquad (A.1)$$

Often the signs of off-diagonal terms are different in the literature. This issue and the errors which can result are addressed in [72]. If the orientation of $\vec{H}_o$ is changed, the tensor is also modified. As an example, if $\vec{H}_o = H_o\hat{y}$ the following cyclic change in subscripts is made; z replaces y, y replaces x and x replaces z to yield:

$$\overleftrightarrow{\mu} = \begin{bmatrix} \mu_{yy} & \mu_{yz} & \mu_{yx} \\ \mu_{zy} & \mu_{zz} & \mu_{zx} \\ \mu_{xy} & \mu_{xz} & \mu_{xx} \end{bmatrix} = \begin{bmatrix} \mu & 0 & -jK \\ 0 & 1 & 0 \\ jk & 0 & \mu \end{bmatrix} . \qquad (A.2)$$

For $\vec{H}_o = H_o\hat{x}$; z replaces x, x replaces y, y replaces z in the Equation (A.2) to give:

$$\overleftrightarrow{\mu} = \begin{bmatrix} 1 & 0 & 0 \\ 0 & \mu & jK \\ 0 & -jK & \mu \end{bmatrix} . \qquad (A.3)$$

If we replace K by SK, then we can orient the static field along the $\pm z$ axis by setting $S = \pm 1$ in the above tensor. For our case, where $\vec{H}_o$ is directed along the $\pm y$ axis, the permeability tensor is:

$$\overleftrightarrow{\mu} = \begin{bmatrix} \mu & 0 & -jSK \\ 0 & 1 & 0 \\ jSK & 0 & \mu \end{bmatrix}. \tag{A.4}$$

where recall that $\mu$ and K are given by

$$\mu = 1 + \frac{\omega_o \omega_m}{\omega_o^2 - \omega^2} \tag{A.5}$$

$$K = \frac{\omega_o \omega_m}{\omega_o^2 - \omega^2} \tag{A.6}$$

Some helpful definitions of important parameters are given below:

$\omega_o$ = precessional angular frequency of spins about $H_o$.

$\omega_m = \gamma_s(4\pi M_s)$, the saturation angular frequency. This is a constant of the system. The value is $3.096 \times 10^{10}$ rad/sec if $4\pi\mu_s = 1760$ Oe.

$\gamma_s = \frac{g|e|}{2m^*} \mu_o$ = gyromagnetic ratio = 2.8 MHz/Oe = $2\pi(2.8 \times 10^6)$ rad/Oe for the electron.

Notice that in general the precession angular frequency can be written as:

$$\omega_o = \gamma_s H_i + j\tfrac{1}{2}\gamma_s \Delta H + \omega_{ex} a^2 k^2 \tag{A.7}$$

or

$$\omega_o = \gamma_s H_i + j\tfrac{1}{2}\gamma_s \Delta H + \gamma_s D \frac{\omega^2}{c^2} \left[\frac{\mu - (SK)^2}{\mu}\right] \tag{A.8}$$

where again $H_i$ is the static internal dc field given by:

$$H_i = H_o - H_{DM} - H_A \tag{A.9}$$

The terms $H_o$, $H_{DM}$ and $H_A$ represent the external applied field, the demagnetizing field and the anisotropy field respectively. The latter two components must be accounted for if the slab dimensions are finite with respect to a wavelength and the slab is not fabricated from single crystalline material.

The parameter represented by $\Delta H$ is the ferrimagnetic resonance linewidth. This term gives a measure of the wave attenuation in the ferrite sample. It is inversely proportional to the precessional relaxation time. This gives a measure also of the degree of heating that occurs within the ferrite due to energy dissipated by a wave in lossy material. As the value of $\Delta H$ is increased, the losses which tend to relax the spin precession increase. This explains the decrease in the relaxation time T. Typical values can range from .3 to 7 oersteds in YIG films. For our analysis we would like to use films with $\Delta H$ values of approximately 1 oersted.

If the wave energy is of high enough frequency, the exchange field effects must be accounted for. This can take two forms:

$$(1)\ \omega_{ex} a^2 k^2 \tag{A.10}$$

$$(2)\ \gamma_s D \left[\frac{\mu-(SK)^2}{\mu}\right] \tag{A.11}$$

where the parameter D is a phenomelogical, inhomogeneous exchange constant with a value of approximately $4.4 \times 10^{-9}$ Oe-cm for YIG. Recall that in the magnetostatic regime i.e. $k \leq 10^4 cm^{-1}$ exchange effects can be neglected. Another loss parameter can also be found in the literature. This is designated as $\lambda$ and is related to the $j\frac{1}{2}\Delta H$ term in the Landau-Lifshitz loss formulation which is used in this report.

In this report, the units are those normally encountered in the literature and for reference we include some conversion factors

$$4\pi M \text{ (in Gauss)} \times 79.5 = M \frac{\text{amp}\cdot\text{Turn}}{\text{m}} \tag{A.12}$$

$$H(\text{in Oe}) \times 79.5 = H \frac{\text{amp}\cdot\text{Turn}}{\text{m}} \tag{A.13}$$

$$B(\text{in Gauss}) \times 10^{-4} = B \text{ Wb/m}^2 \tag{A.14}$$

The above notation conforms to that given by Collin [73], Johnson [74], Ramo, Whinnery and Van Duzer [75] and Beam [76]. It also appears to conform with the work due to Bini et al. [77] and also to that by Matsuo and Chang [78].

Finally, it should be noted that the analysis included in this report assumes that $\partial/\partial y \rightarrow 0$ i.e. that the problem is a two dimensional one. This is done for simplicity; the TE and TM modes then become uncoupled [79].

# APPENDIX B

## DERIVATION OF DISPERSION POLYNOMIALS

### B.1. Dispersion Polynomial for YDS

From Section 3.3, the dispersion relation for the YDS case was developed as

$$e^{-2kg} = \frac{(\gamma_s + k)[SK - \mu + D]}{(\gamma_s - k)[SK - \mu - D]} \tag{B.1-1}$$

where

$$A_1 = SK - \mu + D \tag{B.1-2}$$

$$A_2 = SK - \mu - D \tag{B.1-3}$$

$$D = K^2 - \mu^2. \tag{B.1-4}$$

If an exponential approximation is used then,

$$e^{-2kg} = \frac{12 - 12gk + 4g^2k^2}{12 + 12gk + 4g^2k^2} = \frac{N_1(k)}{D_1(k)}. \tag{B.1-5}$$

Solving for $\gamma_s$ yields

$$\gamma_s = k\,\frac{(B_1 + 1)}{(B_1 - 1)} \tag{B.1-6}$$

where

$$B_1 = \frac{A_2 N_1}{A_1 D_1}. \tag{B.1-7}$$

The proper approximation for $\gamma_s$ is,

$$\gamma_s \doteq k + \frac{SA}{k} + SB \tag{B.1-8}$$

where SA and SB are defined in Appendix C. This gives us the following for (B.1-6).

$$k + \frac{SA}{k} + SB = k\,\frac{(B_1 + 1)}{(B_1 - 1)}. \qquad \text{(B.1-9)}$$

Since $A_1$ and $A_2$ are constant with respect to g, $B_1$ will vary as $N_1$ and $D_1$. The exponential approximation (see Appendix C) requires the consideration of two cases. They are for $kg \leq 1.75$ and $kg \geq 1.75$.

Case I $kg \leq 1.75$

For this case

$$N_1 = 12 - 12gk + 4g^2k^2 \qquad \text{(B.1-10)}$$

$$D_1 = 12 + 12gk + 4g^2k^2 = N_1 + 24gk \qquad \text{(B.1-11)}$$

We write

$$B_1 = \frac{A_2}{A_1}\,\frac{N_1}{N_1 + 24gk} \equiv A_3\,\frac{N_1}{N_1 + 24gk} \qquad \text{(B.1-12)}$$

so that

$$\frac{B_1 + 1}{B_1 - 1} = \frac{A_3N_1 + N_1 + 24gk}{A_3N_1 - N_1 - 24gk} \qquad \text{(B.1-13)}$$

or

$$\frac{B_1 + 1}{B_1 - 1} = \frac{N_1(A_3 + 1) + 24gk}{N_1(A_3 - 1) - 24gk} \qquad \text{(B.1-14)}$$

This gives, for (B.1-9) after multiplying both sides by k:

$$k^2 + SBk + SA = k^2\,\frac{N_1(A_3 + 1) + 24gk}{N_1(A_3 - 1) - 24gk} \qquad \text{(B.1-15)}$$

If we cross-multiply and expand the LHS and RHS of (B.1-15), we obtain

$$(A_3 - 1)\,N_1k^2 + (A_3 - 1)\,N_1SBk + (A_3 - 1)\,N_1SA - 24gk^3$$

$$-24gSBk^2 - 24gSAk = (A_3 + 1)\,N_1k^2 + 24gk^3. \qquad \text{(B.1-16)}$$

Further expansion yields

$$-2N_1k^2 + (A_3 - 1)\,SBN_1k + (A_3 - 1)\,SAN_1 - 48gk^3 - 24gSBk^2$$

$$- 24gSAk = 0$$

$$-2(12k^2 - 12gk^3 + 4g^2k^4) + (A_3 - 1)\,SB\,(12k - 12gk^2 + 4g^2k^3)$$

$$+(A_3 - 1)\,SA\,(12 - 12gk + 4g^2k^2) - 48gk^3 - 24gSBk^2 - 24gSAk = 0. \qquad \text{(B.1-17)}$$

This expression is rearranged to obtain

$$(-8g^2)k^4 + [24g + 4g^2\,(A_3 - 1)\,SB - 48g]k^3 +$$

$$[-24 - 12g\,(A_3 - 1)\,SB + 4g^2\,(A_3 - 1)\,SA - 24gSB]k^2 +$$

$$[12\,(A_3 - 1)\,SB - 12g\,(A_3 - 1)\,SA - 24gSA]k + [12SA\,(A_3 - 1)] = 0. \qquad \text{(B.1-18)}$$

which is the YDS dispersion for thin gap spacings.

Case II $kg \geq 1.75$

In this case we have

$$N_1 = EB = 0.11072 \qquad \text{(B.1-19)}$$

$$D_1 = 2kg \qquad \text{(B.1-20)}$$

so that the expression for $B_1$ becomes

$$B_1 = A_3\,\frac{EB}{2kg} \qquad \text{(B.1-21)}$$

and

$$\frac{B_1 + 1}{B_1 - 1} = \frac{A_3EB + 2kg}{A_3EB - 2kg} \qquad \text{(B.1-22)}$$

or for (B.1-6), we have

$$k^2 + SBk + SA = k^2\,\frac{A_3EB + 2kg}{A_3EB - 2kg}. \qquad \text{(B.1-23)}$$

Upon expansion the following expression results

$$A_3EBk^2 + A_3EBSBk + A_3EBSA - 2gk^3 - 2gSBk^2 - 2gSAk$$

$$= A_3EBk^2 + 2gk^3 \qquad \text{(B.1-24)}$$

The dispersion relation for the case of thick spacings is therefore,

$$(-4g)k^3 + (A_3EB - 2gSB - A_3EB)k^2 + (A_3EBSB - 2gSA)k +$$

$$(A_3EBSA) = 0. \qquad \text{(B.1-25)}$$

## B.2. Dispersion Polynomial for SINGLE-SURFACE (EXACT $\gamma_s$)

The dispersion relation for the SINGLE-SURFACE case is given again by

$$\gamma_s (K^2 - \mu^2) + (SKk - \mu\gamma_f) = 0 \tag{B.2-1}$$

or

$$\gamma_s = \frac{\mu\gamma_f - SKk}{K^2 - \mu^2} \tag{B.2-2}$$

squaring both sides

$$\gamma_s^2 = \frac{(\mu\gamma_f - SKk)^2}{(K^2 - \mu^2)^2} \tag{B.2-3}$$

Recall that

$$\gamma_s^2 = k^2 - k_s^2 + j\left(\frac{k_s}{\omega}\right)^2 \omega_c (\omega - ku_o) \tag{B.2-4}$$

and

$$K^2 - \mu^2 = \frac{\omega^2 - (\omega_m + \omega_o)^2}{\omega_o^2 - \omega^2} = D \tag{B.2-5}$$

so that

$$D^2\gamma_s^2 = \mu^2\gamma_f^2 - 2\mu\gamma_f SKk + (SKk)^2 \tag{B.2-6}$$

$$D^2\gamma_s^2 = \mu^2\left[k^2 + \frac{k_o^2}{\mu} D\right] - 2\mu SK\gamma_f k + (Kk)^2 \tag{B.2-7}$$

let $\gamma_f \doteq k$ so that

$$D^2\gamma_s^2 \doteq \mu^2k^2 + \mu k_o^2 D - 2\mu SKk^2 + (Kk)^2 \tag{B.2-8}$$

$$= k^2(\mu^2 + K^2) + \mu k_o^2 D - 2\mu SKk^2 \tag{B.2-9}$$

$$= (\mu^2 - 2\mu SK + K^2)k^2 + \mu k_o^2 D \tag{B.2-10}$$

$$D^2\gamma_s^2 = (\mu - SK)^2k^2 + \mu k_o^2 D \tag{B.2-11}$$

using the expression for $\gamma_s$ gives

$$D^2\left[k^2 - k_s^2 + j\left(\frac{k_s}{\omega}\right)^2 \omega_c(\omega - ku_o)\right] = (\mu - SK)^2k^2 + \mu k_o^2 D \tag{B.2-12}$$

$$D^2k^2 - D^2k_s^2 + j\left(\frac{k_s}{\omega}\right)^2 \omega_c(\omega - ku_o)D^2 = (\mu - SK)^2k^2 + \mu k_o^2 D \tag{B.2-13}$$

which yields

$$\left[D^2 - (\mu - SK)^2\right]k^2 - \left[j\left(\frac{k_s}{\omega}\right)^2 \omega_c u_o D^2\right]k - \left[D^2k_s^2 - j\left(\frac{k_s}{\omega}\right)^2 \omega_c \omega D^2 + \mu k_o^2 D\right] = 0 \tag{B.2-14}$$

## B.3. Dispersion Polynomial for SINGLE-SURFACE (Approximate $\gamma_s$)

Again for the SINGLE-SURFACE dispersion we have

$$\gamma_s D = \mu\gamma_f - SKk \tag{B.3-1}$$

and if $\gamma_f \simeq k$ then

$$\gamma_s D = (\mu - SK)k \tag{B.3-2}$$

The expression for $\gamma_s$ is

$$\gamma_s = k^2 - k_s^2 + j\left(\frac{k_s}{\omega}\right)^2 \omega_c(\omega - ku_o) \tag{B.3-3}$$

$$\doteq k^2 + j\left(\frac{k_s}{\omega}\right)^2 \omega_c(\omega - ku_o) \tag{B.3-4}$$

if $k^2 >> k_s^2$ which is true for a slow wave

$$\gamma_s = k^2 + j\frac{\left(\frac{k_s}{\omega}\right)^2 \omega_c(\omega - ku_o)k^2}{k^2} \tag{B.3-5}$$

$$= k^2\left[1 + j\left(\frac{k_s}{\omega}\right)^2 \frac{\omega_c(\omega - ku_o)}{k^2}\right] \tag{B.3-6}$$

Then by the complex root approximation we have

$$\gamma_s \doteq k\left[1 + j\left(\frac{k_s}{\omega}\right)^2 \frac{\omega_c\,(\omega - ku_o)}{2k^2}\right] \tag{B.3-7}$$

so that the original dispersion becomes

$$k\left[1 + j\left(\frac{k_s}{\omega}\right)^2 \frac{\omega_c\,(\omega - ku_o)}{2k^2}\right] D = (\mu - SK)k \tag{B.3-8}$$

$$\left[1 + j\left(\frac{k_s}{\omega}\right)^2 \frac{\omega_c(\omega - ku_o)}{2k^2}\right] = \frac{(\mu - SK)}{D} \tag{B.3-9}$$

$$j\left(\frac{k_s}{\omega}\right)^2 \omega_c\,(\omega - ku_o) + 2k^2 = \frac{\mu - SK}{D}\,2k^2 \tag{B.3-10}$$

$$j\left(\frac{k_s}{\omega}\right)^2 \frac{\omega_c}{2}\,(\omega - ku_o) = \left[\frac{\mu - SK}{D} - 1\right] k^2 \tag{B.3-11}$$

Which in final form is

$$\left[\frac{\mu - SK}{D} - 1\right] k^2 + j\left[\left(\frac{k_s}{\omega}\right)^2 \frac{\omega_c}{2}\,u_o\right]k - j\left(\frac{k_s}{\omega}\right)^2 \frac{\omega_c}{2}\,\omega = 0 \tag{B.3-12}$$

## B.4. Dispersion Polynomials for YIGSLAB and YIGSLAB-GAP

The dispersion relation for YIGSLAB-GAP was found to be

$$\left[e^{-2kg} - \left(\frac{\gamma_s + k}{\gamma_s - k}\right)\right]\left[(SK + \mu)(Sk - \mu - D)e^{-2kd} + (\mu - SK)(SK + \mu - D)\right] - D\left[e^{-2kg} + \left(\frac{\gamma_s + k}{\gamma_s - k}\right)\right]$$

$$[SK - \mu - D)e^{-2kd} - (SK + \mu - D)] \tag{B.4-1}$$

Using the exponential approximation for the thin slab/gap case, after considerable algebra we obtain,

$$[2f_4(b_3-b_1+b_2-b_o)]k^6 + [2f_3(b_1-b_3) + 2g_3(b_o-b_2) -2SBf_4(b_o+b_1)]k^5 +$$

$$\{2[f_2(b_3-b_1) + g_2(b_2-b_o) - SAf_4(b_o+b_1)] - SB[f_3(b_o+b_2+b_3-b_1) +$$

$$g_3(b_1+b_3+b_2-b_o)]\}k^4 + \{2[f_1(b_1-b_3) + g_1(b_o-b_2)] - SA[f_3(b_o+b_2+b_3-b_1)$$

$$+ g_3(b_1+b_3+b_2-b_o)] - SB[f_2(b_o+b_2-b_3+b_1) + g_2(b_1+b_3-b_2+b_o)]\}k^3 +$$

$$\{2[f_o(-b_1+b_3+b_2-b_o)] - SA[f_2(b_o+b_2-b_3+b_1) + g_2(b_1+b_3-b_2+b_o)]$$

$$-SB[f_1(b_o+b_2+b_3-b_1) + g_1(b_1+b_3+b_2-b_o)]\} k^2 + \{SA[f_1(b_o+b_2+b_3-b_1) + g_1$$

$$(b_1+b_3+b_2-b_o)] + 2[SBf_o(b_o+b_1)]\} k + [2SAf_o(b_o+b_1)] = 0 \quad (B.4\text{-}2)$$

In the case of kd and kg being greater than 1.75 we obtain

$$[8gd(b_3-b_1)]k^4 + [4gb(b_2-b_o) + 4SBgd(b_3-b_1)]k^3 + [2SB(b_2-b_o)gEB$$

$$-2SB(b_1+b_3)dEB + 4SA(b_3-b_1)gd]k^2 + [2SA(b_2-b_o)gEB -2SA(b_1+b_3)$$

$$dEB - SB(b_o+b_2)(EB)^2]k - [SA(EB)^2(b_o+b_2)] = 0 \quad (B.4\text{-}3)$$

where again the following definitions hold

EB = 0.1172

d = YIG slab thickness

g = spacing between YIG and GaAs

The terms $b_o$, $b_1$, $b_2$, $b_3$ are expressions which are related to the YIG magnetostatic wave parameters. They are defined as

$$b_o = Da_2 \quad (B.4\text{-}4)$$

$$b_1 = -Da_3 \quad (B.4\text{-}5)$$

$$b_2 = -a_2 a_4 N_1 N_2 \tag{B.4-6}$$

$$b_3 = -a_3 a_5 \tag{B.4-7}$$

where

$$a_1 = SK - \mu + D \tag{B.4-8}$$

$$a_2 = SK - \mu - D \tag{B.4-9}$$

$$a_3 = SK + \mu - D \tag{B.4-10}$$

$$a_4 = SK + \mu \tag{B.4-11}$$

$$a_5 = \mu - SK \tag{B.4-12}$$

We represent the exponentials as

$$e^{-2kd} = \frac{N_2}{D_2} \tag{B.4-13}$$

$$e^{-2kg} = \frac{N_1}{D_1} \tag{B.4-14}$$

similar to the previous section. The terms $f_1$, $f_2$, $f_3$ and $f_4$ are related to the exponential terms $N_1$, $D_1$, $N_2$ and $D_2$ from multiplication operations that result from the simplification of (B.4-1). The same holds true for $g_1$, $g_2$ and $g_3$. These are not included for brevity since they can be readily obtained.

In order to obtain the polynomial for the YIGSLAB case the spacing between the YIG and GaAs regions goes to zero. This produces the following conditions.

$$f_4 \to 0$$

$$f_3 \to 0$$

$$g_3 \to 0$$

The following polynomials result for the two separate cases,

Case I $kd \leq 1.75$

$$\left\{2[f_2(b_3-b_1) + g_2(b_2-b_o)]\right\} k^4 + \left\{2[f_1(b_1-b_3) + g_1(b_o-b_2)]\right.$$

$$-SB[f_2(b_o+b_2-b_3+b_1) + g_2(b_1+b_3-b_2+b_o)]\Big\} k^3 + \Big\{ 2[f_o(-b_1+b_3+b_2-b_0)]$$

$$-SA[f_2(b_o+b_2-b_3+b_1) + g_2(b_1+b_3-b_2+b_o)] - SB[f_1(b_o+b_2+b_3-b_1) + g_1$$

$$(b_1+b_3+b_2-b_o)] \Big\} k^2 + \Big\{SA[f_1(b_o+b_2+b_3-b_1) + g_1(b_1+b_3+b_2-b_o)] +$$

$$2SBf_o(b_o+b_1) \Big\} k + [2SAf_o(b_o+b_1)] = 0. \qquad \text{(B.4-15)}$$

Cast II $kd \geq 1.75$

The dispersion polynomial in this case is,

$$[-2SBEB(b_1+b_3)d]k^2 - [2SAEB(b_1+b_3) + SB(EB)^2(b_o+b_2)]k +$$

$$[SA(EB)^2(b_o+b_2)] = 0. \qquad \text{(B.4-16)}$$

## B.5. Dispersion Polynomial for the GENERAL case

The algebraic manipulations for the GENERAL case are exceedingly long. For this reason only the dispersion in its final symbolic form will be given. The method used in the development of previous polynomials was used here, as well as the following approximations:

$$\gamma_s \doteq k \text{ (only in exponents)} \qquad \text{(B.5-1)}$$

$$\gamma_f \doteq k \qquad \text{(B.5-2)}$$

Using the above information along with the dispersion relation for GENERAL developed in Chapter 3, the following polynomial results for the case of thin slabs and gap spacings,

$$M_{T19}k^{19} + M_{T18}k^{18} + M_{T17}k^{17} + M_{T16}k^{16} + M_{T15}k^{15} + M_{T14}k^{14} +$$

$$M_{T13}k^{13} + M_{T12}k^{12} + M_{T11}k^{11} + M_{T10}k^{10} + M_{T9}k^{9} + M_{T8}k^{8} +$$

$$M_{T7}k^{7} + M_{T6}k^{6} + M_{T5}k^{5} + M_{T4}k^{4} + M_{T3}k^{3} + M_{T2}k^{2} + M_{T1}k^{1} = 0 \quad \text{(B.5-3)}$$

The coefficients of this polynomial depend in a complicated way on YIG parameters S, K and $\mu$, as well as the thicknesses of the various layers which make up the device.

A separate dispersion polynomial for GATE was not developed due to the similarity of this case with others which were studied. In order to analyze the GATE model, the following conditions were applied to the GENERAL case:

(1) The semiconductor region is allowed to be as thick as possible for the thin region approximation.

(2) The gap between the GaAs and the heat sink is as large as the approximation will allow.

These conditions provide for a semiconductor region that appears semi-infinite in the transverse plane which is the basic difference between the GATE and GENERAL geometries.

# APPENDIX C

## COMPLEX ROOT AND EXPONENTIAL FUNCTION APPROXIMATION

In the derivation of certain dispersion polynomials, it is necessary to use $\gamma_s$ or $\gamma_f$ which cannot be expressed exactly since they depend on k, which is to be found. It is possible, however, to obtain $\gamma_s^2$ and $\gamma_f^2$, and these are in general complex quantities. Thus, an approximation to the complex square root is required in order to obtain workable dispersion polynomials.

The exponential approximation is also discussed. This is because the general form of the more complex relations is $e^{-x}$. An appropriate choice for this approximation is important because we want to restrict the function $e^{-x}$ to positive values.

### C.1. Complex Root Approximation

Here we look at the square root of a complex number

$$Z = A + jB$$

$$\text{MAG } Z = (A^2 + B^2)^{\frac{1}{2}} \tag{C.1-1}$$

$$\text{ANG } Z = \tan^{-1}(B/A) \tag{C.1-2}$$

If $B \ll A$, then

$$\tan^{-1}(B/A) \doteq B/A \tag{C.1-3}$$

and

$$\text{MAG } Z = (A^2 + B^2)^{\frac{1}{2}} \doteq A \tag{C.1-4}$$

$$\text{ANG } Z \doteq B/A \tag{C.1-5}$$

so for the $\sqrt{Z}$,

$$\text{MAG } \sqrt{Z} = \sqrt{A} \tag{C.1-6}$$

$$\text{ANG } \sqrt{Z} = B/2A \tag{C.1-7}$$

In rectangular form you have

$$\sqrt{Z} = \sqrt{A}\ \cos\left(\frac{B}{2A}\right) + j\sin\left(\frac{B}{2A}\right) \qquad \text{(C.1-8)}$$

and for B << A again, we have

$$\sqrt{Z} \doteq \sqrt{A}\left[1 + j\left(\frac{B}{2A}\right)\right] \qquad \text{(c.1-9)}$$

because we recall that

$$\cos\left(\frac{B}{2A}\right) \doteq \cos 0 = 1 \qquad \text{(C.1-10)}$$

$$\sin\left(\frac{B}{2A}\right) \doteq \frac{B}{2A} \qquad \text{(c.1-11)}$$

Now we obtain $\gamma_f$ the transverse wavenumber in the ferrite.

$$\gamma_f^2 = k^2 + \frac{k_o^2}{\mu}\left(K^2 - \mu^2\right) \qquad \text{(C.1-12)}$$

Recall that when losses are included in the YIG, $\omega_o$ becomes complex and therefore $(K^2 - \mu^2)$ is also complex. We write

$$(K^2 - \mu^2) = D_r + jD_i \qquad \text{(C.1-13)}$$

Thus

$$\gamma_f^2 = k^2\left[1 + \frac{k_o^2}{\mu k^2}\ (K^2 - \mu^2)\ \right] \qquad \text{(C.1-14)}$$

$$= k^2\left[1 + \frac{k_o^2 D_r}{\mu k^2} + j\,\frac{k_o^2 D_i}{\mu k^2}\right] \qquad \text{(C.1-15)}$$

hence

$$\gamma_f = k\left[1 + \frac{k_o^2 D_r}{\mu k^2} + j\,\frac{k_o^2 D_i}{\mu k^2}\right]^{1/2} \qquad \text{(C.1-16)}$$

$$\doteq k\left[\left(1 + \frac{k_o^2 D_r}{\mu k^2}\right)^{1/2}\left(1 + j\,\frac{D_i}{2D_r}\right)\right] \qquad \text{(C.1-17)}$$

$$\doteq k\left[\left(1 + \frac{k_o^2 D_r}{2\mu k^2}\right)\left(1 + j\,\frac{D_i}{2D_r}\right)\right] \qquad \text{(C.1-18)}$$

so that finally

$$\gamma_f \doteq k\left[1 + j\,\frac{D_i}{2D_r}\right] \tag{C1-19}$$

For the semiconductor we have,

$$\gamma_s^2 = k^2 - k_s^2 + j\left(\frac{k_s}{\omega}\right)^2 \omega_c\,(\omega - ku_o) \tag{C.1-20}$$

then

$$\gamma_s^2 \doteq k^2\left[1 + j\left(\frac{k_s}{\omega}\right)^2 \frac{\omega_c(\omega - ku_o)}{k^2}\right] \tag{C.1-21}$$

Upon taking the square root we have

$$\gamma_s \doteq k\left[1 + j\left(\frac{k_s}{\omega}\right)^2 \frac{\omega_c(\omega - ku_o)}{2k^2}\right] \tag{C.1-22}$$

or

$$\gamma_s \doteq k\left\{1 + j\left[\left(\frac{k_s}{\omega}\right)^2 \frac{\omega_c\omega}{2}\right]\frac{1}{k^2} + j\left[-\left(\frac{k_s}{\omega}\right)^2 \frac{\omega_c u_o}{2}\right]\frac{1}{k}\right\} \tag{C.1-23}$$

$$\doteq k\left[1 + \frac{SA}{k^2} + \frac{SB}{k}\right] \tag{C.1-24}$$

$$\gamma_s \doteq k + \frac{SA}{k} + SB \tag{C.1-25}$$

where

$$SA = j\left(\frac{k_s}{\omega}\right)^2 \frac{\omega_c\omega}{2} \tag{C.1-26}$$

$$SB = -j\left(\frac{k_s}{\omega}\right)^2 \frac{\omega_c u_o}{2} \tag{C.1-27}$$

In order to obtain (C.1-19) and (C.1-25), we assume that $k = k_r + jk_i$ and that $k_r >> k_i$.

## C.2. Description of the Exponential Approximation

The exponential function is approximated by the first few terms of the continued fraction expansion [79] and has the form

$$e^{-x} = 1 + \frac{12x}{12 - 6x + x^2} \qquad \text{(C.2-1)}$$

or

$$e^{-x} = \frac{12 + 6x + x^2}{12 - 6x + x^2} = p(x) \qquad \text{(C.2-2)}$$

This approximation does not allow $e^{-x}$ to become negative as $e^{-x} = 1 - x$ would when $|x| > 1$. Because we are searching for $x = 2kd$, we cannot check the magnitude of x in any step of the analysis. A sketch of Equation (C.2-1) and 1/x is shown in Figure C-1. We will use (C.2-2) when $x \leq 3.5$ (i.e., kd, $kg \leq 1.75$). Thus, the thicknesses of concern are less than $.279\lambda$ for reasonable accuracy. For larger values, we let $e^{-x} = \frac{EB}{x}$. The solution of this equation for $x = 3.46$ gives a value for EB of 0.11072.

With the above approximations, we can determine the dispersion polynomials for the various geometries of concern in this report.

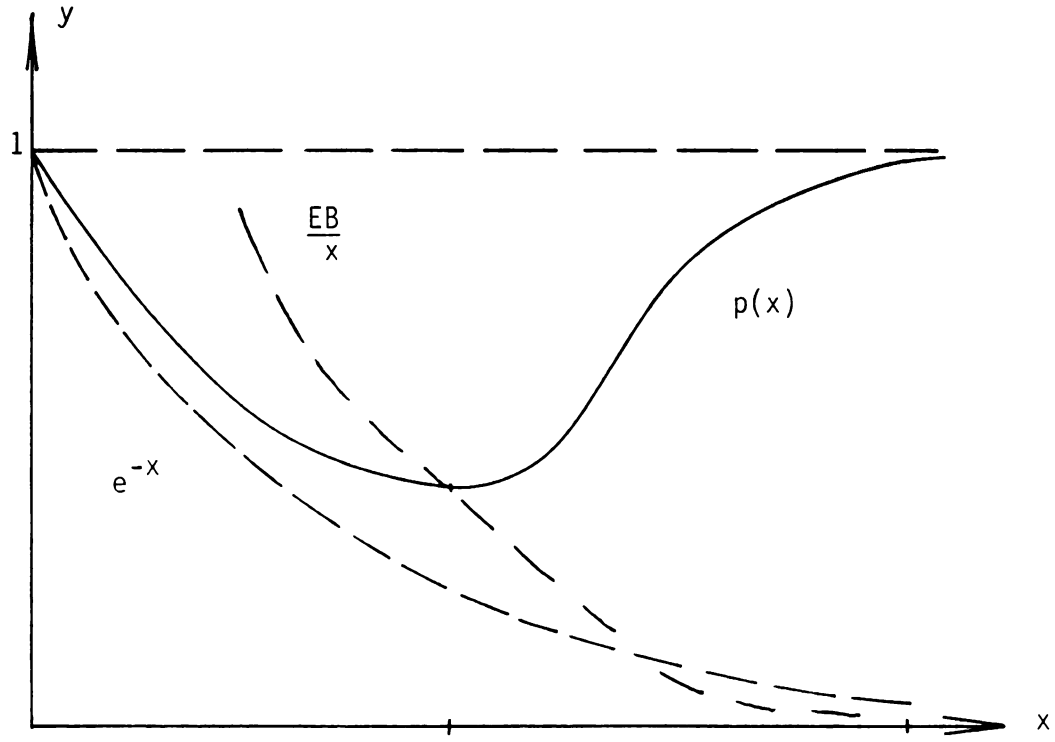


Figure C-1. Comparison of the continued fraction expansion approximation to 1/x for $e^{-x}$.

# APPENDIX D

## YIGSLAB PASSBAND CALCULATION

The starting equation is the dispersion relation for this model. We will take the limits of $n_o \to 0$, $n_o \to \infty$, to model the extreme cases of the GaAs being a dielectric or a prefect conductor. In the first limit (i.e., the dielectric case), if we let $\gamma_f = \gamma_s \doteq k$, then

$$e^{-2kd} = \frac{[\mu + SK + 1][\mu - SK + 1]}{[\mu - SK - 1][\mu + SK - 1]} \tag{D.1}$$

Notice that the expression is invariant with the sign of S; thus,

$$e^{-2kd} = \frac{[\mu + K + 1][\mu - K + 1]}{[\mu - K - 1][\mu + K - 1]} \tag{D.2}$$

We now take the limit of the above expression as $k \to 0$ and $k \to \infty$. If k is assumed pure real (i.e., we examine the lossless case), then for $k \to 0$ after considerable algebra, we have

$$\omega \equiv \omega_A = \gamma[H_o(H_o + 4\pi M_S)]^{\frac{1}{2}} \tag{D.3}$$

$$= [\omega_o(\omega_o + \omega_m)]^{\frac{1}{2}} \tag{D.4}$$

For $k \to \infty$ we obtain for $\omega$,

$$\omega \equiv \omega_B = \omega_o + \frac{\omega_m}{2} \tag{D.5}$$

The terms $\omega_m$, $M_S$ and $H_o$ are defined in Appendix A.

For a representative bias field $H_o$ = 500 Oe, where

$4\pi M_s$ = 1760 Oe we find

$\omega_B = 2.43 \times 10^{10}$ rad/sec

$\omega_A = 1.87 \times 10^{10}$ rad/sec

which gives a frequency passband $f_B - f_A$ of 888 megahertz.

In the limit as $n_o \to \infty$, $\gamma_s \to j\infty$, the original dispersion gives

$$e^{-2kd} = \frac{[\gamma_s(\mu + SK)][\mu - SK + 1]}{[\gamma_s(\mu - SK)][\mu + SK - 1]} \tag{D.6}$$

$$= \frac{(\mu + SK)(\mu - SK + 1)}{(\mu - SK)(\mu + SK - 1)} \tag{D.7}$$

$$= \frac{\mu^2 - K^2 + \mu + SK}{\mu^2 - K^2 - \mu + SK} \tag{D.8}$$

For $k \to 0$,

$$\omega^2 = \omega_o^2 + \omega_o\omega_m \tag{D.9}$$

or

$$\omega = \omega_A \tag{D.10}$$

Therefore, in the limit as $k \to 0$, the value of $\omega$ is $\omega_A$ for the dielectric or the metal cases. For $k \to 0$ we set the numerator of (D.8) to zero and let

$$\mu^2 - K^2 - \mu + SK \neq 0 \tag{D.11}$$

Using

$$\mu^2 - K^2 = \frac{\omega^2 - (\omega_m + \omega_o)^2}{\omega_o^2 - \omega^2} \tag{D.12}$$

so that the numerator of (D.8) is

$$\frac{\omega^2 - (\omega_m + \omega_o)^2}{\omega_o^2 - \omega^2} + \mu + SK = 0 \tag{D.13}$$

After considerable algebra, we have

$$\omega = \frac{1}{S}(\omega_o + \omega_m) \tag{D.14}$$

which for positive $\omega$ implies that $S = +1$.

Thus,

$$\omega \equiv \omega_c = \omega_o + \omega_m \tag{D.15}$$

for the case of S = +1 only. As a check for Equation (D.15), if this is substituted into Equation (D.11) we have

$$\omega\omega_o \neq 0 \tag{D.16}$$

which always holds. Therefore, (D.15) is correct. Therefore, the mode for which $\vec{k} \times H_o\hat{y}$ points away from the YIG exists up to $\omega_o + \omega_m$. Our geometry is given in Figure D1.

For the geometry shown, this wave must propagate in the +Z-direction, and its energy is concentrated along the YIG-GaAs interface. If the wave is to travel in -Z (for S = +1 still) it must propagate along the YIG-air surface.

In this report we will restrict ourselves to the $k > 0$ case. We examine only the wave moving in the +Z-direction in detail.

If we allow S = -1, the mode of concern propagates on the YIG-air surface. Since $S \neq -1$ for the passband edge given in (D.15), we must investigate the complete dispersion equation for -k. Setting k = -k, the dispersion yields

$$e^{2kd} = \frac{\mu^2 - K^2 + \mu + SK}{\mu^2 - K^2 - \mu + SK} \tag{D.17}$$

For $k \to \infty$ we have

$$\mu^2 - K^2 - \mu + SK = 0 \tag{D.18}$$

and

$$\mu^2 - K^2 + \mu + SK \neq 0 \tag{D.19}$$

Using Equation (D.18) gives

$$\left(\omega + \frac{S\omega_m}{4}\right)^2 = \left(\omega_o + \frac{3\omega_m}{4}\right)^2 \tag{D.20}$$

Now the -k wave must travel on the upper surface. Since $\vec{k} \times \vec{H}_o$ must

point away from the YIG, we must let S = +1. If this is used in (D.20), we obtain

$$\omega + \frac{\omega_m}{4} = \pm\left(\omega_o + \frac{3\omega_m}{4}\right) \qquad \text{(D.21)}$$

or

$$\omega \equiv \omega_B = \omega_o + \frac{\omega_m}{2}$$

Therefore, the -k wave at the YIG-semiconductor surface must have S = -1. Therefore, for S = -1, the +k wave must be concentrated on the YIG-air surface. For wave propagating in the +Z direction we assume the generator is at the left edge in Figure D1 and a matched termination exists on the right edge so that no reflections are possible. For S = -1, the passband is $(\omega_A, \omega_B)$ and the wave is on the YIG-air surface. When S = +1, the passband is $(\omega_A, \omega_C)$ and the wave is on the YIG-GaAs interface. Figure D1 provides a summary for the $n_o \to 0$ case. Figure D2 gives a summary for $n_o \to \infty$ along with representative numerical values. The reader should be careful to distinguish between $\omega_c$ in the $\gamma_s^2$ expression (the conductivity frequency) and the upper cutoff $\omega_c$ referred to in this appendix.

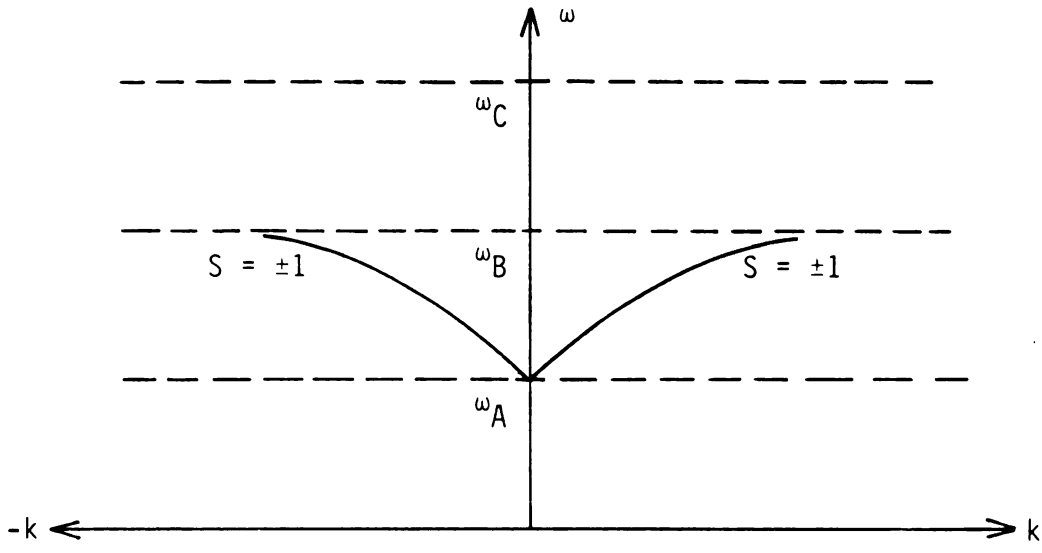


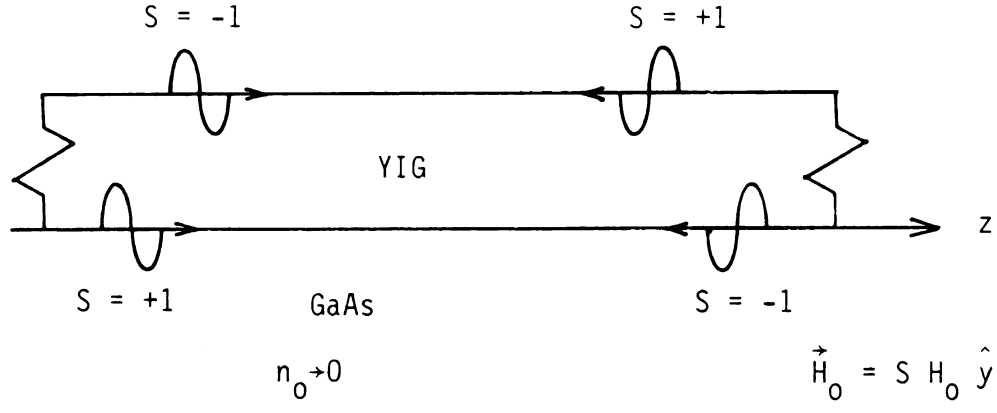


Figure D-1. Passband of dispersion behavior and propagation orientation for the dielectric case.

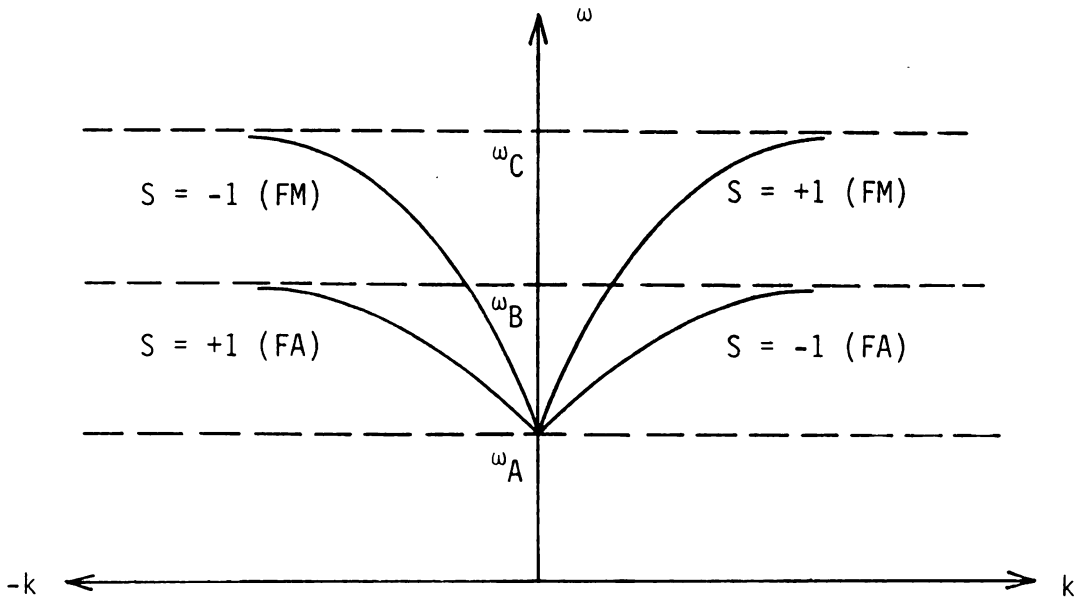


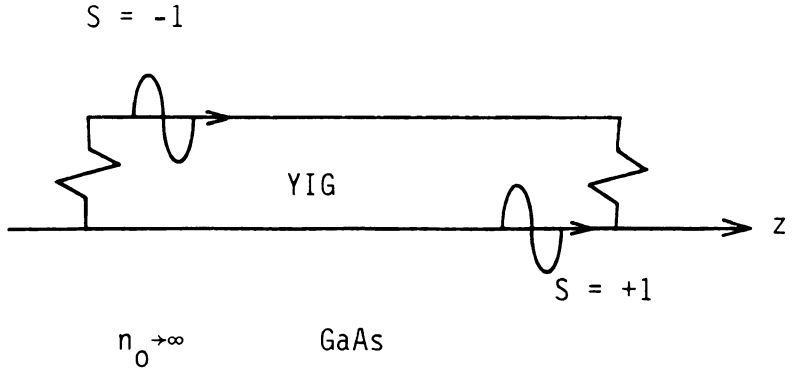


$n_o \to \infty$ GaAs

$H_o$ = 500 Oe
$\omega_A = 1.87 \times 10^{10}$ rad/sec
$\omega_B = 2.43 \times 10^{10}$
$\omega_C = 3.98 \times 10^{10}$
$f_C$ = 6.33 GHz
$f_B$ = 3.86 GHz
$f_A$ = 2.9 GHz

$\omega_o = 8.796 \times 10^9$
$\omega_m = 3.096 \times 10^{10}$
$f_o$ = 1.4 GHz
$f_n$ = 0.49 GHz

Figure D-2. Passband summary for the metal case.

# APPENDIX E

## REVIEW OF PREVIOUS RESEARCH

### E.1. Review of work by Bini, et al.

This work is presented in references [80-83]. Bini obtains the growth factor $k_i$ by using an approximate formula that is the ratio of power and/or energy terms; thus, the name "energetic analysis approach". In the first paper [84], the fields were obtained by first assuming the carrier density in the semiconductor is zero. This is his "cold mode" approach. The introduction of carriers in subsequent calculations was assumed to be a small perturbation. In the subsequent papers, it was not clear when $n_o$ was finite or zero during particular calculations. They predicted active coupling only for MSSW (surface waves) stating that volume waves did not look promising. These surface waves are TE and $\rho = 0$ i.e., no space charge. The interaction is derived from the $\bar{v} \times \bar{B}$ term in the Lorentz force equation. They assume a single boundary (YIG-SEMI interface) supports a slow surface wave. The passband is between $f_A$ and $f_B$ and it occurs when $\bar{k} \times \bar{H}_o$ points away from the YIG. Their eq. (14) in [85] is the basic "single-surface" dispersion which they study in detail. The letter [86] in 1977 did not use the "cold mode" concept. The YIG was a thin film with thickness $h \sim \lambda$. Bini assumes YIG losses can be directly subtracted from the gain. In the third paper [87] in 1978, a slab is considered at the beginning of the paper. The complexity of the resulting dispersion was noted and a mapping technique to track roots was discussed. Subsequently, they returned to the "single surface" case and obtained approximate results in this limit. For no YIG loss ($\Delta H = 0$), they find both weak and strong interaction regions.

The weak regime is for low conductivity; the strong for large conductivities. In the weak regime, the gain increases with $\sigma$, whereas in the strong one, it decreases with increasing $\sigma$. Thus, an optimum carrier density was predicted. (For GaAs, this corresponds to $n_o \sim 10^{14} cm^{-3}$). When loss was introduced, the gain, and bandwith for gain, decreased. A lower limit on $\sigma$ occurs now, which means that practically only the strong regime is feasible. Thus, the optimum value for $n_o$ calculated when $\Delta H = 0$, will not be realized in practice. We now summarize in more detail.

1. They say <u>all</u> experiments conducted have used <u>thick</u> YIG samples, thus, the "single-surface" model should apply. The semiconductors used were Ge and InSb.

2. For single-surface, the gain occurs quite close of $f_B$, where $\omega_b = 2\pi f_B = \omega_o + \frac{\omega_m}{2}$. The bandwidth is about 17 kHz when $\Delta H = 0$ and about 9 kHz when $\Delta H = 10$ Oe.

3. We question this result since Bini says $\Delta H$ gets very large near $f_A$ or $f_B$; so is $\Delta H = 10$ Oe a realistic value to assume? With no loss, the gain goes to infinity at $f_B$.

4. He calculates loss contributions under the condition $n_o = 0$ i.e., "cold mode" again.

5. In the first paper, Equations (11) and (12) are in error; it is not clear how, or if this jeopardizes some of the results.

6. Says one cannot use the magnetostatic limit $\nabla \times \bar{H} = 0$ as this yields zero net power flow.

7. For single-surface, the approximate growth constant is

$$\beta_i \doteq \beta_r \left( \frac{v_o}{v_\rho} - 1 \right) \frac{\omega_c}{\omega} A$$

8. For a finite slab

$$\beta_i = h \frac{\omega_c}{\omega} \left( \frac{v_o}{v_\rho} - 1 \right) A_1$$

9. For the film thin ($h \leq \lambda$)

$$\beta_i \sim \frac{1}{h}$$

10. Notice the approximations in Items 7-9 are independent of h, directly proportional to h, then inversely respectively. Thus, a trend is not at all evident.

11. The carriers and wave energy are in the same direction for gain, and $v_o > v_p$.

12. Says loss reduction of $\beta_i$ is

$$\beta_{im} = -\gamma \frac{\Delta H}{2v_g}$$

$$v_g = h \frac{\omega_\beta^2 - \omega^2}{\omega}$$

but how is this developed?

13. They did not use the Bers-Briggs criteria as it would be complicated due to their numerical scheme. Instead, they used the direction of the Poynting vector. It was not clear if actual or cold mode fields were used; and no calculations were presented.

14. They pointed out several serious errors in previous theoretical treatments.

    a) Vural [88], Robinson [89], had $v_p$ and $v_o$ in opposite directions, so only an evanescent mode was studied!

    b) Kawasaki et al. [90] chose the wrong root; i.e., it becomes unbounded at infinity.

15. After studying the thick slab case ($h>>\lambda$) in detail, they conclude slabs should not be used; only thin films seem feasible. However, only the letter [91] addressed this case!

16. The bandwidth for thin films (~3μ) was ~200 MHz at 3-4 GHz.

17. Their comments on the existing experimental results were quite informative.

    a) Vural [92] saw electronic gain; whereas Szustakowski [93] under very similar conditions observed no interaction!

    b) The experimental data (obtained from pulsed conditions) is not suitable for comparison with theory.

    c) Vaskovskii's [94] data are unclear since the measurement frequency is out of the passband for the proposed modes!

18. The predicted 10 kHz bandwidth (for $h>>\lambda$, single surface) clashes with reported data, since the spectrum is about 10 MHz wide about the carrier (0.2μsec pulse widths).

19. Surprisingly they claim "all the theoretical work has now been completed"; and "subsequent analysis is not needed."

20. They state all reported experimental results are questionable; and we agree.

21. Concludes that the device must be a thin film operated in pulsed mode at $77^{o}$K with excellent heat sinking.

22. Since the magnetic saturation occurs at tens of microwatts, low power applications are the only foreseeable ones.

23. Surprisingly, the Hall-effect that would accumulate the surface was not mentioned at all. No balancing bias plate was envisioned.

24. We agree with their expressions for $\gamma_f^2$ and $\gamma_s^2$, but not necessarily with some of the approximations for $\gamma_s$.

25. The "idle modes" introduced are not clear at all; are they evanescent modes?

E.2. Review of Awai et al.

1. The case analyzed is YIGSLAB; an optimum carrier density is predicted. The gain increases for increasing frequency [95].

2. They mention that there is no mode (slow) at the interface of an infinite half-space of YIG on a dielectric. They reference Damon and Eshbach for this result. Therefore, the work by Robinson et al. is in jeopardy.

3. Notice Bini mentioned Robinson's error of $u_o$ and $v_p$ in opposite directions. However, now we see the single-surface concept of Bini is also in jeopardy, since no "cold mode" actually exists.

4. Therefore, Awai used a finite slab. A slow mode exists with or without the carriers. Assumes $\Delta H = 0$ always.

5. Used $u_o = 8 \times 10^7$ cm/sec, which is not realizable. Finds $k_i \sim 1\text{-}100$ $cm^{-1}$. Says optimum $n_o$ occurs for $n_o \sim 10^{17}$.

6. Used the Bers-Briggs criteria to verify actual convective instability.

E.3. Review of Lukomskii et al.

1. Finds gain for 4μ YIG on 20μ InSb at 3.5 GHz. $\Delta H$ = 0.4 Oe, $n_o$ = $3 \times 10^{15}$. Says heating reduces operation to pulse mode only, and pulse width should be less than 5μ sec, for a temperature rise of 10°C [96].

2. They state for a film of YIG of thickness a,

$$\omega^2 = \omega_o^2 + \frac{\omega_m^2}{4}\left(1-e^{-2ka}\right)$$

$$v_g = \frac{\omega_m^2}{4\omega} ae^{-2ka}$$

Notice if $a \to \infty$ (for single surface), $\omega^2 \to \omega_o^2 + \frac{\omega_m^2}{4}$ and $v_g \to 0$; Thus no passband.

3. States YIG films ~5μ can have $\Delta H \sim 0.5$-1.0 Oersted, but T = 300°K.

4. Says $\Delta H > 1$ reduces gain to zero, in general. Lower $H_o$ widens the bandwidth and shifts it to lower frequencies.

5. States the experimental data are probably due to current filament formation; thus, the apparent amplification may be just reduced damping.

6. The gain calculated assumes $k_i \sim 10\,cm^{-1}$.

## E.4. Review of Vashkovskii et al.

1. They are one the experimentalists. They found reduced loss by about 8 dB with Ge during the pulse. The YIG was $1000\mu$ thick [97].

2. They say that measurements of delay time vs $H_o$ show that a surface wave is present. This does not agree with our results, however. Bini mentions the passband descrepancy!

3. When $u_o$ and $v_p$ are in opposite directions, only attenuation occurs.

4. The results are not very clear or conclusive.

5. They analyze the case we called GATE. They state the presence of the metal gate always enhances the gain. The separation between the YIG and bias plate alters the gain and bandwidth.

6. The dispersion is practically independent of the carrier density $n_o$, but is sensitive to the plate position.

7. They employed the Bers-Briggs test, as well as including losses via $\Delta H$.

8. They chose $u_o = 5 \times 10^7$ cm/sec. which is not realizable.

9. Best gain occurs when the gate is directly against the YIG.

10. Best gain-BW for b = 0, d $\simeq 17\mu$ (d = YIG thickness) (b = gate separation). The $k_i \sim 1$ to 2 $cm^{-1}$.

11. Says absolute (oscillation) instability is possible by using the Bers-Briggs conditions.

E.5. Review of Yukawa et al.

1. They analyze a YIG slab between two semiconductor slabs and this structure between two metal plates [98].

2. They find gain for the special case of a $10\mu$ semiconductor and a $100\mu$ YIG slab with metal on both sides. For $n_o$ $10^{15}$-$10^{16}$, $k_i$~1-10. (But $u_o = 8 \times 10^7$ cm/sec)

3. They predict absolute instability in some conditions.

E.6. Review of Schlömann

1. Explains in detail the Hall-effect action that causes the magnetostatic wave to grow [99].

2. Analyses a "single surface model" almost (the semiconductor is a slab). Assumes real $\vec{k}$ and complex $\vec{\omega}$.

E.7. Review of Shapiro

1. He assumes a single surface geometry [100].

2. Assumes $\vec{k}$ is real but $\vec{\omega}$ complex; hence only oscillation is sought.

E.8. Review of Kawasaki et al.

1. Recall Bini mentions their incorrect root choice.

2. They point out that the additional $H_0$ due to the current pulse was not included in analysis of previous experiments; thus, the variation of delay with or without the current pulse does not necessarily imply gain [101].

3. Their experiment using Ge showed gain.

4. The analysis used a YIG slab, and a semiconducting slab and metal on the YIG face.

5. They obtain the dispersion for this case, but simplify it, and ultimately reach the single surface limit.

6. The experiment used YIG with $\Delta H \leq 0.5$ Oersted, and 900μ thick. The semiconductor was 300μ thick.

7. The input power was less than 0.1 mW to prevent saturation. The measurements were pulsed at 4.1 GHz. Room temperature conditions prevailed.

8. The measured attenuation implied $\Delta H = 0.7$ Oersted.

9. A peculiar situation occurs in Figure 2 of the paper. For the value of $H_0$ given, the lower cutoff frequency for the surface waves is about 4.65 GHz. However, the measurement frequency (center) was 4.1 GHz. This implies that a volume wave was being generated and detected. No other author has mentioned this problem. Bini mentioned a similar situation occurred in Vashkovskii's work.

10. Electronic gain occurred when the holes drifted with the wave. Attenuation when drifted in opposite direction. The maximum magnitude of this gain was 3 dB at field strength of 2 KV/cm.

11. Was there real gain or reduced damping due to current filament production? Lukomskii made this statement in reference to Vashkovskii's experiments with Ge.

12. The initial insertion loss when the Ge was placed on the YIG was 25-30 dB.

13. The experimental values for interaction were only poorly reproducable.

14. In defense of Comment #11. If the interaction was due to filament production, then why does the direction of drift make a difference? Item #10 shows the interaction is not reciprocal.

15. In response to the previous item, we can easily see that holes drifting to the right (with the wave) are pushed away from the YIG, and

de-damping is possible. When drifted to the left, they are pushed toward the YIG and cause more loss.

16. A verification of interaction was instituted by replacing the Ge with a copper plate. No change in attenuation was observed for either polarity of potential applied to the copper.

17. They state reduced insertion loss even for carriers drifting slower than wave. (This again sounds like filament production).

18. They mention most authors find gain for $\vec{u}_o$ about $10^8$cm/sec; an unrealizable condition.

E.9. Chang, et al.

1. The first paper [102] looked at the intersection of dispersion curves for a semiconductor rod in an annular YIG wrapped in metal. The $u_o \doteq 5 \times 10^8$cm/sec was used. A backward branch of the dispersion was used. The thermal velocity is set to zero.

2. The next paper finds dispersion curves versus carrier density. The carriers do not drift. $\Delta H = 0$ [103].

3. A fifth order polynomial is found in $\omega$. Anticipates lowest damping occurs for $n_o \sim 10^{17}$cm$^{-3}$. The YIGSLAB model is used here.

4. The next several papers analyze special cases of the GENERAL model. They supposedly let various gaps$\to\infty$; but with assumed terms such as

$$\phi_i = a_i e^{-fx} + b_i e^{+fx}$$

the $b_i$ term blows up! How this is handled is not clear [104-105].

5. They obtain $k_i \sim 1$-10 near 4 GHz but $u_o \sim 5 \times 10^7$ to $1 \times 10^8$cm/sec, which is unrealizable.

6. They get best gain when the gap between the semiconductor and YIG goes to zero.

7. The next paper covers the GATE case. They use $u_o = 10^8$cm/sec. The values found for $k_i \sim 10^{-2}$-$10^1$ [106].

8. Increasing $\Delta H$ (from 0 to 1 Oe) reduces gain and raises the value of the low frequency wherein gain starts. This shift was about 2 GHz.

9. The next paper develops an energy analysis for the interaction. They use a GATE model [107].

10. Their energy expression is applicable for the case of <u>small</u> loss (nearly transparent media). We question this transparency assumption, since the carrier stream is very lossy. During the change from loss to gain, however, the system can be considered low loss; hence transparent.

11. Here they use $n_o = 10^{15}$ and $u_o = 2 \times 10^7$cm/sec. This is one of the few calculations where realizable parameter values were used.

12. Gain is lost when $\Delta H = 4$ Oe, but here $u_o = 10^8$cm/sec. For $u_o = 2 \times 10^7$, $\Delta H = 0.05$ apparently reduces the gain to zero; this is for the YIG energy concentrated on the face away from the semiconductor.

13. The next paper treats the GENERAL model but without the bias plate. Their signs for S = ±1 appear to be confused [108].

14. They plot the threshold velocity versus $\Delta H$. If we assume $u_o \leq 2 \times 10^7$ cm/sec, then $\Delta H \leq 1.0$ Oe or the gain is lost.

15. The values for $k_i$ before $\Delta H$ reaches 0.4 are about 1 to 3 $cm^{-1}$. The gain increases monotonically as $u_o$ increases. States this is unique to the MSSWA.

16. This condition of $k_i$ increasing monotonically with $u_o$ was also found by Awai et al.

17. They finally perform a calculation wherein most parameters are reasonable.

    $u_o = 2 \times 10^7$ cm/sec
    $\Delta H = 0.2$ Oe
    $H_o = 600$ Oe
    semiconductor thickness, 5μ
    insulator between semiconductor and heat sink, .01μ
    YIG thickness, 10μ
    $n_o \doteq 2 \times 10^{15}$

    They found $k_i \sim 0.5$ to 3 $cm^{-1}$.

18. Finally, the experimental results were published in 1982; the first paper was published in 1968 [109].

19. The experimental parameters are

    Ga As: $n_o = 8.1 \times 10^{15}$, $\mu_e = 6 \times 10^3$, thickness = 80μ
    YIG: $\Delta H = 0.5$ Oe, thickness = 90μ

20. They state the previous experiments used YIG slabs that were too thick 500-1000μ; and Ge, which has a low saturated drift velocity. The references are to Vashkovskii, Szustakowski, and Kawasaki.

21. Therefore, only four groups have performed experiments.

22. Surprisingly, they used spacers between the slabs. No metal plates were used. The parameters for the spacers are, thickness = 65-155μ, polyimide, $\tan\delta = 10^{-3}$

23. Using pulsed signals at 4.2 GHz, they were able to completely recover (to within 2-3 dB) the insertion loss. The I.L.~10-38 dB. $P_{in}$ = 7 dBm.

24. The reported data was for the 65μ spacer. The GaAs loading loss was ~17 dB. Apparently, the spacers were used.

25. The repetition rate was several tens of hertz to keep heating low.

26. They state the next experiments will use thin epitaxial GaAs YIG films.

27. Note they obtained interaction when the electrons were closest to the YIG by the Hall deflection. Thus, the concept of de-damping definitely was not occuring as could be assumed in the previous experiments.

E.10. Review of Spector

1. It appears he treats the forward and backward volume mode cases only. The only conclusion is that gain occurs when $u_o > v_p$. A rather interesting conclusion is drawn about the role of collisions. When $\nu \to 0$, the carriers and spin system cease to interact in a manner wherein energy exchange occurs. The material is a ferromagnetic semiconductor [110].

E.11. Review of Vural

1. This paper appeared in 1966. Here spin and helicon waves are considered. $H_o$ and drift are collinear; thus, the system is considerably different from our cases [111].

2. They point out several descrepancies between their work (with Bloom) and that of Akhiezer et al.

# REFERENCES

## LIST OF REFERENCES


[1] R.W. Damon and J.R. Esbach, "Magnetostatic Modes of a Ferromagnet Slab," J. Phys. Chem. Solids, Vol. 19, p. 308, 1961.

[2] L.K. Brundle and N.J. Freedman, "Magnetostatic Surface Waves on a YIG Slab," Electronics Letters, Vol. 4, p. 132, 1968.

[3] S.R. Seshadri, "Surface Magnetostatic Modes of a Ferrite Slab," Proc. IEEE (Lett.), Vol. 58, pp. 506-507, Mar. 1970.

[4] J.B. Merry and J.C. Sethares, "Low Loss Magnetostatic Surface Waves at Frequencies up to 15 GHz," IEEE Trans. on Magnetics, Vol. MAG-9, No. 3, p. 527, Sept. 1973.

[5] K. Kawasaki and M. Umeno, "Influence of Surface Metallization on the Propagation Characteristics of Surface Magnetostatic Waves in an Axially Magnetized Rectangular YIG Rod," IEEE Trans. on Microwave Theory and Techniques, Vol MTT-22, No. 4, Apr. 1974.

[6] D.F. Vaslow, "Group Delay Time for the Surface Wave on a YIG Film Backed by a Grounded Dielectric Slab," Proc. IEEE (Lett.), p. 142-143, Jan. 1973.

[7] J.D. Adam and J.H. Collins, "Microwave Magnetostatic Delay Devices Based on Epitaxial Yttrium Iron Garnet," Proc. IEEE, Vol 64, No. 5, p. 794, May 1976.

[8] J.M. Owens and C.V. Smith, "Beyond SAW Filters: Magnetostatics Show Promise," MSN, p. 44, June 1979.

[9] J.B. Merry and J.C. Sethares, as in Reference 4.

[10] W.L. Bongianni, "Magnetostatic Propagation in a Dielectric Layered Structure," Journal of Applied Physics, Vol. 43, No. 6, p. 2541, June 1972.

[11] T. Yukawa et al., "Effects of Metal on the Dispersion Relation of Magnetostatic Surface Waves," Japanese Journal of Applied Physics, Vol. 16, No. 12, p. 2187, Dec. 1977.

[12] K. Kawasaki et al., "Passband Control of Surface Magnetostatic Waves by Spacing a Metal Plate Apart from the Ferrite Surface," IEEE Trans. on Microwave Theory and Techniques, Vol. MTT-22, No. 11, p. 924, Nov. 1974.

[13] A.V. Vashkovskii et al., "Instability of Surface Magnetostatic Waves in a Semiconductor-Ferromagnetic-Dielectric Metal Structure," Radio Electronics and Electron Physics, 1974.

[14] M.R. Daniel et al., "A Linearly Dispersive Magnetostatic Delay Line at X-Band," IEEE Trans. on Magnetics, Vol. MAG-15, No. 6, p. 1735, Nov. 1979.

[15] W.S. Ishak and K.W. Chang, "Magnetostatic-Wave Devices for Microwave Signal Processing," Hewlett Packard Journal, p. 10, Feb. 1985.

[16] J.D. Adam and J.H. Collins, as in Reference 7.

[17] M. Bini et al., "Energetic Derivation of the Amplification of Magnetic Waves Interacting with a Flow of Charges in a Semiconductor," Journal of Applied Physics, Vol. 47, No. 7, P. 3209, July 1976.

[18] M. Bini et al., "Thin-Film Magnetostatic Amplifier: Analytical Expressions of Dispersion and Gain Properties," Electronics Letters, Vol. 13, pp. 114-115, Feb. 1977.

[19] M. Bini et al., "Amplification of Surface Magnetic Waves in Transversely Magnetized Ferrite Slabs," Journal of Applied Physics, Vol. 49, No. 6, p. 3554, June 1978.

[20] M. Bini et al., "Interaction of Magnetic Waves with Drifting Charges," IEEE Trans. on Magnetics, Vol. MAG-14, No.5, p. 811, Sept. 1978.

[21] I. Awai et al., "Interaction of Magnetostatic Surface Waves with Drifting Carriers," Japanese Journal of Applied Physics, Vol. 15, No.7, p. 1297, July 1976.

[22] J.D. Adam and J.H. Collins, as in Reference 7, p. 796.

[23] K. Kawasaki et al., "The Interaction of Surface Magnetostatic Waves with Drifting Carriers in Semiconductors," IEEE Trans. on Microwave Theory and Techniques, Vol. MTT-22, No. 11, p. 918, Nov. 1974.

[24] R.F. Soohoo, Microwave Magnetics, New York, Harper and Row, 1985, Chapter 5.

[25] Ibid, p. 107.

[26] B. Lax and K.J. Button, Microwave Ferrites and Ferrimagnetics, New York, McGraw-Hill, 1962, Chapter 4.

[27] Ibid, pp. 146-147.

[28] B. Lax and K.J. Button, as in Reference 26, p. 149.

[29] Ibid.

[30] B. Lax and K.J. Button, as in Reference 26, p. 148.

[31] Ibid.

[32] R.F. Soohoo, as in Reference 24, pp. 109-113.

[33] E. Schlömann, "Amplification of Magnetostatic Surface Waves by Interaction with Drifting Charge Carriers in Crossed Electric and Magnetic Fields," Journal of Applied Physics, Vol 40, No. 3, p. 1422, Mar. 1969.

[34] R.F. Soohoo, as in Reference 24, pp. 119-122.

[35] Ibid, p. 120.

[36] B. Lax and K.J. Button, as in Reference 26, pp. 167-169.

[37] W.S. Ishak and K.W. Chang, as in Reference 15, p. 14.

[38] B.A. Auld, "Walker Modes in Large Ferrite Samples," Journal of Applied Physics, Vol. 31, No.9, p. 1642, Sept. 1960.

[39] J.C. Freeman, private communication.

[40] J.C. Freeman, private communication.

[41] E. Schlomann, as in Reference 33.

[42] W.S. Ishak and K.W. Chang, as in Reference 15, p. 11.

[43] B.B. Robinson et al., "Spin-Wave/Carrier-Wave Interactions," IEEE Trans. on Electron Devices, Vol. ED-17, No.3, p. 224, Mar. 1970.

[44] S.F. Adam, Microwave Theory and Applications, New Jersey, Prentice-Hall, 1969, Chapter 4, pp. 118-122.

[45] C.T. Hui, The Field and Carrier Waves Interaction in a Semi-Infinite Semiconductor, M.S. Thesis, Michigan State University, 1982.

[46] S.R. Seshadri, as in Reference 3.

[47] R.E. De Wames and T. Wolfram, "Characteristics of Magnetostatic Surface Waves for a Metallized Ferrite Slab," Journal of Applied Physics, Vol. 41, No. 13, p. 5243, Dec. 1970.

[48] P. Young, "Effect of Boundary Conditions on the Propagation of Surface Magnetostatic Waves in a Transversely Magnetized Thin YIG Slab," Electronics Letters, Vol. 5, No. 18, p. 429, Sept. 1969.

[49] S.R. Seshadri, as in Reference 3.

[50] J.D. Adam and G.A. Bennett, "Identification of Surface-Wave Resonances on a Metal-Backed YIG Slab," Electronics Letters, Vol. 6, No. 24, p. 789, Nov. 1970.

[51] K. Kawasaki et al., as in Reference 12.

[52] R. Pauchard et al., "Electromagnetic Surface Waves in a Metallized Ferrite Slab," Electronics Letters, Vol. 7, No. 24, p.428, July 1971.

[53] H. Van De Vaart, "Influence of Metal Plate on Surface Magnetostatic Modes of Magnetic Slab," Electronics Letters, Vol. 6, No. 19, p. 601, Sept. 1970.

[54] W.K. Bongianni, as in Reference 10.

[55] W.K. Bongianni, as in Reference 10.

[56] T. Yukawa et al., as in Reference 11.

[57] R. Pauchard et al., as in Reference 52.

[58] K. Kawasaki et al., as in Reference 12.

[59] M. Bini et al., as in Reference 19, p. 3554.

[60] Ibid, p. 3555.

[61] I. Awai et al., as in Reference 21.

[62] B.Vural, "Interaction of Spin Waves with Drifted Carriers in Solids," Journal of Applied Physics, Vol. 37, No. 3, Mar., 1966.

[63] M.C. Steele and B. Vural, Wave Interactions in Solid State Plasmas, New York, Mc Graw Hill, 1969.

[64] C.T. Hui, as in Reference 45.

[65] Ibid.

[66] A. Bers and R.J. Briggs, "Criteria for Determining Absolute Instability and Distinguishing Between Amplifying and Evanescent Waves," Quarterly Progress Report, No. 71, Research Laboratory of Electronics, M.I.T., Cambridge, MA, Oct. 15, 1963.

[67] J.C. Freeman, private communication.

[68] J.C. Freeman, private communiction.

[69] I. Awai et al., as in Reference 21.

[70] J.C. Freeman, private communication.

[71] A.V. Vashkovskiy et al., as in Reference 13.

[72] P.M. Bolle and L. Lewin, "On the Definition of Parameters in Ferrite-Electromagnetic Wave Interactions," IEEE Trans, on Microwave Theory and Techniques, Vol. MTT-21, p. 118, Feb. 1973.

[73] R.E. Collin, Foundations for Microwave Engineering, New York McGraw-Hill, 1966.

[74] C.C. Johnson, Field and Wave Electrodynamics, New York, McGraw-Hill, 1965.

[75] S. Ramo, J.R. Whinnery and T. Van Duzer, Field and Waves in Communication Electronics, New York, John Wiley and Sons, 1965.

[76] W.R. Beam, Electronics of Solids, New York, McGraw-Hill, 1965.

[77] M. Bini et al., as in Reference 17.

[78] N.S. Chang and Y. Matsuo, "Ferromagnetic Loss Effect on Magnetostatic Surface Wave Amplification by YIG-Semiconductor Coupled System," IEEE Trans. on Magnetics, Vol. MAG-13, No. 5, Sept. 1977.

[79] J.C. Freeman, private communication.

[80] M. Bini, et al., as in Reference 17.

[81] M. Bini, et al., as in Reference 18.

[82] M. Bini, et al., as in Reference 19.

[83] M. Bini, et al., as in Reference 20.

[84] M. Bini, et al., as in Reference 17.

[85] Ibid.

[86] M. Bini, et al., as in Reference 18.

[87] M. Bini, et al., as in Reference 19.

[88] M.C. Steele and B. Vural, as in Reference 63, Chapter 10.

[89] B.B. Robinson, et al., as in Reference 43.

[90] K. Kawasaki, et al., as in Reference 23.

[91] M. Bini, et al., as in Reference 18.

[92] B. Vural, "Interaction of Spin Waves with Drifting Carriers in Solids," Journal of Applied Physics, Vol. 37, No.3, March 1966.

[93] M. Szustakowski and B. Wecki, "Amplification of Magnetostatic Surface Waves in the YIG-Ge Hybrid System," Proc. of Vibr. Probl., Vol. 14, p. 155, 1973.

[94] A.V. Vashkovskiy et al., Interaction of Surface Magnetostatic Waves with Carriers on a Ferrite-Semiconductor Interface," ZhETF Pis. Red., Vol. 16, No. 1, p. 4, July, 1972.

[95] V.P. Lukomskii and Yu. A. Tavirko, "Amplification of Magnetostatic Waves in Ferromagnetic Films Due to the Drift Current of Carriers, Fiz. Tverd. Tela., Vol. 15, p. 700, Mar. 1973.

[96] I. Awai, as in Reference 21.

[97] A.V. Vashkovskii, et al., as in Reference 94.

[98] T. Yukawa et al., "Absolute Instability of Magnetostatic Surface Waves Interacting with Drifting Carriers in Closed Ferrite-Semiconductor Structure," Trans. on Magnetics, Vol. MAG-14, No. 5, Sept. 1978.

[99] E. Schlomann, as in Reference 33.

[100] R. Kh. Shapiro, "Spectrum of Surface Electromagnetic Waves in Ferromagnet-Semiconductor Structures,"Soviet Physics-Solid State, Vol. 14, No. 11, May 1973.

[101] K. Kawasaki, et al., as in Reference 23.

[102] N.S. Chang and Y. Matsuo, "Possibility of Utilizing the Coupling Between a Backward Wave in YIG and Waves Associated with Drift Carrier Stream in Semiconductors," Proc. IEEE (Lett.), p. 765, April 1968.

[103] M. Masuda, N.S. Chang, Y. Chang, "Magnetostatic Surface Waves in Ferrite Slab Adjacent to Semiconductor," IEEE Trans. on Microwave Theory and Techniques, p. 132, Feb. 1974.

[104] N.S. Chang, et al., "Characteristics of Magnetostatic Surface Waves in a Layered Structure Consisting of Metals, Dielectrics, a Semiconductor and YIG," Electronics Letters, No. 11, p. 83, Jan. 1975.

[105] N.S. Chang, et al., "Amplification of Magnetostatic Surface Wave Propagation in a Layered Structure Consisting of Metals, Dielectrics, a Semiconductor and YIG," Journal of Applied Physics, Vol. 47, No. 1, Jan. 1976.

[106] N.S. Chang, et al., as in Reference 104.

[107] N.S. Chang, et al., "Energy Analysis for the Amplification Phenomena of Magnetostatic Surface Waves in a YIG-Semiconductor Coupled System" IEEE Trans. on MIcrowave Theory and Techniques, Vol. MTT-25, No. 7, July 1977.

[108] N.S. Chang, et al., as in Reference 78.

[109] N.S. Chang, et al., "Experimental Investigation of Magnetostatic Surface Wave Amplification in GaAS-Yttrium Iron Garnet Layered Structure," Journal of applied Physics, Vol. 53, No. 8, Aug. 1982.

[110] H.N. Spector, "Amplification of Spin Waves in Ferromagnetic Semiconductors," Solid State Communications, Vol. 6, p. 811, 1968.

[111] B. Vural, as in Reference 92.